CHEMOTAXIS OF *ESCHERICHIA COLI* TOWARDS

NOREPINEPHRINE METABOLITES

A Dissertation

by

SASI KIRAN PASUPULETI

Submitted to the Office of Graduate and Professional Studies of
Texas A&M University
in partial fulfillment of the requirements for the degree of

DOCTOR OF PHILOSOPHY

Chair of Committee,	Arul Jayaraman
Committee Members,	Michael D. Manson
	Arun R. Srinivasa
	Katy C. Kao
Head of Department,	M. Nazmul Karim

December 2017

Major Subject: Chemical Engineering

ABSTRACT

The co-existence of ~10^{14} commensal bacteria and host cells in the human gastrointestinal (GI) tract creates an environment rich in molecules produced by both. The close-proximity of different signals and cells in the GI tract is thought to lead to inter-kingdom (IK) signaling where bacteria and human cells recognize and respond to signals produced by each other. One such IK signaling molecule abundant in the GI tract is Norepinephrine (NE), which is known to increase the virulence and pathogenesis of GI tract pathogen, enterohemorrhagic *E. coli* (EHEC). It has also been shown that NE is a potent chemoattractant for EHEC as well as for non-pathogenic *E.coli*. While the effects of NE on virulence are well studied, its role as a chemoeffector is not fully understood. The overall goal of this work is to comprehensively characterize the chemotaxis response of *E. coli* toward NE and to elucidate the underlying mechanisms. A part of this work is also aimed at developing a probabilistic model to simulate the bacterial migration towards attractants.

We showed that attraction of *E. coli* RP437 towards NE requires prior exposure to a lower concentration of NE during cell growth, and that *de novo* expression of two enzymes - TynA and FeaB - is required for *E. coli* chemotaxis towards NE. We discovered that NE is not the actual chemoattractant but the molecule that *E. coli* RP437 responds to is dihydroxymandelic acid (DHMA) generated from NE. We observed that chemotaxis to DHMA requires the Tsr chemoreceptor and the minimum concentration required for a detectable chemotaxis response was ~5 nM. We also observed that the chemotaxis

response to DHMA was significantly reduced at concentrations greater than 50 μM and concluded that negative cooperativity between the two serine-binding sites resulted in attenuation of chemotaxis response.

We investigated the molecular mechanism underlying the conversion of NE to DHMA in *E. coli* RP437, and identified that it requires the QseC histidine kinase and its cognate response regulator QseB, and to a lesser extent, the response regulator QseF. We also determined that the *feaR* transcription factor is required for *tynA* and *feaB* expression. This work is significant as it suggest that host-derived signals such as NE can be converted by commensal bacteria to a potent chemoattractant, which can then recruit pathogens that possess Tsr-like receptors to the site of infection.

A probabilistic model was also developed to simulate the chemotaxis behavior of bacteria in microfluidic devices. The time-dependent distribution of bacteria in the chemotaxis chamber was simulated using MATLAB®. We determined that the time dependent bacterial migration in the microfluidic device is influenced by bulk motion of the fluid and existing concentration gradient of chemoeffector. The probabilistic model can be used to reduce the experimental space required to test the response of an unknown chemoeffector in the microfluidic device.

DEDICATION

To my parents, my brother, and my wife

ACKNOWLEDGEMENTS

CONTRIBUTORS AND FUNDING SOURCES

Contributors

Faculty committee recognition

This work was supervised by a dissertation committee consisting of Professor Arul Jayaraman [advisor], and Professor Katy C. Kao in the Department of Chemical Engineering, Professor Michael D. Manson in the Department of Biology, and Professor Arun R. Srininvasa in the Department of Mechanical Engineering.

Student/collaborator contributions

The experiments presented in Chapter III were conducted in part by Nitesh Sule, and Daniel Howsmon of the Department of Chemical Engineering and were published in 2014. The experiments presented in Chapter IV were conducted in part by Nitesh Sule of the Department of Chemical Engineering and were published in 2017.

All other work conducted for the dissertation was completed by the student under the advisement of Professor Arul Jayaraman of the Department of Chemical Engineering.

Funding Sources

TABLE OF CONTENTS

LIST OF FIGURES

LIST OF TABLES

CHAPTER I

INTRODUCTION

I.1 Background

The human gastrointestinal (GI) tract harbors approximately 10^{14} bacteria that belong to over 1000 distinct bacterial species and exhibit symbiotic relationships with the host (1). Gut bacteria help produce essential B vitamins and vitamin K, help metabolize dietary carbohydrates, proteins, and polyphenols in the food, combat against colonization by pathogenic bacteria (both foodborne and opportunistic), and play an important role in maintaining human health (2). The symbiosis between the resident bacteria of the gut and the host is disturbed when pathogenic bacteria enter the GI tract, and a disturbed microbial equilibrium is one of the factors that contribute to enteric infections. A diverse group of pathogens, the most prevalent being *Clostridium, Campylobacter*, *Escherichia coli*, and various strains of *Listeria, Salmonella, Shigella*, *Vibrio*, and *Yersinia,* contribute to foodborne infections. Of these, *Salmonella* and *E. coli* account for over 80% of the multistate outbreaks that have occurred in the US over the past decade (3). Specifically, enterohemorrhagic *E. coli* O157:H7 (EHEC, also known as Shiga toxin producing *E. coli*, STEC, or verocytotoxin-producing *E. coli*, VTEC) is the single most frequently occurring pathogen in these incidents. EHEC causes severe and bloody diarrhea as well as hemolytic uremic syndrome (HUS). The clinical course of an EHEC infection is shown in **Fig. 1.1**. Approximately three days after the ingestion of EHEC, the patient develops diarrhea, abdominal pain, and fever.
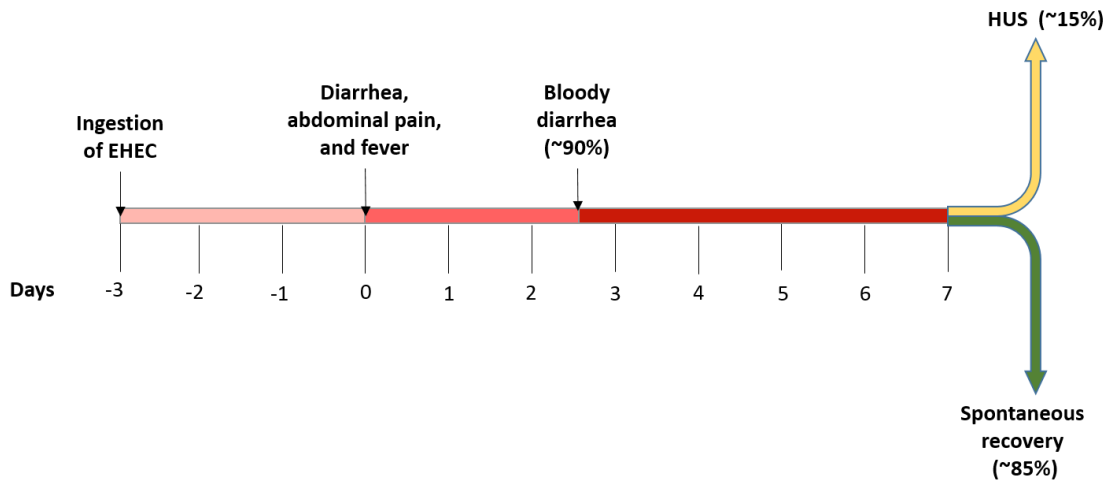
FIG. 1.1. Clinical course of EHEC infections in children. 3 days after the ingestion of pathogen patient develops diarrhea, abdominal pain, and fever. In next 2 – 4 days, the diarrhea will become bloody in almost 90% of the cases. A week after the onset of diarrhea ~15% of the patients develop HUS. Adapted from Mellmann et al. (4).

The diarrhea will become bloody in almost 90% of the cases over the next 2 – 4 days. About one week after the onset of diarrhea, ~15% of the patients (children younger than 10 years of age) develop HUS (4). HUS is characterized by hemolytic anemia (anemia caused by destruction of red blood cells), uremia (acute kidney failure), and thrombocytopenia (low platelet count) (5). HUS can cause life-threatening complications such as stroke, coma, high blood pressure, and heart problems (6).

After ingestion, EHEC travels through the digestive system and attaches to the mucosal epithelium of the large intestine to induce typical attaching and effacing (A/E) lesions which promote colonization (7). A/E lesions are characterized by intimate attachment, microvillous effacement, and actin polymerization under the adherent bacteria to form pedestal-like structure (8). The genes responsible for the formation of A/E lesions on the host epithelial cells are encoded on a 35.6 kb pathogenicity island known as locus

of enterocyte effacement (LEE). This locus contains 41 genes that are divided into five major operons (*LEE1 through LEE5*). They encode a type 3 secretion system (T3SS) and various regulators, chaperones, and effector proteins. The LEE-encoded regulator (Ler), the first gene encoded in *LEE1*, acts as the master transcription factor of the pathogenicity island, regulating the expression of all other LEE genes (9, 10).

EHEC infections occur through a three-step mechanism: (a) migration of pathogens towards the gut epithelium by recognizing the intestinal luminal environment, (b) attachment and colonization of pathogens on the epithelial cells, and (c) infection of cells by release of toxins (11, 12). The host factors influencing EHEC infection are not completely understood. However, recent studies on diarrheagenic *E. coli* virulence reveal that the neuroendocrine environment present in the gastrointestinal (GI) tract modulates the extent of infection (13), including upregulation of EHEC virulence factors by the neuroendocrine hormone norepinephrine (NE). NE, a neurotransmitter and stress hormone associated with the 'fight or flight' response, is released during mental or physical stress, trauma, and injury (14, 15). In the GI tract, NE is released by the sympathetic nerves innervating the gut. NE has shown to stimulate the expression of Shiga-toxins and LEE-encoded proteins in EHEC O157:H7 (16), and accordingly, NE increases the adhesion of EHEC O157:H7 to cecal mucosa, colonic mucosa, and the ileum (13).

Of the three steps in the model for EHEC infection, the first (i.e., recognition of the GI tract environment and migration) may offer the best opportunity for early intervention. The major goal of this work was to investigate the role of NE in modulating the migration of bacteria to sites of colonization on the epithelial layer of the GI tract.

I.2 Motivation

Foodborne illness affects approximately 1 in 10 people worldwide and annually results

in 420,000 deaths (17). According to the Center for Disease Control and Prevention, ~48

million people in the United States get sick by consuming contaminated food every year,

resulting in 128,000 hospitalizations and 3000 deaths (18). EHEC alone causes

approximately 73,000 infections, with 2000 hospitalizations and 60 deaths per year (19).

Symptoms of an EHEC infection range from abdominal cramps, diarrhea (sometimes

bloody), and nausea, and can lead to infection of the systemic circulation and death. The

cost associated with the EHEC infections is very high; it is estimated that the total cost

associated with EHEC infections just in the United States is ~2 billion dollars /yr (20),

when hospitalization charges, physician services, drugs, insurance coverage, etc. are taken

into account. Another important consequence of EHEC infections is the decrease in

quality of life, and in extreme cases, permanent disability or even mortality. Because the

infectious dose required for EHEC infections is extremely small (10-100 CFU/mL) (21),

even a few cells entering the GI tract can lead to infection.

Unlike infection by other GI tract pathogens like *Salmonella*, EHEC infections are

typically not treated with antibiotics, because the genes encoding for the *stx* (Shiga toxin)

genes are harbored in a prophage and use of antibiotics such as ciprofloxacin triggers the

SOS response in EHEC (4). This, in turn, results in the induction of the phage lytic cycle

and leads to excision of the prophage from the chromosome and co-transcription of *stx*

and phage genes. As a result, the levels of Stx in the environment increases significantly.

Although EHEC does not invade the host cells, Stx can enter the circulation and bind to

the Gb3 receptor in renal microvascular endothelial cells, resulting in inhibition of protein synthesis, cellular damage, and eventually HUS (22). HUS is particularly dangerous in children and elderly people with weakened immune systems. Given the seriousness of EHEC infections, understanding the mechanisms underlying EHEC infection can lead to the development of approaches for combating human GI tract infections.

I.3 Research importance, objectives, and novelty

Colonization of the GI tract by EHEC is not random and does not occur at all locations and sites (e.g., there is no significant colonization in the small intestine). In human subjects, EHEC has been shown to preferentially colonize gut-associated lymphoid tissues (GALTs) in the large intestine (23). Therefore, it is reasonable to speculate that the colon microenvironment plays a significant role in the events (i.e., initial migration of EHEC towards intestinal epithelial cells) that lead to colonization of EHEC. It is likely that the multitude of microbial and host signaling molecules in the colon microenvironment play an important role in promoting EHEC colonization in the GALTs.

One such molecule that is abundant in the GI tract (24, 25) and has been previously shown to promote the expression of virulence genes and Shiga toxin production in EHEC is the neuroendocrine hormone and neurotransmitter NE (26). A majority of prior studies have focused on investigating the effect of NE on EHEC virulence gene expression and pathogenesis at the epithelial surface (i.e, after EHEC colonization) (13, 16, 26). In contrast, this work focuses on events that occur prior to colonization of the GI tract; specifically, on the role of NE in EHEC migration towards the epithelial surface. Our

overall hypothesis is that EHEC senses NE as a chemoattractant and uses local NE gradients to reach preferred colonization sites. This hypothesis is supported by previous work from our laboratory showing that NE is a chemoattractant for EHEC as well as for non-pathogenic *E.coli* in vitro (27, 28). However, the mechanisms underlying the chemotaxis of *E. coli* towards NE is not known. Thus, the overall goal of this work is to undertake a comprehensive characterization of chemotaxis of *E. coli* toward NE and to elucidate the underlying mechanisms. In addition, we have developed a probabilistic model to simulate the bacterial migration towards attractants.

E. coli chemotaxis towards nutrients such as amino acids has been extensively used as a model for studying signal transduction in bacteria (29). However, few studies have investigated chemotaxis towards non-energy sources such as NE. Therefore, this work extends our knowledge about the full repertoire of chemical signals that serve as attractants for *E. coli*. In addition, this study also supports the role of metabolism in the generation of a broad range of chemoeffectors starting from a smaller subset of host molecules. This paradigm could be especially important in environments such as the GI tract, where the generation of chemoeffectors by metabolism carried out by the diverse microbiota will be important for controlling the virulence of enteric pathogens such as EHEC, as we have observed for NE and DHMA (30).

This study used the non-pathogenic and more easily manipulated laboratory strain *E. coli* RP437 as a model for investigating chemotaxis toward GI tract molecules. However, because *E. coli* RP437 and EHEC possess the same five chemoreceptors (Tar, Tsr, Tap,

Trg, and Aer) and share a high degree of gene and protein sequence homology (31), the

results from this work will certainly be applicable to EHEC as well.

The specific objectives were to:

- Characterize the chemotaxis response of *E. coli* RP437 towards NE and its

  metabolites

- Investigate the mechanisms underlying the conversion of NE to other metabolites

  in *E. coli*.

- Model the chemotaxis behavior of bacteria in microfluidic devices using a

  probabilistic approach

CHAPTER II

LITERATURE REVIEW

II.1 Human microbiota

The human microbiota is an aggregate of trillions of microorganisms that reside in and on the human body. The number of single-celled microorganisms in the human microbiota is estimated to be 10 times greater than the number of cells of the human host (1). In addition to the bacteria, the human microbiota includes archaea, fungi, and viruses (32). Microorganisms colonize all different parts of the human body **(Fig. 2.1),** including the skin, nose, ear, mouth, lung, GI tract, kidney, and urogenital tract. They make up 1 – 3 % of the human body mass (33).

Although the composition of the microbiota depends on anatomical location, interpersonal variation is also substantial (34). For example, twins share less than 50 % of their bacterial taxa at species level (35). Despite this diversity, the human microbiota has conserved core functions, such as maintenance of basic biological processes, provision of resistance against colonization by pathogens, and regulation of the immune system. The microhabitats of different organs and body parts each have their own specialized properties. For example, the gut microbiota help to digest complex carbohydrates, participate in lipid metabolism, and produce essential vitamins (32). Microbiota present on the skin inhibit surface pathogens by secreting toxic metabolites (36).
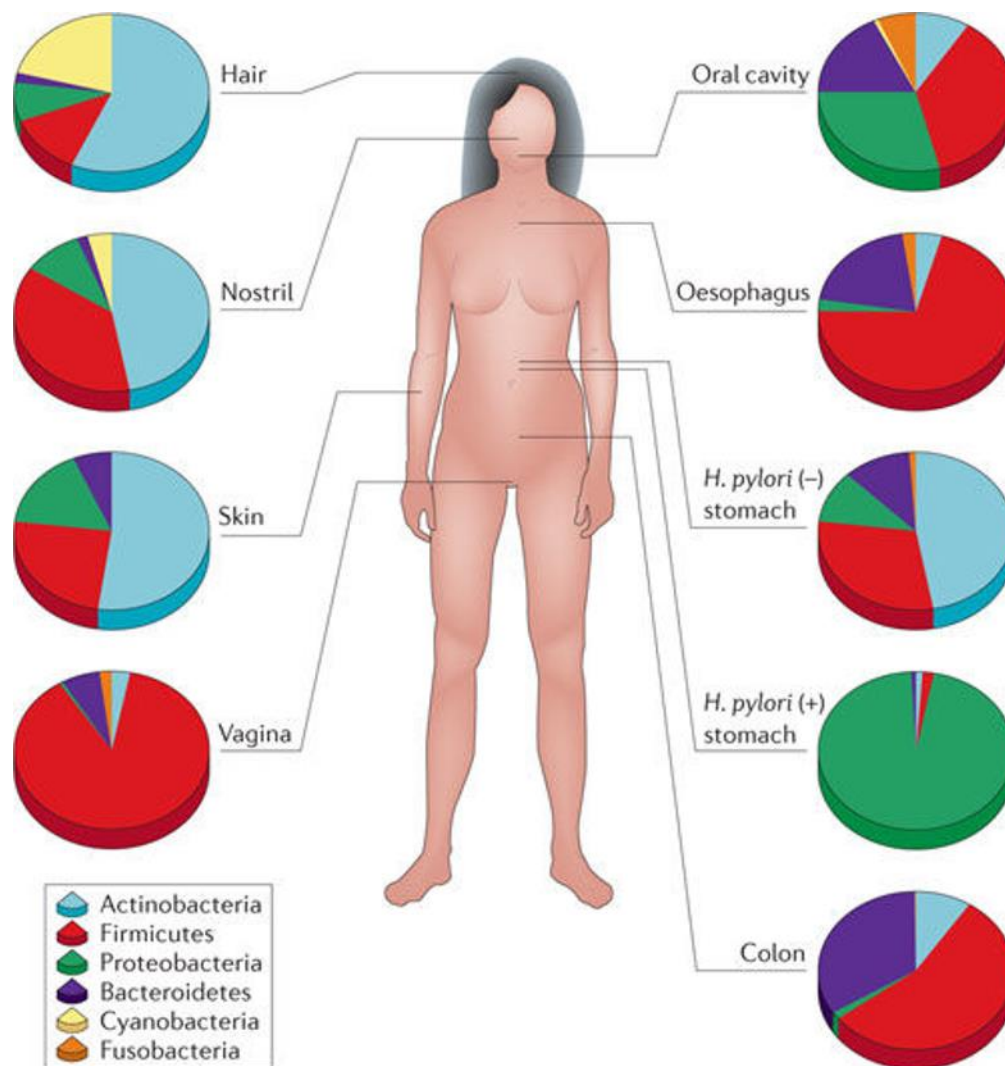
FIG. 2.1. Colonization of different parts of the human body by microorganisms. The figure indicates the taxonomy of the microbiome at the phylum level for different anatomical sites. Reprinted by permission from Macmillan Publishers Ltd: Nature Reviews Genetics (37), copyright 2012.

II.1.1 Human gut microbiota

The human GI tract, commonly referred to as the gut, spans from the mouth to the anus and comprises a connected system of organs that takes in food, extract nutrients and energy, and secretes waste material. The GI tract can be divided into upper and lower parts. The upper GI tract consists of the mouth, pharynx, esophagus, and stomach, whereas the lower GI tract comprises the small intestine, large intestine, and rectum (38). Besides its major functions in ingestion, digestion, absorption, and excretion, the human gut is also a major component of the immune system. With an estimated surface area of 32 m^2 (39), the gut and its associated immune components provide protection against entry of exogenous pathogens into the blood and lymph circulatory systems (40) as well maintaining a healthy and nutrient rich environment for the resident microbiota. The human gut microbiota contains ~10^{14} organisms belonging to more than 1000 species (1).

Microorganisms display a great deal of heterogeneity with respect to their density and composition in different parts of the GI tract. The stomach and the upper part of the small intestine (duodenum, jejunum) contains a relatively low number of bacteria (10^3 to 10^4 cells/g) due to the low pH (41). The major microbial types present in the stomach and upper part of small intestine are acid resistant lactobacilli and streptococci (41). In addition, *Helicobacter pylori* is present in the stomach of a large percentage of people (42). The number of resident bacteria increase to 10^8 cells/g in the distal small intestine (the ileum) and mainly contains certain *Clostridium* spp. and certain members of the phylum Proteobacteria (43). The colon is the primary site of microbial colonization in humans with 10^{12} to 10^{14} cells/g, and 99.9 % of them are obligate anaerobes. The most

abundant bacteria are the member of the genus *Bacteriodes*, *Peptostreptococcus,*

Eubacterium, Clostridium, Fusobacterium, and *Bacillus* (41, 44).

In spite of the fact that our GI tract is germ-free upon birth, it is quickly colonized by

microorganism from the environment and mother's birth canal (42). The microbiota is

dynamic and rapidly evolves into a complex microbial ecosystem. Studies have shown

that the microbial community of 3-year old infant already resembles that of an adult (42,

45). Although the composition of gut microflora depends on several factors, such as diet,

age, medications, illness, stress, and lifestyle (46), it has recently been found that over

90% of the bacterial component of gut microbiota can be represented by four major

microbial phyla: *Bacteroides, Firmicutes, Proteobacteria* and *Actinobacteria* (47).

The gut microbiota maintains a symbiotic relationship that confers benefits to both the

members of the microbial community and the host. The host benefits from the microbiota

because of its metabolic, immunological and protective functions (48, 49). Production of

short chain fatty acids (SCFAs), such as acetate, propionate, and butyrate, from dietary

fibers and complex carbohydrates by the colonic bacteria is one example of metabolic

function of gut microbiota (50). The SCFAs plays an important role in the control of

epithelial cell proliferation and differentiation in the colon (44). The gut microbiota also

plays an important role in the synthesis of essential vitamins such as vitamin K, vitamin

B_{12}, folate, and biotin, which are not produced by the host. Gnotobiotic studies on

colonization of germ-free mice with specific microorganisms have revealed the important

role of the microbiota on the development and maturation of the immune system (51). For

example, studies with germ-free animals show extensive defects in the organization and

function of gut-associated lymphoid tissue (GALT) along with reduced antibody production, fewer Peyer's patches, and impaired development and maturation of isolated lymphoid follicles (ILFs) (46, 51). However, some of these defects can be reversed by colonizing germ-free animals with the commensal bacteria (52). The gut microbiota also provides resistance to colonization by enteric pathogens through the production of antimicrobial substances (such as bacteriocins) and by competing for nutrients required by pathogens to establish themselves in the GI tract (53) .

Several studies have also shown that alterations in the conmposition of the microbiota (dysbiosis) is correlated wtih numerous diseases such as metabolic syndrome, cancer, inflammatory bowel disease (IBD), Crohn's disease, and ulcerative colitis (54-58). The Human Microbiome Project (HMP), a National Institutes of Health (NIH) initiative started in 2008, focuses mainly on understanding the correlation between changes in the microbiome and the disease state using metagenomics and genomic DNA-sequencing techniques (57).

II.2 Important signaling molecules in the GI tract

The gut microbiota produce several metabolites that serve as microbe-microbe and host-microbe signaling agents. For example, indole functions as an interspecies and interkingdom signaling molecule (59), and autoinducer-2 (AI-2) works primarily as quorum sensing (QS) molecule (60). In addition to metabolites produced by gut microbiota, the GI tract contains numerous host-derived signaling molecules, such as catecholamines (dopamine, epinephrine, norepinephrine, etc.). Epinephrine and

12

norepinephrine, in particular, have been shown to affect microbial populations in the GI tract and can also influence virulence factors production in the invading pathogens (26, 61-63).

II.2.1 Norepinephrine (NE)

NE is a catecholamine neurotransmitter of the sympathetic nervous system that enervates the GI tract (64). NE is synthesized from tyrosine by a series of enzymatic steps in the adrenal medulla and by postganglionic neurons of the sympathetic nerve system (65). The first step in the synthesis of NE involves conversion of tyrosine to L-DOPA and is catalyzed by the enzyme tyrosine hydroxylase (TH). DOPA is converted into dopamine by the enzyme DOPA decarboxylase. Finally, dopamine is converted into NE by the enzyme dopamine β-hydroxylase (DBH) and released into the gut lumen from the noradrenergic nerve endings in the GI tract. When there is excess NE production (e.g., after a major injury, infection, or stress), NE spills over into the GI tract lumen, where it affects the composition of the microbial community (66-69). Previous studies have shown that NE stimulates the growth of various Gram-negative and Gram-positive bacteria, including *Pseudomonas aeruginosa*, *Yersinia enterolitica*, *Salmonella enterica*, and *Listeria* spp (67). It was found that NE increased adhesion of EHEC O157:H7 to cecal mucosa, colonic mucosa, and the ileum (13). NE also increases the secretion of virulence determinants like elastase, rhamnolipid, and pyocyanin in *P. aeruginosa* PA14 (70), enhances growth, motility, and invasiveness in *Campylobacter jejuni* (61), and up-regulates expression of virulence factors in *S. enterica* Typhimurium (71).

We have found that NE is a chemoattractant for EHEC as well as for non-pathogenic *E.coli* in vitro (27, 28). Experiments with a series mutants of *E. coli* RP437 have revealed that attractant response to NE is primarily mediated by serine chemoreceptor, Tsr, and that pre-exposure to NE results in *de novo* expression of proteins required for NE chemotaxis (28). Wild-type *E.coli* RP437 cells were attracted toward an agarose plug containing 200 µM NE (28), whereas *B. pilosicoli* are attracted to NE even when the NE concentration in a capillary assay (see below) is as low as 0.05 mM (72).

In humans, NE is rapidly degraded to various metabolites. Either monoamine oxidase A (MAO-A) or catechol – O –methyl transferase (COMT) catalyzes the initial step in the NE metabolism (73). MAO-A deaminates NE to 3, 4-dihydroxyphenyl-glycolaldehyde (DOPEGAL) (73). This potentially toxic aldehyde intermediate metabolite rapidly undergoes further metabolism to form either stable alcohol or acid metabolites (73). Aldehyde dehydrogenase converts DOPEGAL to 3,4-dihydroxy-mandelic acid (DHMA) and aldehyde reductase converts DOPEGAL to 3,4-dihydroxy-phenylglycol (DHPG) (73). Finally, vanillylmandelic acid (VMA), the major end product of NE metabolism, is formed by the action of COMT on DHMA (73).

II.3 *Escherichia coli* chemotaxis

Chemotaxis is the directed migration of organisms toward or away from higher concentrations of chemicals that are sensed as attractants or repellents, respectively (74). Chemotaxis of *E. coli* toward metabolizable compounds has been well studied (75-77). *E. coli* migrate toward amino acids (e.g., aspartic acid, serine), sugars (maltose, ribose,

galactose, glucose), dipeptides, pyrimidines and electron acceptors (oxygen, nitrate, fumarate) (78-80). They move away from a broad range of compounds including alcohols, fatty acids, glycerol, and metal ions (e.g., Ni^{2+}) (81-83).

When present in an isotropic chemical environment *E. coli* have two modes of movement (80). They swim smoothly in relatively straight line, called a "run", and then abruptly change direction in a chaotic movement known as a "tumble" (80). Because of the alternating run and tumble modes, the migration of a bacterial cell has been described as a random walk (80). When cells encounter an increasing concentration of an attractant, the tumble frequency is reduced and longer runs are attained, which results in a biased random walk (**Fig.2.2**). As a result, cells migrate toward higher concentrations of an attractant (80). Conversely, bacteria tumble more frequently if they encounter an increasing concentration of repellent (80). In *E.coli*, the run and tumble modes of movement are correlated with the direction of rotation of the flagellar motor. Counterclockwise (CCW) rotation promotes formation of a left-handed helical flagellar bundle that produces a force on the cell body that causes the cell to swim smoothly (84). In contrast, clockwise (CW) rotation of one or more flagella destabilizes the bundle and causes the cell to tumble (84). In a uniform signaling environment, runs last an average of ~2 s and are interrupted by short tumbles of ~0.1 s (85).
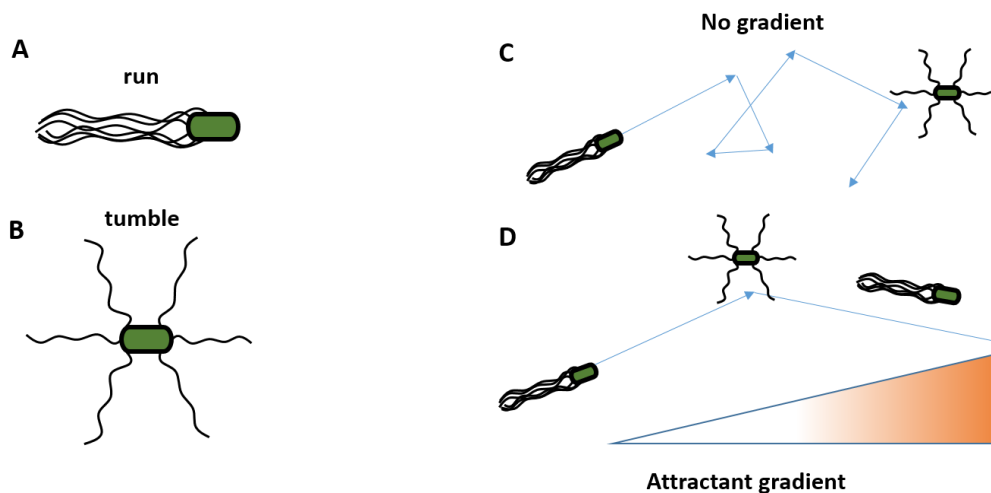
FIG. 2.2. Chemotaxis behavior of *E. coli*. Through alternate (A) Run, (B) Tumble modes of movement, bacteria attains random walk when present in (C) uniform signaling environment. When present in (D) attract gradient, the run gets longer and frequency of tumbling is reduced which results in biased random walk.

E. coli senses chemoeffector gradients in a temporal fashion by comparing the current concentrations to those encountered over the past few seconds of travel (86, 87) . This ability implies that *E. coli* possess a 3–4 s memory that is used to determine whether chemoeffector levels have changed. Upon detecting an increase in attractant concentration, the cells will continue to swim smoothly in the direction of gradient due to suppression of tumbles (**Fig.2.2**).

The sensing of different chemoeffectors is carried out by transmembrane chemoreceptors. *E. coli* has five such chemoreceptors: Tsr (taxis to serine and away from some repellents), Tar (taxis to aspartate and maltose and away from some repellents), Trg (taxis to ribose and galactose/glucose), Tap (taxis to dipeptides and pyrimidines) and Aer (aerotaxis) (88). Of these, four (Tsr, Tar, Tap, and Trg) are methyl-accepting transmembrane receptors or methyl-accepting chemoreceptor protein (MCP) (88). These

16

receptors have a periplasmic domain with distinct ligand-binding sites and a conserved cytoplasmic signaling domain (**Fig.2.3**).

A fifth MCP-like protein, Aer, mediates aerotactic responses by monitoring redox changes in the electron transport chain (86). Aer undergoes sensory adaptation through a poorly understood, methylation-independent mechanism. The five MCP-family receptors in *E. coli* utilize a common set of cytoplasmic signaling proteins to control flagellar rotation and sensory adaptation (**Fig. 2.3)** (86). There are six cytoplasmic signaling proteins: CheA, CheB, CheR, CheW, CheY, and CheZ. When present in a chemoeffector gradient, membrane-bound receptors change their conformation upon binding a ligand. This conformational change results in autophosphorylation of the cytoplasmic histidine kinase CheA, which forms a stable complex with the receptor along with an adaptor protein CheW. CheA then donates its phosphoryl group to two competing response regulators, CheB and CheY. CheY-P binds to flagella motor and induces CW rotation. Binding of attractant to a chemoreceptor inhibits the CheA activity and leads to a lower CheY-P concentration, which promotes smooth swimming. The rapid dephosphorylation of CheY-P is ensured by the phosphatase CheZ. The MCPs record the most recently encountered ligand concentration by reversibly methylating four or five specific glutamic acid residues in the cytoplasmic signaling domain of each monomer of the chemoreceptors (86). The methyltransferase, CheR, and the methylesterase, CheB, mediate the methylation and demethylation of the receptors, respectively. Increased receptor modification increases the activity of the associated CheA, and, as a result, cells adapt to a homogeneous chemical environment (89).
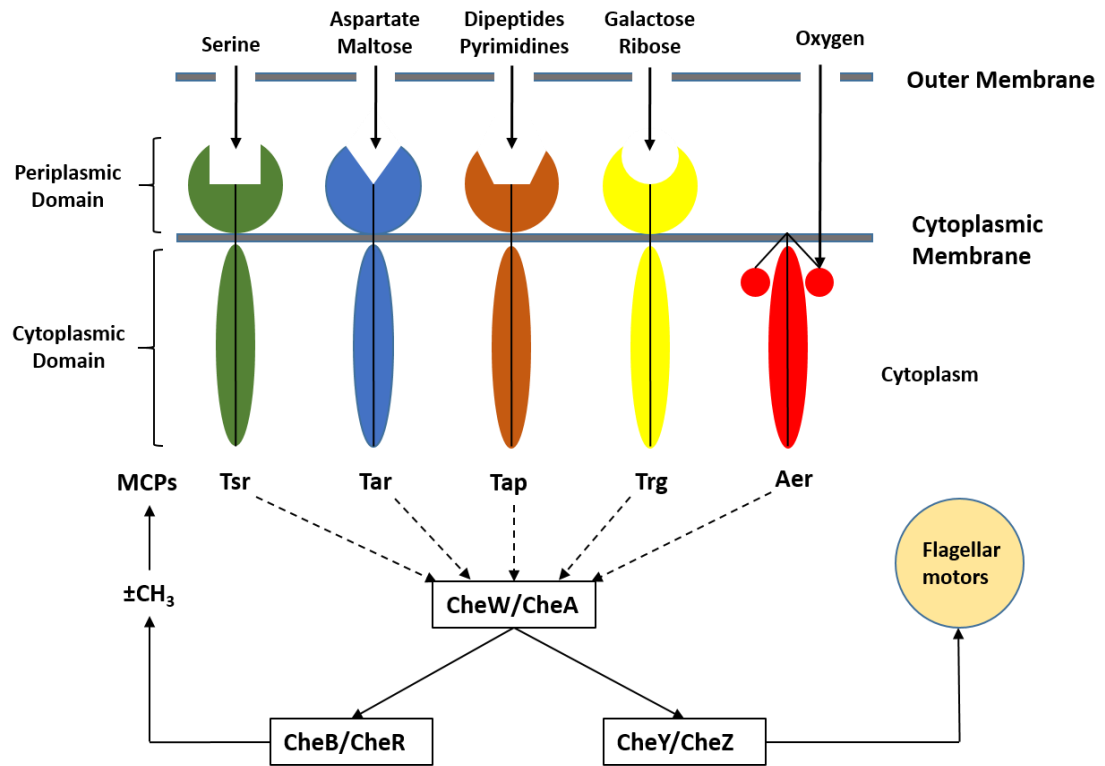
FIG. 2.3. *E. coli* chemotaxis signaling network components. Five *E. coli* chemoreceptors Tsr, Tar, Tap, Trg, and Aer are shown along with their chemoeffector ligands serine, maltose/ aspartate, dipeptides/pyrimidines, galactose/ribose, and oxygen respectively. All five receptors employ a common set of cytoplasmic signaling proteins, CheW and CheA, which interact with cytoplasmic domain of chemoreceptor to form stable ternary complexes that generate stimulus signals in the form of phosphoryl groups. CheY and phospho-CheY signal the CCW and CW flagellar rotation, CheZ controls the phosphorylation or dephosphorylation of cheY, CheR (methyltransferase) and CheB (methylesterase) regulate the MCP methylation state.

II.4 Methods for studying bacterial chemotaxis

II.4.1 Swim and swarm plate assays

Plate assays are generally used to study the chemotaxis behavior of bacteria toward a chemoeffector that can be metabolized (90). For swim plate assays, motility medium containing agar concentrations of 0.25 to 0.4% are used (90). At this low concentration of agar, the bacteria can move through the long aqueous channels formed inside the agar. As the colony grows, its metabolism depletes attractants to create a spatial concentration gradient in the agar. As a result, the cells migrate outward toward higher concentrations of the attractant compound (90). The strength of attraction can be assessed by measuring the rate of formation of the chemotactic ring that is formed by cells in the region of the steepest gradient (90). A variation of the swim plate assay is the swarm assay. In this assay, motility medium containing higher concentrations of agar (0.5% to 0.7%) are used, and the cells swim through the aqueous layer that forms on the agar surface (91). Swarming cells typically produce more, and longer, flagella (91). Neither swimming or swarming assays are useful for measuring repellent taxis or chemotaxis toward chemoeffectors that cannot be metabolized by the bacteria (90).

II.4.2 Capillary assay

The capillary assay is commonly used for investigating bacterial chemotaxis. Adler et al. (79) developed the assay and used it to demonstrate the chemotaxis response of *E. coli* towards a wide range of attractants and repellents. In this assay, chambers on the order of

1 cm^2 made from plastic O-rings with a 60° cut and 1 mm in height are loaded with a suspension of highly motile bacteria in chemotaxis buffer to create a pond under a coverslip (**Fig. 2.4**). A capillary (1 µL column) is sealed by flaming one end and placed with its open end into a solution of an attractant at the desired concentration, which is drawn up into the capillary as it cools. The filled capillary is inserted into the pond and incubated at the desired temperature for 30 to 45 minutes. The chemoeffector in the capillary will diffuse out into the pond to create a gradient that the can be sensed by the bacteria. The bacteria will then migrate into the capillary if the chemoeffector is an attractant and is not present at too high a concentration (above saturation of the receptor being tested). The capillary is then removed, the sealed end carefully broken off, and the contents delivered into dilution buffer. Dilutions are plated on nutrient agar, and colonies are counted the next day. The colony counts allow a calculation of the number of cells that entered the capillary and used to compare the strength and concentration dependence of the chemotaxis response to various compounds. The capillary assay can also be used for measuring repellent taxis, but the results are less sensitive as those for attractants. For example, Tso et al. (83) modified the capillary assay by placing the chemorepellent acetate in the pond of bacteria and filling the capillary with buffer. The number of bacteria that 'flee' into the capillary for 'refuge' is used to measure the repellent response. Not sruprisingly, the number of bacteria that accumulate in the capillary is not as high as for an attractant response, and the threshold concentration for detecting a repellent response is also higher (83).
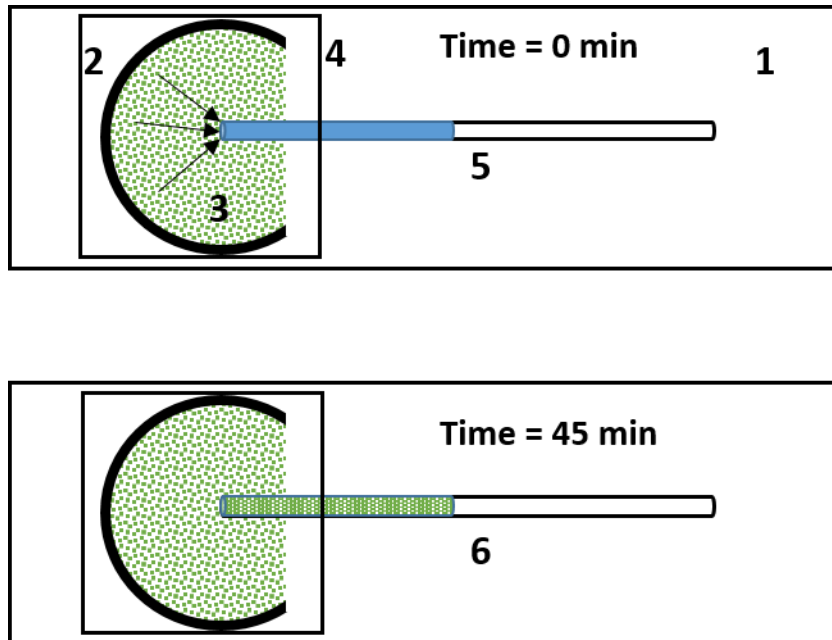
FIG. 2.4. Experimental setup for the capillary assay.
1. Glass slide
2. Plastic o-rings cut at one end
3. Ponds containing highly motile cells
4. Cover slip
5. Capillary tube containing chemoeffector
6. Capillary tube with cells along with the chemoeffector

II.4.3 Plug-in-pond assay

Tso et al. (83) developed the chemical-in-plug assay, a simple and quick way of measuring repellent or attractant chemotaxis. In this assay, a hard agarose plug (2%) containing chemoeffector is surrounded with a turbid suspension of bacteria in soft agar (0.3%). A zone of clearance quickly appears around the hard agar plug if the chemical within the plug is a repellent, and cells aggregate around the plug if it contains an attractant. The variation on chemical-in-plug assay is agarose-in-plug bridge method

developed by Yu et al. (92) later gained popularity as plug-in-pond assay in which molten agarose solution (2-4%) containing potential attractant or repellent is placed on a cover slide, and a coverslip is placed on top of the agarose to form the plug. The coverslip is kept in place using plastic stripes on either side of the plug. About 100 µl of the cell suspension is introduced between the microscope slide and the glass coverslip through capillary action, and the chemotaxis response in terms of distribution of cells around the agarose plug is observed using a microscope. Although this assay is widely used for rapid screening of attractants, it is prone to false positive response if appropriate controls are not used (93).

II.4.4 Micro-plug (µPlug) assay

The µPlug assay (90) is an improved version of the well-established plug-in-pond assay (91). It consists of a 15×15 mm square microfabricated chamber in poly-dimethylsiloxane (PDMS) with a height of ~75 μm. Low-melting agarose mixed with chemoeffector is introduced through a 1.5 mm diameter hole in the middle of the chamber to create plug. Two additional holes are punched with a blunt 19-gauge needle along the diagonal, one of which to introduce cells into the chamber, and the other to provide a vent as shown in **Fig. 2.5.** The chemoeffectors diffuses out of the plug and forms a radial concentration gradient around the plug. The bacteria sense the gradient, and if the molecule being tested is an attractant, they will move up the concentration gradient and
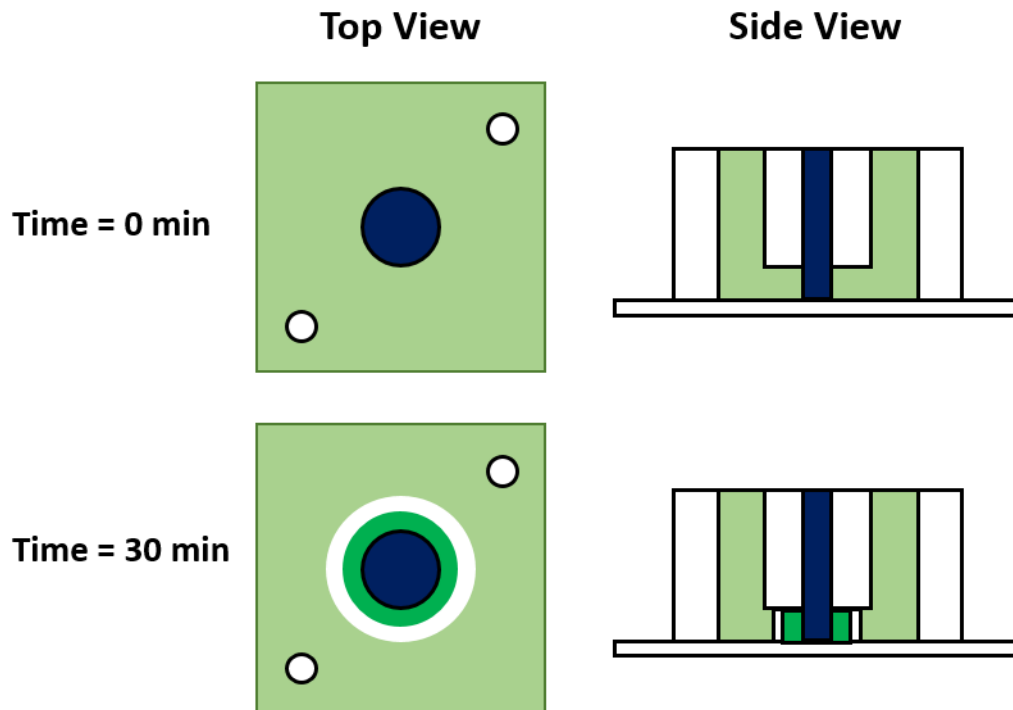
FIG. 2.5. Experimental setup for µPlug assay. GFP-labeled bacteria suspended in CB are introduced at the inlet, and the outlet allows escape of air. The agarose plug contains CB plus chemoeffector at the desired concentration. The plug is visualized by addition of 5% bromophenol blue to provide optical contrast. The cartoon shows the distribution of GFP-labeled cells when they are first introduced (t = 0 min) and at the end of the experiment (t = 30 min)**.**

accumulate at the boundary of the plug. If the molecule being tested is a chemorepellent, fewer cells accumulate at the plug boundary. With bacteria that express fluorescent proteins, the accumulation of cells at the interface can be imaged and the chemotactic response determined. Although the µPlug assay provides a simple and rapid method for determining the chemotaxis response of cells to a molecule, it does not facilitate

quantification of the response. Moreover, this method also suffers from the same drawbacks as the capillary assay in that it is not suited to studying repellent responses.

II.4.5 Micro-flow (µFlow) assay

The µFlow assay (94) was developed in order to address the above mentioned challenges and obtain quantitative information about the chemotactic response of bacteria toward chemoeffectors. The µFlow device builds on a simpler flow cell developed by Mao et al (95), in which bacteria are introduced between two parallel streams containing buffer and a chemoeffector. Bacteria sense the chemoeffector at the interface between the two streams and either swim toward the chemoeffector containing stream (for an attractant) or away from the interface of the two streams (for repellents).

The µFlow device (94) integrates a microfluidic concentration-generator (96) and a chemotaxis observation chamber for visualizing bacterial migration in response to the chemoeffector. The concentration-gradient generator consists of a pyramid-shaped branched network of microfluidic channels fabricated in PDMS. The network of microchannels enables splitting, combining, and mixing of fluid streams as they flow through the network. In a two-inlet µFlow device, the two fluid flow streams containing chemoeffector and buffer are brought together and mixed and then split into three streams. Since the flow is laminar, mixing between the two streams occurs mainly through the process of diffusion among the three fluid streams contain different proportions of chemoeffector. This process of mixing and splitting is repeated several times to generate a nearly linear concentration gradient across the width of the chemotaxis

24

chamber. Non-linear gradients can also be generated either by increasing the number of inlets or changing the flow characteristics. Hegde et al. (97) employed a µFlow device to generate an exponential gradient of 0 – 200 µM by using 5 inlets with different chemoeffector concentrations (0, 0.2, 2, 20, 200 µM).

The gradient generated by µFlow device is stable throughout the length of the observation chamber. Although bacteria entering the chemotaxis observation chamber in the device developed by Mao et al. (95) encounter a sharp interface between the cell buffer and the chemoeffector solutions, cells in the µFlow device encounter the midpoint of the generated concentration gradient. Depending on the flow rate used, bacteria are exposed to the gradient for different times, typically around 20 seconds to traverse the 2 cm length of the chamber. The extent of migration in the corss-gradeint direction is captured by acquiring 100 green and red fluorescence images for 20 min. The images are analyzed using in-house developed Matlab analysis codes to enumerate bacterial counts at different locations across the width of the chemotaxis chamber (98).

In µFlow device the chemotaxis response of bacteria towards the chemoeffector gradient is quantified in terms of chemotaxis migration coefficient (CMC), which weights the migration of cells by the distance they move from the center of the observation chamber (95). For example, a cell that moved to the farthest high-concentration position at the right was given a weighting factor of +1, and a cell that moved to the farthest low-concentration position at the left was given a weighting factor of -1. Therefore, a higher CMC value can be interpreted as a stronger chemotaxis response of the bacteria to the coeffector.

II.5 Mathematical modeling of bacterial chemotaxis

Mathematical modeling of bacterial migration is not only necessary to interpret the experimental data but also is used as an essential tool to predict the behavior of bacterial populations in response to different environmental conditions (99). Several mathematical models have been proposed to describe different aspects of chemotaxis behavior at the single-cell level (100-103) and at the population level (104-109). Most of the population based models are based on the Keller–Segel model of chemotaxis, which was developed to model the movement of slime molds. The generalized Keller–Segel model is of the following form:

$$\frac{\partial u}{\partial t} = \nabla.\mu(v)\nabla u - \nabla.\chi(s)u\nabla v + g(u,v) - h(u,v) \qquad (1.1)$$

$$\frac{\partial v}{\partial t} = D\nabla^2 v - f(u,v) \qquad (1.2)$$

Where $u = u(x,t)$ is the density of bacterial population, $v = v(x,t)$ is the concentration of attractant, $\mu(v)$ is the bacterial diffusion coefficient, $\chi(v)$ is the chemotactic sensitivity coefficient, $g(u,v)$ and $h(u,v)$ are the cell growth and death functions, respectively, $f(u,v)$ is the function describing the degradation of attractant, and D is the diffusion coefficient of attractant.

Although the partial differential equations (PDEs) (1.1) and (1.2) can be solved with appropriate boundary condition for given initial bacterial and attractant distribution it is always challenging to obtain numerical solutions without several assumptions. Also, this model doesn't account for the active motion of the bacteria and single cell dynamics (110).

CHAPTER III

CHEMOTAXIS OF *ESCHERICHIA COLI* TO NOREPINEPHRINE (NE) REQUIRES CONVERSION OF NE TO 3,4-DIHYDROXYMANDLEIC ACID (DHMA)*

III.1 Overview

Norepinephrine (NE), the primary neurotransmitter of the sympathetic nervous system, has been reported to be a chemoattractant for enterohemorhagic *E. coli* (EHEC). Here, we show that non-pathogenic *E. coli* K-12 grown in the presence of 2 μM NE also is attracted to NE. Growth with NE induces transcription of genes encoding the tyramine oxidase, TynA, and the aromatic aldehyde dehydrogenase, FeaB, whose respective activities can, in principle, convert NE to 3,4-dihydroxymandelic acid (DHMA). Our results indicate that the apparent attractant response to NE is in fact chemotaxis to DHMA. DHMA was found to be a strong attractant for *E. coli*. Only strains of *E. coli* K-12 that produce TynA and FeaB exhibited an attractant response to NE. We demonstrate that DHMA is sensed by the serine chemoreceptor Tsr and that the chemotaxis response requires an intact serine-binding site. The threshold concentration for detection is ≤ 5 nM DHMA, and the response is inhibited at DHMA concentrations above 50 μM.

Cells producing a heterodimeric Tsr receptor containing only one functional serine-binding site still respond like wild type to low concentrations of DHMA, but their response persists at higher concentrations. We propose that chemotaxis to DHMA generated from NE by bacteria that have already colonized the intestinal epithelium may recruit *E. coli* and other enteric bacteria that possess a Tsr-like receptor to preferred sites of infection.

III.2 Introduction

The human gastrointestinal (GI) tract harbors an assortment of bacteria, most of which are harmless or helpful commensals. However, infection of the GI tract by pathogenic bacteria can have devastating consequences. It has been suggested that norepinephrine (NE), the predominant neurotransmitter of the enteric sympathetic nervous system, promotes growth and virulence of enteric bacteria (111) through signaling via adrenergic receptors located either on intestinal epithelial cells (112) or in the bacteria themselves (113, 114). In particular, the bacterial quorum sensor kinase QseC has been implicated in the NE-induced expression of genes whose products are involved in adherence, motility, and pathogenesis (113, 115). However, the concentrations of NE required for effective induction of virulence genes, 50 μM in one recent study (71), are higher than those that are expected to occur in the intestinal lumen (69, 116). Thus, for NE to activate expression of virulence factors, bacteria would have to navigate to regions of the intestinal epithelium that have locally high concentrations of NE. An obvious candidate for directing such migration is chemotaxis.

Chemotaxis in *E. coli* is well understood at the molecular level. However, the compounds that have been reported as chemoattractants (31) are primarily nutrients: serine and related amino acids, sensed by the chemoreceptor Tsr; aspartate and maltose, sensed by Tar; ribose and galactose, sensed by Trg; and dipeptides and pyrimidines, sensed by Tap. The significance of chemotaxis to these compounds as virulence factors, except in the general sense of increasing nutrient acquisition to promote growth, is unclear. Another under-appreciated problem with prior studies of the role of chemotaxis in pathogenesis is that wild-type cells are compared with totally non-chemotactic, smooth-swimming mutants rather than with mutants having normal motility patterns but defects in chemotaxis to specific chemoeffectors. Thus, it remains unclear whether it is chemotaxis per se that is responsible for the observed effects or whether an altered pattern of run-tumble motility is responsible for the differences observed.

NE has been reported as an interdomain signaling molecule (27, 115, 117). NE serves as an inducer of virulence and motility genes in enterohemorhagic *E. coli* (EHEC) and in *S. enterica (27, 71).* The primary signaling pathway for induction of virulence appears to go through the membrane-bound quorum-sensing kinase QseC and its associated response regulator, QseB (118). The relationship between stress and microbial infection suggests that increased catecholamine concentrations in the intestine promote bacterial growth (68) and colonization (62). However, the effects of NE in enhancing virulence require higher concentrations than those that are predicted to exist in the gut, and in some cases appear to be independent of QseC and instead related to the ability of NE to serve as an iron chelator (119). However, both α and β-adrenergic receptor antagonists inhibit the

responses of enteric bacteria to catecholamines, and receptors other than QseC, including QseE, BasS, and CpxA, have been reported to contribute to the bacterial response to adrenergic signals (115). The current study was undertaken to determine the mechanisms underlying chemotaxis to NE in order to assess whether chemotaxis may contribute to the virulence of enteric bacteria.

III.3 Materials and methods

III.3.1 Bacterial strains and solutions

Strain CV1 is equivalent to strain RP437 (120) but was renamed to conform to the nomenclature of other strains used in this study. It was used as the wild-type *E. coli* strain for chemotaxis. All relevant strains and plasmids are listed in **Table 3.1**. Liquid cultures were grown in tryptone broth (TB; 10 g/L tryptone and 8 g/L NaCl). Selection for kanamycin resistance was on Luria-Bertani agar containing 1.2 % Difco Bactoagar and 50 µg/ml kanamycin. TB semi-solid agar contained 0.35 % Difco Bactoagar. H1 minimal-glycerol TLHMB$_1$ agar contained 1.2 % Difco Bactoagar and was supplemented with 0.5 % glycerol, 20 µg/mL threonine, leucine, histidine, and methionine, and 1 µg/mL thiamine. Chemotaxis buffer (CB) contains physiological buffered saline with 10 mM potassium phosphate, pH 7.0, containing 0.1 mM EDTA, 0.01 mM *L*-methionine, and 10 mM *DL*-lactate. Expression of Tsr from plasmids pCA24N-*tsr* and pRR53-*tsr*$_{R69E}$ was induced with 100 µM isopropylthiogalactoside (IPTG). This concentration of inducer gave

optimal serine chemotaxis in tryptone semi-solid agar when wild-type Tsr was expressed from pCA24N-*tsr* in Δ*tsr* strain CV5.

III.3.2 Reagents

Norepinephrine (NE) and 3,4-dihydroxymandelic acid (DHMA) of reagent grade and were obtained from Sigma-Aldrich.

III.3.3 Generation of mutants

The *tynA*, *feaB*, and *qseC kan*-insertion knockout mutations in strains SP101-103 were introduced into strain CV1 by phage P1$_{vir}$ transduction from the respective mutants in the Keio collection (121), with selection for resistance to 50 μg/mL kanamycin. The insertions were confirmed by Southern blotting. Chromosomal *tsr* point mutations were introduced into strain CV1 in two steps. First, a *serB-kan* insertion from strain UU2641 was introduced into strain CV1 by P1$_{vir}$ transduction with selection for resistance to 50 μg/mL kanamycin on Luria Broth (LB) agar to generate strain TAMU100. The *tsr* mutations were then introduced into strain TAMU100 by P1$_{vir}$ transduction with lysates prepared on strains UU2375 and UU2376, which contain chromosomal *tsr* alleles encoding Tsr-R69E and Tsr-T156K, respectively, to generate strains TAMU101-102. Selection for Ser$^+$ transductants was accomplished by plating on minimal-glycerol TLHMB$_1$ agar, and the presence of the *tsr* mutations was screened by testing transductants on TB semi-solid agar and picking isolates that did not form the outer (serine) chemotaxis rings. Glycerol was used as the carbon source in minimal medium because glucose adventitiously induces

31

transcription of the *ccdB* (control of cell death) gene from the *rhaB* promoter in the *kan*-insertion that allows counter-selection for loss of the insertion in the presence of rhamnose (122). CcdB is potent gyrase inhibitor (123) that is the toxin of an addiction system of the F plasmid of *E. coli* (124).

III.3.4 Fabrication of the microflow device

Microflow devices were fabricated as previously described (90). Briefly, device designs were drawn in AutoCAD and used to create a high-resolution (>3000 dpi) photolithography mask with a laser printer (Advanced Reproductions, North Andover, MA). Standard photolithography techniques using an SU-8 2050 photoresist (Microchem Corp, MA) generated imprints of the microflow devices on silicon wafers. The silicon-wafer templates were used as negative molds to generate the chemotaxis devices in poly(dimethyl)siloxane (PDMS), using standard soft-lithography protocols (90). Chamber dimensions were measured using a profilometer. Devices were fabricated by bonding the patterned PDMS slab to clean glass slides, using oxygen-plasma bonding in a plasma etcher (100 mTorr, 100 W, 40 sec) to create optically transparent devices. Access ports were punched into the PDMS using a blunt 19-gauge needle.

III.3.5 Microflow assay

The microflow assay for chemotaxis (90) measures the chemotactic response of bacteria, fluorescently labeled by GFP expression. When the cells enter the observation chamber they encounter a stable concentration gradient of chemoeffector established

across the width of the microfluidic chamber. The microflow chemotaxis device consists of two modules – a concentration-gradient generator and a chemotaxis-observation chamber. The gradient generator comprises a network of microfluidic channels that uses diffusive mixing from five inputs to generate non-linear, approximately exponential concentration gradients across the width of the observation chamber. The length of the network is 18.5 mm. The width of each inlet entering the observation chamber is 500 µm. The observation module is a chamber (20 µm x 1050 µm x 2 cm µm) connected to the gradient-generator module. A secondary inlet (50 µm) is used to introduce bacteria into the observation module at the mid-point of the concentration gradient. The bacteria and the concentration gradients are introduced into the device through silicon tubing. The device infused with dyes of different colors is shown in **Fig. 3.1**.

The assay was performed as described previously (90). A mixture of GFP-expressing, motile test cells and RFP-containing, dead TG1 cells was gently resuspended in CB containing the chemoeffector at the concentration expected at the mid-point of the observation chamber and incubated for 20 min. All steps were conducted at room temperature. The flow rate in the microfluidic device was controlled using a PicoPlus programmable pump (Harvard Apparatus, Holliston, MA). The assembled device was positioned on the stage of a Leica TCS SP5 resonant-scanner confocal microscope. Multiple 500 µL gas-tight glass syringes (Hamilton, Reno, NV), containing either CB or CB with chemoeffector, were carefully connected to the inlets of the gradient-generator module to avoid introducing air bubbles into the device. The bacterial mixture was introduced into the chemotaxis chamber through the bacterial inlet port, using a 50 µL
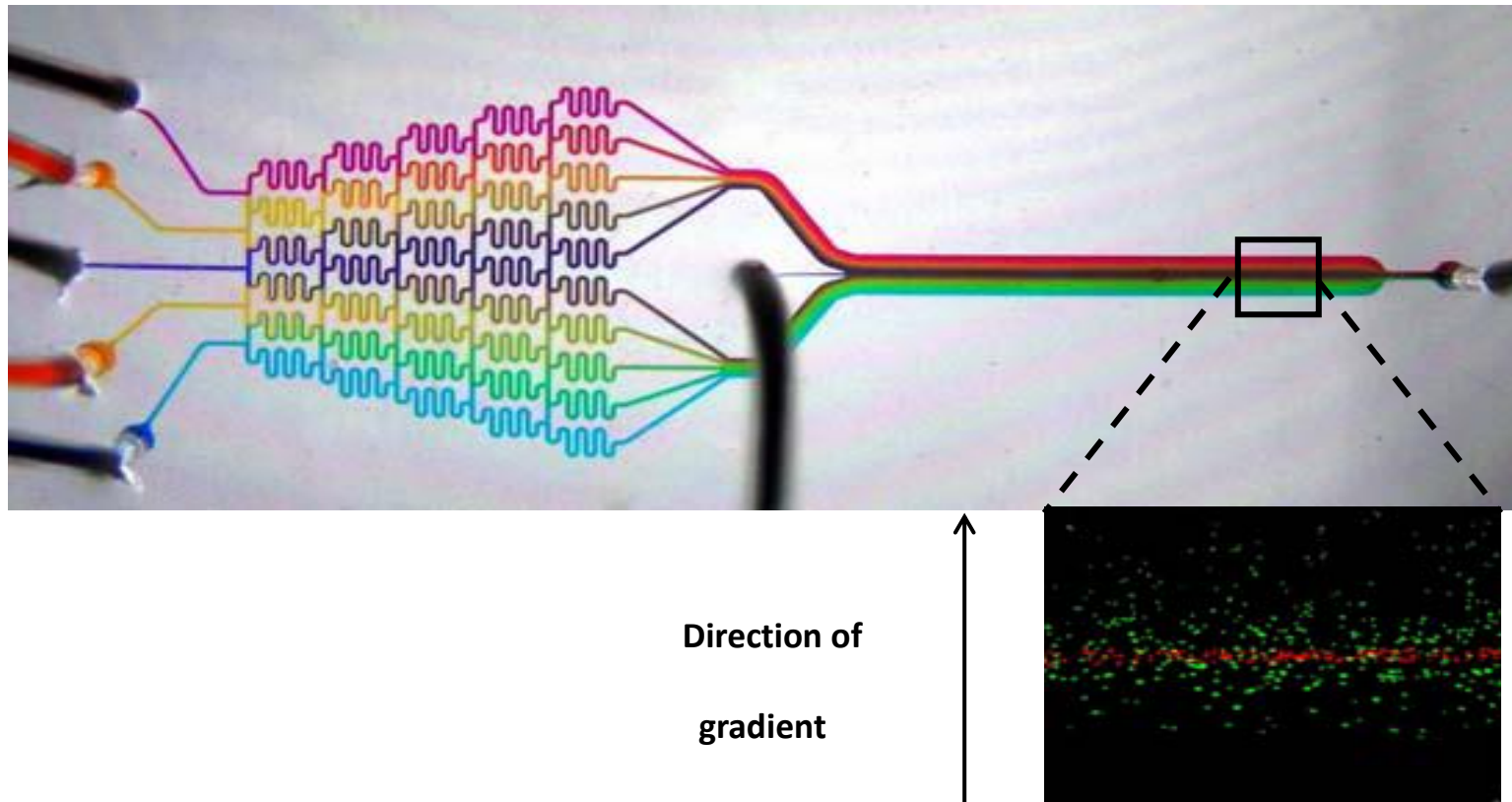
FIG. 3.1. The µFlow assay. In this photograph, a different colored dye is injected by each inlet to illustrate how gradients form and persist for the length of the 20 µm high chemotaxis chamber, whose geometry allows laminar flow. With this device we would typically inject ten-fold higher chemoeffector concentrations at each inlet from top to bottom, generating a steep, exponential gradient. Other inlet configurations allow linear or other shaped gradients to be made. The inset shows the distribution of wild-type *E. coli* cells in a 0 to 50 µM DHMA gradient (inputs of 0, 0.05, 0.5, 5, and 50 µM).

gas-tight glass syringe. The syringes connected to the gradient generator and the bacterial inlet were operated at the same flow rate, using different pumps. The total flow rate in the observation module (from the five gradient inlets and one bacterial inlet) was maintained at 2.1 μL/min. Green and red fluorescent images were acquired for 20 min. For each experiment, 100 images for each fluorophore were collected 7 mm from the inlet at 2.5 sec intervals. The 2.5 sec imaging interval was chosen based on our calculation that free-floating bacteria moving at a flow rate of 2.1 μL/min take an average of 2.5-3 sec to traverse 1000 μm, the imaging field-of-view (90). Therefore, bacteria in the middle of the flow were exposed to the gradient for an average of 18-21 sec prior to imaging. Cells spending more time in contact with the floor or ceiling of the chamber move more slowly (94).

III.3.6 Quantification of chemotaxis in the microflow assay with image analysis

The migration and distribution of bacteria in each image were quantified using a Matlab (Mathworks, Natick, MA) image-analysis subroutine developed in house, as described previously (90). Briefly, the analysis consisted of the following steps: (i) removal of background pixels in the image based on pixel size and intensities; (ii) determination of the center of the image (i.e., where bacteria enter the observation chamber), using the dead cells (red fluorescence) as a reference; (iii) location of green cells (i.e., live bacteria expressing GFP) in the images relative to the center, determined by calculating the centroid; and (iv) quantification of the number of live cells in 16 μm-

wide intervals. These steps were repeated for each image, and the total counts of cells in 100 images were summed for analysis.

The migration profile was used to calculate the chemotaxis migration coefficient (CMC), which weights the migration of cells by the distance they move from the center of the observation chamber, as previously described (95). For example, a cell that moves to the farthest high-concentration position at the right (interval 64) receives a weighting factor of +1, and a cell that moves to the farthest low-concentration position at the left (interval 1) is given a weighting factor of -1. Green cells in the middle of the chamber (intervals 31-34) were excluded from the analysis on the grounds that they could be non-motile or poorly motile cells. The motility migration coefficient (MMC) was determined in the same way as the CMC except that the weighting factor was positive in both directions. Examples of assays used to calculate CMC and MMC values are shown in **Fig. 3.2**.

The CMC value represents the magnitude of the chemotactic response to the steep exponential gradients that are generated with ten-fold increases in the attractant concentration in each of the five inlet ports, from left to right. The cells were pre-incubated for ten minutes with the same concentration of attractant present in the middle (third) inlet, which is the concentration they experience when entering the chamber. The MMC value represents the extent of the smooth-swimming response of cells in chemotaxis buffer (CB) that are introduced into a chamber with a uniform concentration of attractant. The cells do not adapt to the attractant until they spread across the chamber. If they adapt before reaching the point along the channel at which their distribution is imaged, their movement

36

will be random run-tumble behavior that will not significantly affect the final distribution across the chamber.

III.3.7 Preparation of motile bacteria for chemotaxis assays

Bacteria were prepared for chemotaxis assays as described by Mao *et al.* (95). Overnight cultures of GFP-expressing bacteria, grown overnight at 32°C in TB containing 150 µg/mL erythromycin, were inoculated into 25 mL of the same medium lacking erythromycin to a turbidity of ~0.05 at 600 nm. Cultures were grown with swirling in 125 ml Erlenmeyer flasks at 32°C to mid-exponential phase (turbidity of ~0.5 at 600 nm), with addition of 100 µM IPTG for induction of Tsr expression from the pRR53-*tsr* and pCA24N-*tsr* plasmids. A 3-mL aliquot of cells was centrifuged at 400 x *g* for 5 min at room temperature and gently resuspended in 2 mL of CB. TG1 cells expressing RFP were killed by exposure to 1 mM kanamycin for 1 h (complete killing was verified by lack of growth on LB agar plates) and mixed with GFP-expressing motile cells at approximately equal densities. The microflow chemotaxis assay was performed within 20 min after resuspension of the bacteria in CB, which contained attractants at the concentration expected at the midpoint of the observation chamber, *e.g.*, 500 nM in a 0-50 µM exponential gradient. In some experiments, bacteria were prepared as described above but primed by addition of 2 µM NE to the TB growth medium 1 hr before harvesting. Cells introduced into uniform concentrations of attractants were resuspended in non-supplemented CB, except as noted.

37
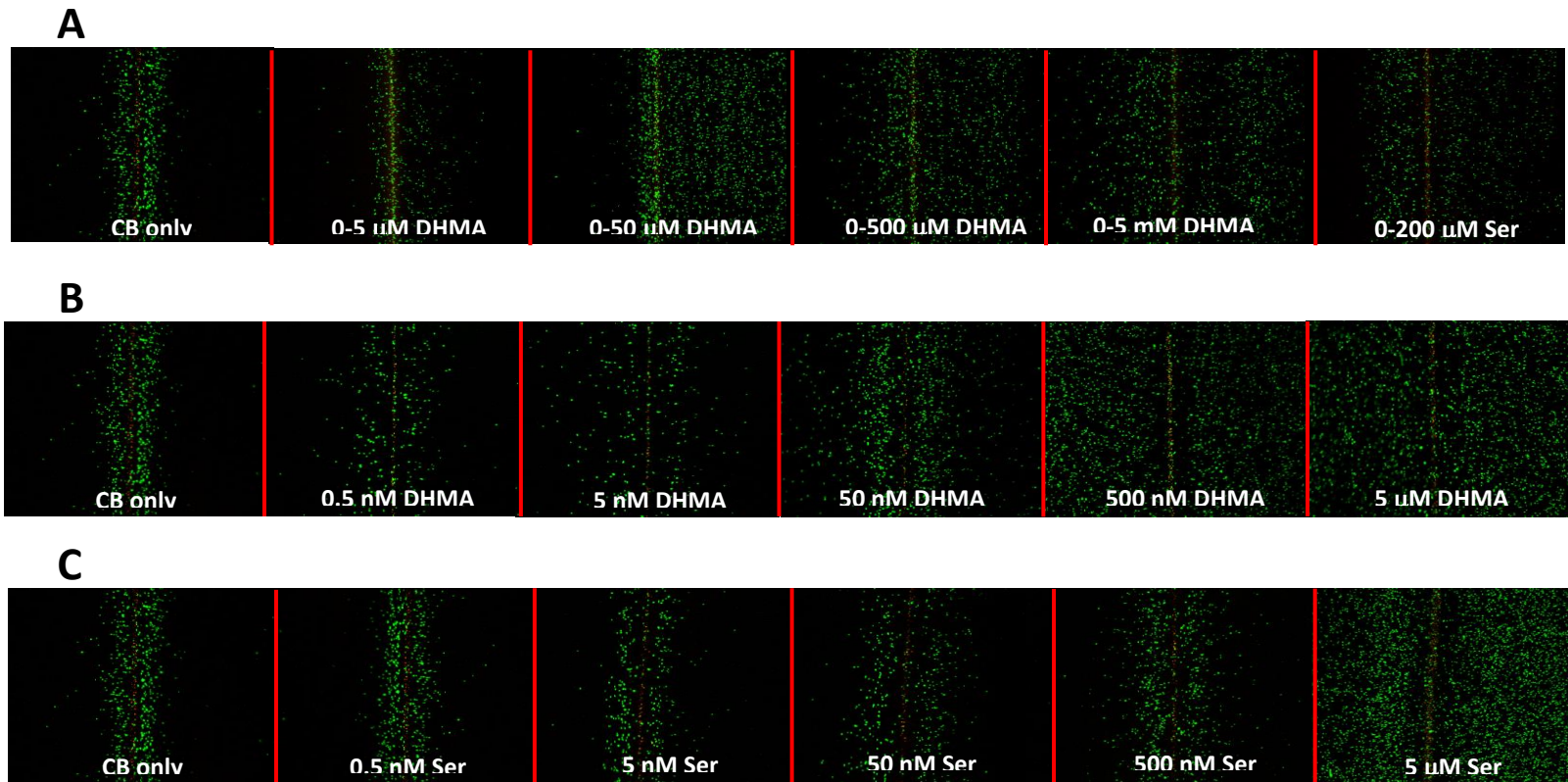
FIG. 3.2. Images of µFlow assays for non-linear gradients and uniform attractant concentrations. A) Non-linear (exponential) gradients over the indicated range of concentrations from left to right across the 1 mm-wide observation channel. Composite images were taken 14-15 mm along the 2 mm channel. Flow from bottom to top. Motile CV1 cells are labeled with GFP, and non-motile TG1 cells are labeled with RFP. Cells suspended in CB containing the midpoint concentration of attractant (e.g., 50 nM for the 0-5 µM gradient) were introduced in the middle of the channel. B) Cells suspended in CB were introduced into the middle of the channel containing the indicated uniform concentrations of DHMA. C) Cells suspended in CB were introduced into the middle of the channel containing the indicated uniform concentrations of serine.

III.3.8 RNA isolation and quantitative RT-PCR (q-RT-PCR)

Bacteria were grown using the protocol described above for the µFlow assay, with or without priming. After 60 min exposure to NE, cells were collected by centrifugation and stored at -80°C prior to RNA extraction. RNA was extracted using the Nucleospin RNA II kit (Clontech, CA) according to the protocol recommended by the manufacturer. Cells grown without NE were used as negative controls. Total RNA was isolated from the cell pellets, and RNA quality was spectrophotometrically assessed. qRT-PCR was performed using iScript one-step RT-PCR kit with SYBR green (Bio-Rad Laboratories, CA) on a MyiQ single-color real-time PCR detection system (Bio-Rad Laboratories). The threshold cycles, as calculated by the MyiQ optical system software (Bio-Rad Laboratories), were used to determine the relative changes between samples. The experiments were run in triplicate in 25 µl reactions, and 50 ng of total RNA was used for each reaction, with the final forward and reverse primer concentrations at 0.15 µM each. After amplification, template specificity was ensured through melting-curve analysis. The *rrsG* (ribosomal RNA G) transcript was used as the housekeeping RNA for normalizing the data.

III.3.9 Determination of the number of molecules of DHMA in the periplasm

The mean volume of an *E. coli* cell grown in a moderately rich medium like TB has been estimated at around 4 femtoliters (4×10^{-15} liter) (125), and the volume of the periplasm has been estimated to be 20-40% of the total cell volume (126). Thus, 1×10^{-15} liter is a reasonable estimate for the average periplasmic volume. At 5 nM (5×10^{-9} moles/liter), a concentration of DHMA that still generates an attractant response, there are

thus about 5 x 10^{-24} moles of DHMA in the periplasm, assuming equilibration with the external medium. Multiplying by Avogadro's number of 6 x 10^{23} molecules/mole, this yields about 3 molecules of DHMA in the periplasmic space of a single cell.

III.4 Results

III.4.1 An *E. coli* K-12 strain shows chemotaxis towards norepinephrine

To examine NE chemotaxis, we used the K-12 strain RP437 (120), a standard for studies of *E. coli* chemotaxis. Strain RP437 is henceforth called CV1 to conform to the nomenclature used for the chemoreceptor-mutant strains used in this study.

We employed a microflow device manufactured in house (90) to monitor chemotaxis to NE. This assay offers several advantages for studying the response to biological signals. First, the microliter volumes involved minimize the amount of a chemical that must be used per assay. Second, the migration of bacteria can be observed in stable gradients of almost any desired profile. These gradients are established in a mixing device and are oriented perpendicular to the direction of flow. Third, because the microflow chamber is only 1 mm wide, the gradients formed can be very steep. Finally, the time for the bulk flow to reach the site of imaging is ∼20 sec, so that the short-term responses of the cells can be recorded.

Cells harvested from TB did not respond to NE in the microflow assay, a result in contrast to the earlier reports with the microplug assay (27) . However, in the microplug assay, cells are exposed to NE for 30 min or longer. We therefore tested whether prior

exposure to NE primes the cells to respond. Cells grown in TB supplemented with 2 μM NE for 1 hr before harvesting showed a robust response to NE (**Fig. 3.3**) that was equivalent to the response observed with similar gradients of serine (**Fig. 3.3**; **Fig. 3.2**). The effects of pre-exposure to NE were eliminated when 12.5 μg/mL chloramphenicol was added at the same time as NE, suggesting that protein synthesis is required for the effect (**Fig. 3.3**). Chemotaxis to serine and aspartate, sensed as attractants by the Tsr and Tar chemoreceptors, respectively, was unaffected by chloramphenicol. These results suggest that preincubation with NE induces the synthesis of proteins that are required for NE to be sensed as an attractant.

III.4.2 Chemotaxis toward NE requires induction of bacterial enzymes

One pathway for NE metabolism in mammals involves deamination to form 3,4-dihydroxyphenyl-glycol-aldehyde (DOPEGAL) followed by oxidation to form 3,4-dihydroxymandelic acid (DHMA) (73). These steps in *E. coli* can potentially be carried out by two enzymes: a periplasmic tyramine oxidase TynA (127) and a cytoplasm aromatic aldehyde dehydrogenase FeaB (127). Quantitative reverse transcription polymerase chain reaction (qRT-PCR) analysis showed that *tynA* transcription increased 4.5-fold and *feaB* transcription increased 3.5-fold after 1 hr of incubation with 2 μM NE, (**Fig. 3.4B**). The SP101 and SP102 mutants, which lack TynA and FeaB, respectively, failed to respond to NE in the microflow assay (**Fig. 3.5**).

The quorum-sensing kinase QseC has been implicated in NE-induced expression of virulence and motility genes in pathogenic *E. coli* and *S. enterica* (71, 113). Induction of
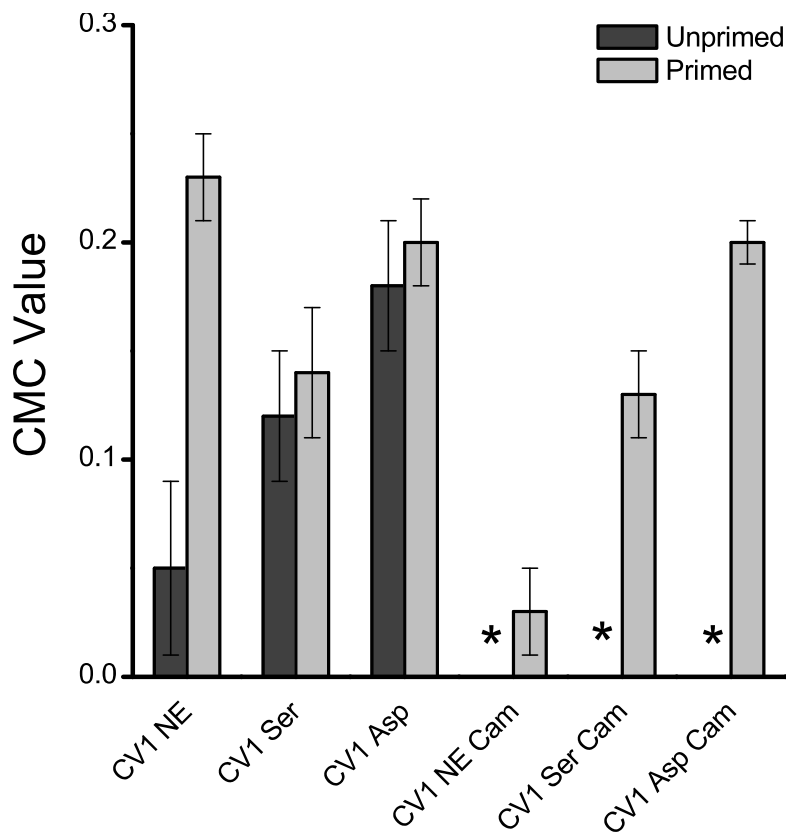
FIG. 3.3. Chemotaxis Migration Coefficient (CMC) values for cells in exponential 1-500 µM NE and 1-200 µM serine and aspartate gradients. Error bars represent the standard deviation of the mean for triplicate experiments. Primed indicates that cells were grown in the presence of 2 µM NE for 1 hr before harvesting. Abbreviations used: CB, chemotaxis buffer; NE, norepinephrine; Asp, aspartate; Ser, serine; Cam, chloramphenicol. *indicates not assayed.

tynA and *feaB* transcription by exposure to NE was abolished in a Δ*qseC* mutant SP103 (**Fig. 3.4B**), which also showed a large decrease in NE chemotaxis (**Fig. 3.5**). These results suggest that NE sensed by QseC induces *tynA* and *feaB* transcription, and hence production of DOPEGAL and DHMA.
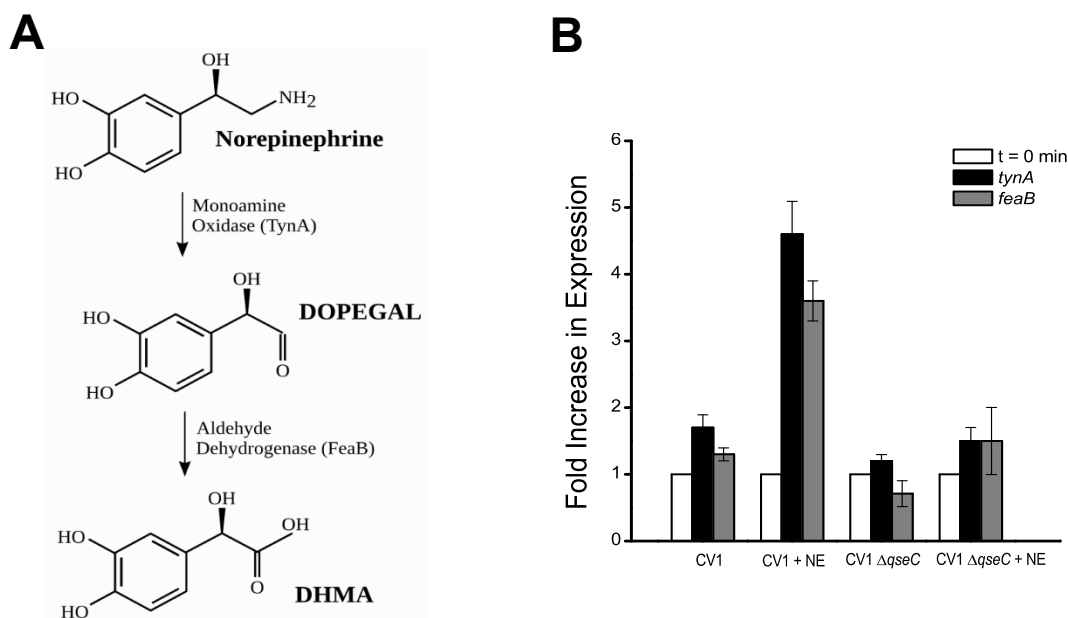
FIG. 3.4. Bacterial genes encode enzymes that can produce DHMA from NE. (A) The chemical pathway shown is present in the human GI tract, and *E. coli* potentially has a similar capability via TynA and FeaB, as indicated. (B) Induction of *tynA* and *feaB* transcription by preincubation with 2 µM NE in wild-type and Δ*qseC* cells. The levels of transcript were measured by q-RTPCR 60 min after addition of 2 µM NE to the culture. Controls were incubated 60 min in the absence of NE. The results are normalized to the level of the *rrsG* transcript. The error bars represent the standard deviation of the mean.

III.4.3 DHMA is a potent attractant for *E. coli*

DOPEGAL is not commercially available, but DHMA proved to be a very strong attractant for strain CV1 (**Fig. 3.6**). Representative images of the microflow assays with DHMA are shown in **Fig. 3.2**. The response to DHMA was strongest in an exponential gradient of 0-50 µM. The CMC value was 0.12 in a 0-5 µM gradient, 0.22 in a 0-50 µM gradient, 0.09 in a 0-500 µM gradient, and 0.06 in a 0-5000 µM gradient (**Fig. 3.6**). The

43

simplest explanation for the decreased response at higher concentrations of DHMA is that

the receptor became saturated. Strain CV12, which contains only Tsr and Aer, gave a
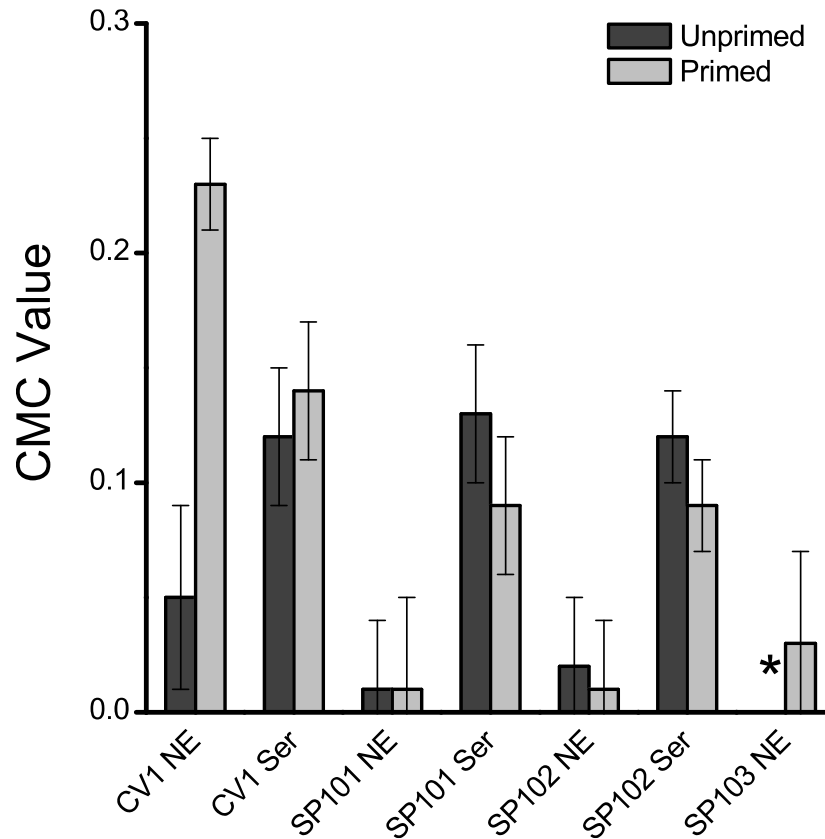
FIG. 3.5. NE chemotaxis in mutants defective in NE metabolism. CMC values in exponential gradients of 0-500 µM NE and 0-200 µM serine. Strains: CV1, wild type; SP101, Δ*tynA*; SP102, Δ*feaB*; SP103, Δ*qseC*. Error bars represent the standard deviation of the mean for triplicate experiments. Primed indicates that cells were grown in the presence of 2 µM NE for 1 hr before harvesting. *indicates not assayed.

much weaker response to DHMA. This difference may be due to altered ligand sensitivity

in strains that contain only one type of high-abundance chemoreceptor (128, 129).
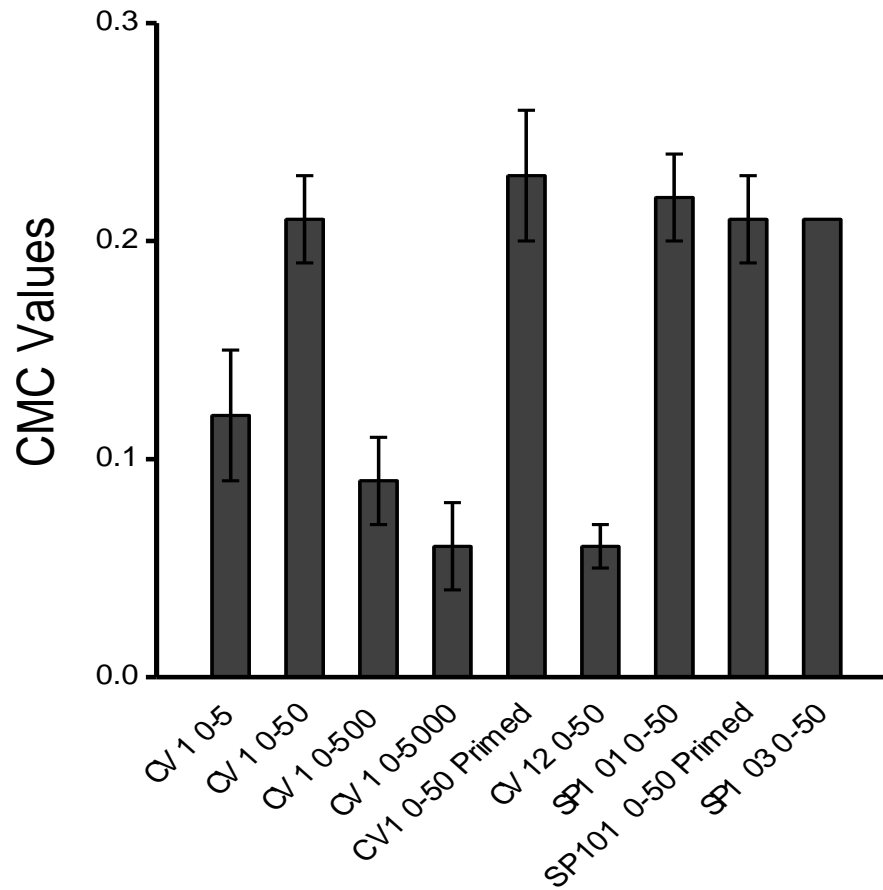
FIG. 3.6. CMC values for cells in exponential DHMA gradients. The gradients ranged from 0 to the indicated value in μM. Strains: CV1, wild type; CV12, Δ*tar-tap*, Δ*trg*; SP101, Δ*tynA*. Error bars represent the standard deviation of the mean for triplicate experiments. Primed indicates that cells were grown in the presence of 2 μM NE for 1 hr before harvesting.

III.4.4 Chemotaxis to DHMA requires the Tsr chemoreceptor and its intact serine-binding site

CV5 cells that lack Tsr did not respond to serine or DHMA, although their response to aspartate was the same as that of CV1 cells (**Fig. 3.7**). We then tested whether the serine-binding site of Tsr is required for sensing DHMA. The T156K and R69E amino acid replacements in Tsr disrupt the majority and minority halves, respectively, of the serine-binding site (130). Strains TAMU101 and TAMU102, which encode Tsr-R69E and Tsr-T156K, respectively, at the chromosomal *tsr* locus, also failed to respond to serine or DHMA in the microflow assay (**Fig. 3.7**). This analysis suggests that the DHMA and serine-binding sites in Tsr overlap.

III.4.5 Heterodimeric Tsr with one functional ligand-binding site mediates responses to DHMA

Tsr contains two rotationally symmetric serine-binding sites that exhibit strong negative cooperativity (131); **Fig. 3.8A**)**.** We therefore tested the possibility that binding of DHMA at the second site inhibits the attractant signal produced by binding at the first site. The Tsr-T156K and Tsr-R69E mutant subunits were produced at approximately equal levels in strain TAMU104 (see Materials and Methods). In this strain, the T156K protein is expressed from the chromosomal *tsr* locus, and the R69E protein is expressed from a plasmid-encoded *tsr* gene under control of an IPTG-inducible promoter. After induction with 100 μM IPTG, this strain produces approximately the same amount of Tsr as the chromosomal gene. Under these conditions, half of the Tsr molecules should be

46
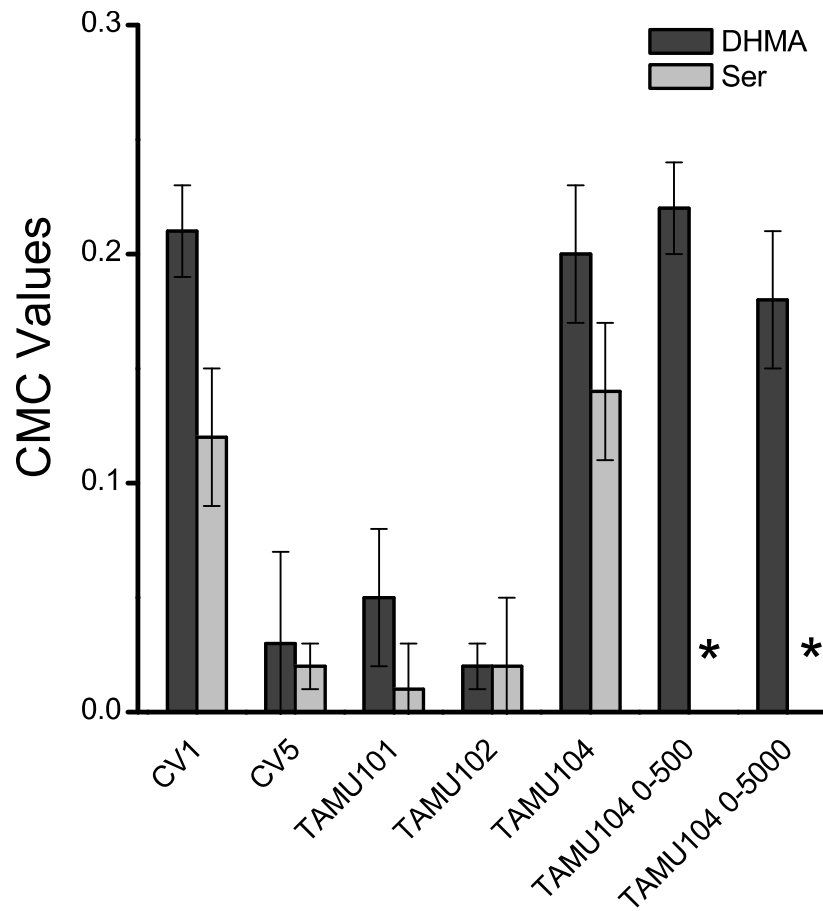
FIG. 3.7. DHMA chemotaxis in *tsr* mutant strains. CMC values in exponential gradients of 0-50 μM DHMA and 0-200 μM serine. Strains: CV1, wild type; CV5, Δ*tsr*; TAMU101, *tsr*-R69E; TAMU102, *tsr*-T156K; TAMU104, expresses a chromosomal *tsr*-T156K gene and a plasmid-borne *tsr*-R69E gene at approximately the same levels. CMC values are also given for TAMU104 in gradients of 0-50 μM and 0-5000 μM DHMA for comparison with the CMC values in those gradients for strain CV1 shown in **Fig. 3.6**. Error bars represent the standard deviation of the mean for triplicate experiments. Primed indicates that cells were grown in the presence of 2 μM NE for 1 hr before harvesting. *indicates not assayed.

heterodimers with one intact ligand-binding site and one doubly defective site (**Fig. 3.8B**). A similar approach has been used to show that Tar (132, 133) and Tsr (134, 135) heterodimers of this type still mediate attractant responses to their respective ligands. In contrast to CV1 cells, TAMU104 cells exposed to 100 μM IPTG responded robustly to DHMA in gradients of 0-50 μM up to 0-5000 μM (**Fig. 3.7**). Thus, when Tsr has only one functional ligand-binding site, it mediates good chemotaxis responses at higher concentrations of DHMA.
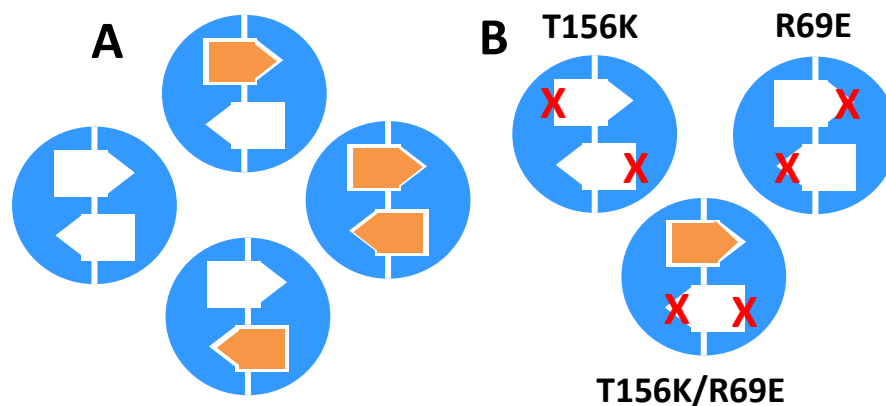
FIG. 3.8. Complementation of mutations that disrupt the majority and minority half-binding sites for serine. **A)** The periplasmic domain of the Tsr homodimer. Squares indicate the majority site, triangles the minority site. The ligand is shown in blue, with the square end representing the α-amino and α-carboxyl groups of and amino acid ligand and the pointed end the R group. Ligands can bind with equal affinity to either one of the rotationally symmetric binding sites. Both sites can be occupied, but binding to the second typically occurs with strong negative cooperativity. **B)** The residue substitutions introduced by mutations, indicated by the red Xs, are T156K for the majority site and R69E for the minority site. Neither mutant homodimer is capable of binding ligand. If the two mutant receptors are co-expressed at equal levels, half of the Tsr dimers will be heterodimers (T156K/R69E) that retain one intact ligand-binding site.

In a second assay, cells resuspended in chemotaxis buffer (CB) in the absence of DHMA were introduced into the microflow chamber containing various uniform concentrations of DHMA in CB. In this assay, a smooth-swimming response is indicated by enhanced spreading of cells in both directions from the midpoint at which they enter the channel. This spreading is quantified in a term we call the motility migration coefficient (the MMC value, as described in Materials and Methods). The difference in the responses used to determine the CMC and MMC values is illustrated in **Fig. 3.9A**, and the full spectrum of responses to uniform concentrations of DHMA and serine is presented in **Fig. 3.2**. A more complete discussion of the behaviors quantified in the CMC and MMC assays is given in Materials and Methods under the heading Quantification of chemotaxis in the µFlow assay with image analysis.

Wild-type CV1 cells had an MMC value of 0.16 in chemotaxis buffer (CB). In comparison, exclusively smooth-swimming CV16 cells, which lack all four canonical chemoreceptors, had an MMC value of 0.40 in CB. The increased spreading probably occurs with smooth-swimming cells because they rapidly reach the floor or ceiling of the 20 µm tall chamber and move laterally in the channel without being caught up in the bulk flow that would quickly wash them through the chamber. As shown in **Fig. 3.9B**, CV1 and TAMU104 cells already showed increased MMC values at 5 nM (0.0005 µM) DHMA, whereas TAMU101 (Tsr$_{R69E}$) and TAMU102 (Tsr$_{T156K}$) cells first showed increased MMC values at 500 nM (0.5 µM) and 5 µM DHMA, respectively. Thus, the two point mutations in *tsr* do not make the cells totally unresponsive to DHMA, but they decrease the response sufficiently to prevent detectably higher CMC values in exponential
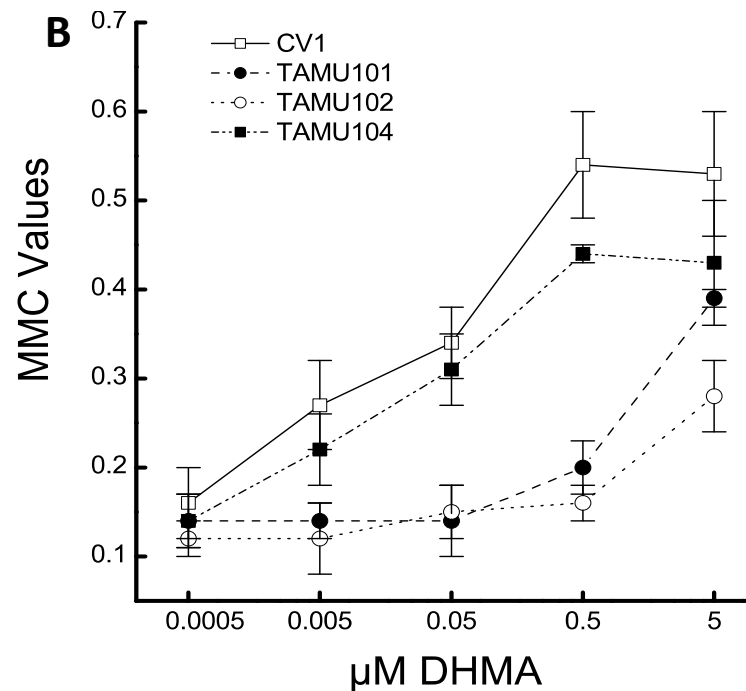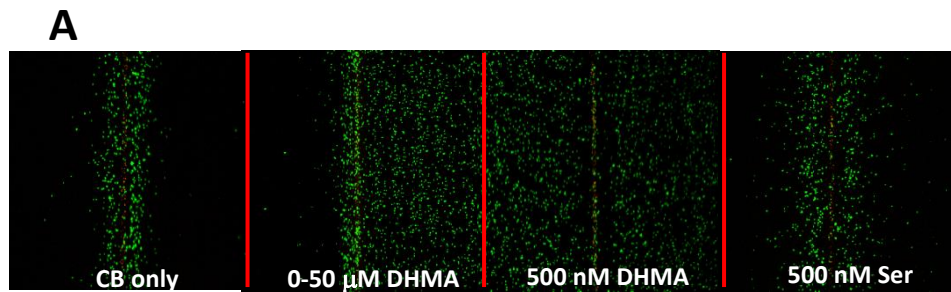
FIG. 3.9. A) Representative images of the microflow assay illustrating both CMC and MMC assays. 1 is chemotaxis buffer only; 2 is a 0-50 μM exponential gradient of DHMA; 3 is a uniform concentration of 500 nM DHMA; 4 is a uniform concentration of 500 nM serine. B) MMC values for different *tsr* mutants in exponential gradients of DHMA from 0 to the indicated concentration. Strains: CV1, wild type; CV5, Δ*tsr*; TAMU101, *tsr*-R69E; TAMU102, *tsr*-T156K; TAMU104, chromosomal *tsr*-T156K, plasmid-borne, salicylate-inducible *tsr*-R69E. Error bars represent the standard deviation of the mean for triplicate experiments.

DHMA gradients in our microflow assay. CV1 cells introduced into the chamber after being exposed to DHMA for 20 min at the same concentration they encounter in the chamber did not show MMC values above 0.16 at any DHMA concentration, so the cells did adapt to the presence of DHMA, as they do to serine. CV1 cells first showed an increase in MMC value at 500 nM serine, indicating that Tsr senses DHMA about 100 times more sensitively than it senses serine (**Fig. 3.10**). The MMC values for serine plateaued at 5 μM and remained between 0.40 and 0.45 up to 5 mM. The MMC values plateaued at 0.5 to 0.55 with 0.5 and 5 μM DHMA but then dropped significantly at 500 μM. The MMC values at 500 μM and 5 mM DHMA were the same as the buffer control. In contrast, TAMU104 cells expressing heterodimeric Tsr with only one ligand-binding site responded with increased MMC values at concentrations up to 5 mM, although they reached their plateau value of 0.40 to 0.5 at the same 0.5 μM concentration as CV1 cells. This result is consistent with the idea that DHMA interacts with the second Tsr ligand-binding site to cancel out the attractant signal evoked by binding at the first site. We saw no obvious increase in tumbling at high concentrations of DHMA, which should be reflected in lower MMC values. Therefore, binding to the second site does not generate an obvious repellent response. Binding at the second site must occur with lower affinity, as is expected because of the negative cooperativity that exists between the two sites (131, 136).
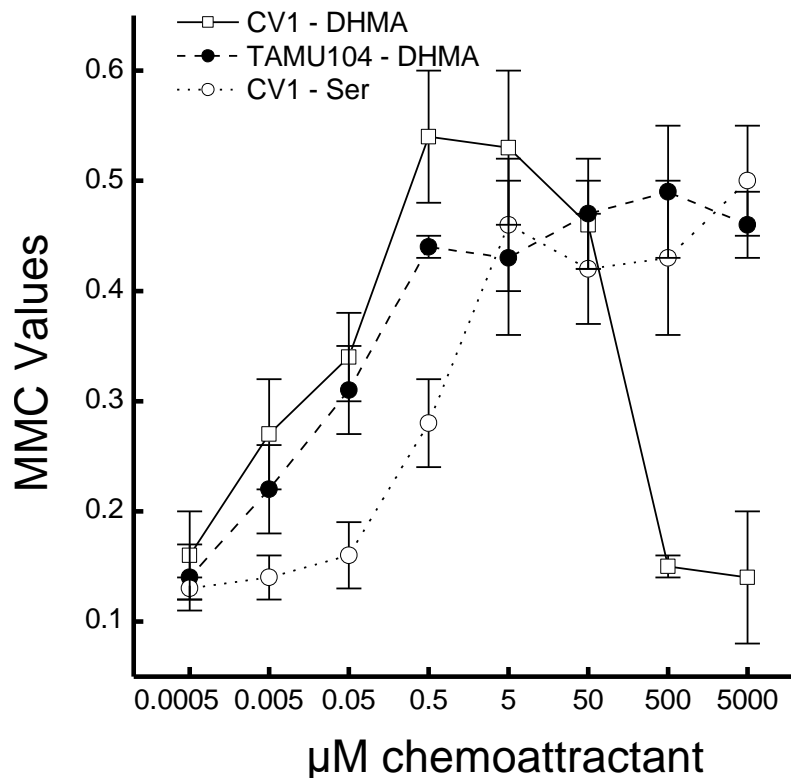
FIG 3.10. MMC values for different *tsr* mutants in exponential gradient from 0 to the indicated concentration of DHMA or serine. Strains: CV1, wild type; TAMU104, chromosomal *tsr*-T156K, plasmid-borne, salicylate-inducible *tsr*-R69E. The DHMA data for CV1 are an extension of those shown in **Fig. 3.9B**. Error bars represent the standard deviation of the mean for triplicate experiments.

III.5 Discussion

This study made the following discoveries. 1) The RP437 K-12 strain of *E. coli* exhibits chemotaxis to norepinephrine (NE). This highly motile, non-pathogenic strain possesses all of the chemoreceptors found in enterohemorhagic *E. coli* (EHEC) (137) and shares the high-abundance chemoreceptors Tar and Tsr with *S. enterica*. 2) Chemotaxis to NE requires induction of the periplasmic tyramine oxidase, TynA, and the aromatic

52

aldehyde dehydrogenase, FeaB, through a signaling pathway that requires the quorum-sensing histidine protein kinase QseC. Thus, the observed chemotactic response to NE is indirect. 3) 3,4-dihydroxymandelic acid (DHMA), a metabolite of NE that could be made by the combined activities of TynA and FeaB, is a potent chemoattractant for *E. coli* K-12 with effective concentrations ≤ 5 nM, suggesting that chemotaxis to NE is actually chemotaxis to DHMA. 4) DHMA is sensed by the serine chemoreceptor Tsr. 5) Mutant variants of Tsr defective in the majority (Tsr-T156K) or minority (Tsr-R69E) halves of the cross-dimer serine-binding site are defective in DHMA chemotaxis. 6) A heterodimeric receptor consisting of one subunit of Tsr-T156K and one subunit of Tsr-R69E, which has only one functional serine-binding site, mediates good chemotaxis to DHMA. 7) Cells expressing wild-type Tsr show a decreased response to DHMA at concentrations above 50 μM, whereas cells expressing the Tsr-156K/Tsr-R69E heterodimer do not show a decreased chemotaxis response at high concentrations of DHMA. Although these results make the basic mechanism of chemotaxis to NE and DHMA clear, they leave several questions unanswered.

III.5.1 How can cells respond to such low concentrations of DHMA?

Assuming equilibration between the concentration of unbound small molecules in the environment and the periplasm, at an external DHMA concentration of 5 nM there should be about 3 molecules of free periplasmic DHMA (see Material and Methods). Diffusion of small molecules trapped within the periplasmic space is very rapid, so that localization of the chemoreceptors at a sub-polar patches (138) should not be limiting for the kinetics

53

of detection of DHMA. If Tsr binds DHMA very tightly, the number of Tsr receptors occupied by DHMA at 5 nM DHMA may be considerably higher than 3. In any case, the response to DHMA is exquisitely sensitive.

The binding of one additional attractant molecule per second is adequate to cause a measurable increase in counterclockwise flagellar bias (139, 140). Rates of change in bound DHMA should certainly occur in cells moving laterally in the steep gradients present in the observation chamber of our microflow device. The sensitivity of the response is enhanced by the high amplification seen within the receptor patch (the activity of ~35 CheA kinases inhibited per molecule of attractant bound) (129) and by the high positive cooperativity (Hill coefficient of ~11) in adjusting the rotational bias of the flagellar motor to changes in intracellular CheY-phosphate (141).

III.5.2 The microflow assay is ideal for studying chemotaxis to biological signals

The observation chamber in the microflow assay is only 20 μm high. Thus, chemotaxis in the microflow assay is essentially a two-dimensional excursion. This geometry may provide a good simulation of the spatial context in which chemotaxis occurs in the intestine. The physiologically relevant response to NE or its metabolites in the intestine could be largely a surface phenomenon that occurs when the cells swim within or under the mucosal layer, which is only a few hundred μm thick and lies in close proximity to the intestinal epithelium. The gradients in the microflow assay can be made very steep, a condition that may also reflect the situation in vivo. With conventional assays for chemotaxis, it is unlikely that we could have observed a response that peaks at 5-50 μM

DHMA and then disappears at higher concentrations. We anticipate that the microflow assay will be suitable for screening bacterial chemotaxis to a wide range of biological signaling molecules in a spatial and temporal context similar to that in which chemotaxis probably occurs in the host intestine.

III.5.3 Why do cells respond only to low concentrations of DHMA?

Unlike the typical situation in which responses plateau at high concentrations of attractant, the smooth-swimming response to DHMA disappears at higher concentrations (**Fig. 3.10**). This effect is not seen if the second of the two ligand-binding sites of the Tsr homodimer is eliminated, as in the R69E/T156K heterodimer (**Fig. 3.8B**). One possible explanation is that DHMA binds to the second site with negative cooperativity (131, 136), and, by so doing, cancels out the attractant signal generated by binding to the first site. The mechanism for this phenomenon remains to be elucidated, but in vivo it would be expected to cause cells to congregate in regions with intermediate concentrations of DHMA.

III.5.4 Is NE/DHMA chemotaxis an important factor in gut/microbe interactions?

The DHMA that bacteria encounter in the GI tract could be generated by the host or by bacterial metabolism. The ability of NE to induce the synthesis of bacterial enzymes that convert NE to DHMA suggests that resident bacteria play an important role in generating localized DHMA gradients. Because FeaB and the other aldehyde dehydrogenases are presumably confined to the cytoplasm, to respond to NE the

DOPEGAL generated by periplasmic TynA would have to be taken up by the cells and converted to DHMA, which would then be released back into the periplasm. A similar mechanism is observed for *E. coli* chemotaxis to lactose (142). Lactose must be taken up into the cell by lactose permease (143) and split into glucose and galactose by β-galactosidase (144). One or both of these monosaccharides must then reenter the periplasm and bind to the MglB binding protein (145), which then has to interact with the Trg chemoreceptor (146). However, in the intestine, motile cells probably respond to DHMA gradients generated by bacteria that have already colonized the intestinal epithelium. Thus, sensitivity to low concentrations of DHMA is consistent with the idea that chemotaxis to DHMA has biological significance.

Endogenous DHMA production is normally low in sympathetic neuronal tissues (73), but it may be produced from NE by bacteria that have already colonized NE-rich areas on the intestinal epithelium. Among such sites would be the Peyer's patches near the junction of the jejunum and ileum, which are favored locations for colonization and invasion by enteric bacteria (147). By navigating to loci of NE leakage, cells could encounter the higher concentrations of NE that are required for induction of virulence genes (71). Furthermore, stress increases release of NE by the sympathetic innervation of the gut and heightens the severity of bacterial infection in the GI tract (116), and high levels of NE enhance growth of *E. coli* in serum-based media in vitro (68). This effect is also seen as a temporary and reversible increase in fecal coliforms in the mouse intestine in the presence of pharmacologically induced high levels of NE in the mouse (62). The combination of induction of virulence genes by NE and chemotaxis to its metabolite DHMA may work

together to heighten the pathogenicity of enteric bacteria that possess a Tsr-like chemoreceptor.

It is intriguing that the serine receptor Tsr, typically reported to be the most abundant of the *E. coli* chemoreceptors (148), also senses two biological signaling molecules, the intradomain quorum-sensing compound AI-2 (97) and the interdomain signaling molecule DHMA. It is exciting to contemplate that microfluidic assays may uncover other secrets about old friends in the chemotaxis signaling pathways of bacteria.

Table 3.1. List of strains and plasmids

Strain or plasmid	Relevant genotype or other characteristics	Antibiotic resistance[a]	Source
E. coli strains			
CV1	Wild type for chemotaxis; equivalent to RP437 _thr(_Am_)-1 leuB6 his-4 metF(_Am_)159 rpsL136 [thi-1 ara-14 lacY1 mtl-1 xyl-5 eda tonA31 tsx-78]_	Str	(120)
CV5	CV1 Δ_tsr thr_+	Str	(97)
CV12	CV1 (_tar-tap_)Δ_5201 trg_::Tn_10 eda_+	Str;Tet	(97)
CV16	CV1 Δ_tsr thr_+ (_tar-tap_)Δ_5201 trg_::Tn_10 eda_+	Str;Tet	(97)
BW25113 Δ_tynA_	BW25113 _tynA_ΩKan	Kan	(121)
BW25113 Δ_feaB_	BW25113 _feaB_ΩKan	Kan	(121)
BW25113 Δ_qseC_	BW25113 _qseC_ΩKan	Kan	(121)
SP101	CV1 Δ_tynA_	Str; Kan	This study

Table 3.1. Continued

Strain or plasmid	Relevant genotype or other characteristics	Antibiotic resistance	Source
SP102	CV1 Δ*feaB*	Str; Kan	This study
SP103	CV1 Δ*qseC*	Str; Kan	This study
UU2641	RP437 *serB*::*kan-ccdB*	Str; Kan	Parkinson (personal communication)
UU2375	RP437 *tsr-R69E (tar-tap)Δ5201 (aer)Δ1 ygjG*::Gm *(trg)Δ4543*	Str	Parkinson (personal communication)
UU2376	RP437 *tsr-R69E (tar-tap)Δ5201 (aer)Δ1 ygjG*::Gm *(trg)Δ4543*	Str	Parkinson (personal communication)
TAMU100	CV1 *serB*::*kan-ccdB*		This study
TAMU101	CV1 tsr-r69E		This study
TAMU102	CV1 tsr-T156K		This study
TAMU104	TAMU101/pRR53-*tsr*R69E		This study
TG1	*supE thi-1 Δ(lac-proAB) Δ(mcrB-hsdSM)5, (*r$_K^-$m$_K^-$*)*; F' [*traD36 proAB$^+$ lacI^q lacZΔM15*]		Stratagene

Table 3.1. Continued

Strain or plasmid	Relevant genotype or other characteristics	Antibiotic resistance	Source
Plasmids			
pCM18	GFP expression vector	Erm	(149)
pDS-Red Express	RFP expression vector	Amp	Clontech
pRR53-*tsr*$_{R69E}$	Expresses Tsr-R69E under control of IPTG	Amp	(135)

[a] Abbreviations for antibiotics: Str, streptomycin; Tet, tetracycline; Kan, kanomycin; Erm, erythromycin; Cm, chloramphenicol; Amp, ampicillin

CHAPTER IV

CONVERSION OF NOREPINEPHRINE TO 3,4-DIHDROXYMANDELIC ACID IN *ESCHERICHIA COLI* REQUIRES THE QSEBC QUORUM-SENSING SYSTEM AND THE FEAR TRANSCRIPTION FACTOR*

IV.1 Overview

The detection of norepinephrine (NE) as a chemoattractant by *E. coli* K-12 requires the combined action of the TynA monoamine oxidase and the FeaB aromatic aldehyde dehydrogenase. These role is to convert NE into 3,4-dihydroxymandelic acid (DHMA), which is a potent chemoattractant sensed by the Tsr chemoreceptor. These two enzymes must be induced by prior exposure to NE, and cells that exposed to NE for the first time initially show minimal chemotaxis toward it. The induction of TynA and FeaB requires the QseC quorum-sensing histidine kinase, and the signaling cascade requires new protein synthesis. Here, we demonstrate that the cognate response regulator for QseC, the transcription factor QseB, is also required for induction. The related quorum-sensing kinase QseE appears not to be part of the signaling pathway, but its cognate response regulator, QseF, which is also a substrate for phosphotransfer from QseC, plays a non-essential role.

––––––––

The promoter of the *feaR* gene, which encodes a transcription factor that has been shown to be essential for the expression of *tynA* and *feaB*, has two predicted QseB-binding sites. One of these sites appears to be in an appropriate position to stimulate transcription from the P_1 promoter of the *feaR* gene. This study unites two well-known pathways: one for expression of genes regulated by catecholamines (QseBC) and one for expression of genes required for metabolism of aromatic amines (FeaR, TynA and FeaB). This cross talk allows *E. coli* to convert the host-derived and chemotactically inert NE into the potent bacterial chemoattractant DHMA.

IV.2 Introduction

Catecholamine hormones and neurotransmitters, an overlapping set of host-derived molecules, profoundly affect the resident microbiota of the mammalian gut (66, 69, 116). It is apparent that these molecules are also important in regulating the virulence of invading pathogens (16, 27, 150, 151). In particular, the QseBC and QseEF two-component systems of enteric bacteria have been shown to mediate these responses to catecholamines (71, 113, 152-156).

We recently demonstrated (157) that some of the effects reported for norepinephrine (NE) and other catecholamines in enterohemorrhagic *E. coli* (EHEC) (158) can also be evoked by a non-amine metabolite of NE, 3,4-dihydroxymandelic acid (DHMA). In addition to inducing virulence gene expression in EHEC, DHMA is a chemoattractant for both EHEC (157) and a non-pathogenic K-12 strain of *E. coli*, RP437 (159). The chemotaxis response to DHMA is mediated by the Tsr chemoreceptor, which is present in

both EHEC and non-pathogenic K-12 strains of *E. coli*. Tsr homologs are present in a number of other enteric bacteria, as well, including *Salmonella enterica* (160, 161), *Enterobacter aerogenes* (162) , and *Pseudomonas aeruginosa* (163).

DHMA is made in two enzymatic steps from NE. The first step is carried out by a primary amine oxidase, TynA, which produces the intermediate 3,4-dihydroxyphenyl-glycol-aldehyde (DOPEGAL), and the second step is catalyzed by an aromatic aldehyde dehydrogenase, FeaB (127). TynA and FeaB are also produced by other enteric bacteria, where their characterized function is the utilization of aromatic amines as nitrogen sources and, in at least one case, as a carbon source (164). The expression of TynA and FeaB in *E. coli* RP437 requires prior exposure to NE and subsequent protein synthesis, and the induction of *tynA* and *feaB* transcription depends upon the presence of the histidine protein kinase QseC (159).

FeaR is a transcriptional regulator of the AraC family (164) and has been characterized as an essential transcription factor for the expression of *tynA* and *feaB* in response to exposure to aromatic amines. The *feaR*, *feaB* and *tynA* genes are adjacent but are divergently transcribed (164). The *feaB* and *tynA* genes have separate promoters and are somewhat differently regulated, although both promoters have two well-defined, tandem FeaR-binding sites upstream of the -35 region of their respective promoters (164).

In this study, we investigated the QseC-dependent signaling pathway by which NE is converted to DHMA. We found that the QseC signaling pathway requires its cognate response regulator QseB and, to a lesser extent, the related response regulator QseF. One output of this pathway is the expression of FeaR. We conclude that cross talk between the

63

regulatory systems for virulence and metabolism of aromatic amines may depend upon the ability of QseBC and, to a lesser extent, QseF to regulate *feaR* as well as genes directly involved in virulence.

IV.3 Materials and methods

IV.3.1 Bacterial strains, growth conditions and materials.

E. coli RP437 ((120); noted here as CV1) was used as the wild-type *E. coli* strain. GFP-expressing CV1 cells were obtained by transforming with plasmid pCM18 (149) and used to visualize migration to NE in the microfluidic chemotaxis assay. The pCM18 plasmid was maintained in cultures using 100 μg/mL erythromycin. CV1 *qseB*, *qseE*, *qseF*, or *feaR kan*-insertion mutations were generated as described previously (159). Briefly, mutations were introduced into strain CV1 by phage P1$_{vir}$ transduction using lysates generated from the respective mutants in the Keio collection (121). Mutants were selected for kanamycin resistance on lysogeny broth containing 1.2% Difco Bacto agar and 50 μg/mL kanamycin. All gene disruptions were confirmed by PCR.

Liquid cultures were grown in tryptone broth (TB; 10 g/L tryptone and 8 g/L NaCl) containing the appropriate antibiotics. Norepinephrine (>99% purity) was obtained from Spectrum Chemicals (Gardena, CA).

IV.3.2 Microfluidic chemotaxis assay

Motile bacteria were prepared for chemotaxis assays as described by Mao et al (95). Cultures of GFP-expressing bacteria were grown in TB containing 100 µg/ml erythromycin. Overnight cultures were inoculated into the same medium to a turbidity at 600 nm of ~0.05. The cultures were grown with swirling in Erlenmeyer flasks at 30°C. At a turbidity of ~0.35, 8 µM NE or solvent blank was added to the cultures and further incubated to mid-exponential phase (turbidity at 600 nm of ~0.5) before harvesting for experiments. Mid-exponential phase cells were centrifuged at 400g for 10 min at room temperature and gently resuspended in chemotaxis buffer (CB; physiological buffered saline with 10 mM potassium phosphate, pH 7.0, containing 0.1 mM EDTA, 0.01 mM L-methionine, and 10 mM DL-lactate).

All microflow chemotaxis experiments were performed within 20 min after resuspension of the bacteria in CB. The assay was performed as described previously (159). A mixture of GFP-expressing, motile test cells and red fluorescent protein (RFP)-containing, dead TG1 cells was gently resuspended in CB. 500 µl gas-tight glass syringes (Hamilton, Reno, NV), containing either CB or CB with chemoeffector, were carefully connected to the inlets of the gradient generator module to avoid introducing air bubbles into the device. The bacterial suspension was introduced into the chemotaxis chamber, using a 50 µl gas-tight glass syringe. The flow rate in the microfluidic device was maintained at 2.1 µl/min, using a Fusion 400 programmable pump (Chemyx Inc., Stafford, TX). The assembled device was positioned on the stage of a TCS SP5 confocal resonant-scanner microscope (Leica Microsystems Inc., Buffalo Grove, IL). For each assay, 100

images for each fluorophore were collected 7 mm from the inlet at 2.5 sec intervals. The 2.5-sec imaging interval was chosen based on our calculation that free-floating bacteria moving at a flow rate of 2.1 μl/min take an average of 2.5 s to traverse 1,000 μm, the imaging field of view (94). The bacteria in the middle of the flow were exposed to the gradient for an average of 18 to 21 s prior to imaging. Cells spending more time in contact with the floor or ceiling of the chamber move more slowly (94).

IV.3.3 Quantification of chemotaxis in the microflow assay with image analysis

The migration and distribution of bacteria in each image were quantified using an in-house developed program. Briefly, the analysis consisted of the following steps: (i) removal of background pixels in the image, based on pixel size and intensities; (ii) determination of the center of the flow chamber (i.e., where bacteria enter the observation chamber), using dead cells (red fluorescence) as a reference; (iii) location of green cells (i.e., live bacteria expressing GFP) in the images relative to the center, by determining the centroid; and (iv) calculation of the motility migration coefficient (MMC) based on the location of the migrated motile cells. These steps were repeated for each image, and the total counts of cells in 100 images were summed for analysis to generate migration profiles. The MMC is calculated by weighting the migration of cells by the distance they move in either direction from the center of the observation chamber, as previously described (159). The MMC value represents the extent of the smooth-swimming response of cells in CB that are introduced into a chamber with a uniform concentration of attractant. The cells do not adapt to the attractant until they spread across the chamber. If

66

they adapt before reaching the point along the channel at which their distribution is imaged, their movement will be random run-and-tumble behavior that will not significantly affect the final distribution across the chamber.

IV.3.4 RNA isolation and qRT-PCR

Bacteria were grown in TB as described above, and the mutant strains were grown in the presence of 50 µg/ml kanamycin. At mid-exponential phase (after 60 min of exposure to NE), cell pellets were collected by centrifugation and stored in RNAprotect® (Qiagen, CA) at -80°C prior to RNA extraction. Total RNA was isolated from the cell pellet using RNeasy Mini kit (Qiagen, CA) with the protocol provided by the manufacturer. RNA purity was assessed using the ratio of absorbance at 260 and 280 nm. All samples had A_{260}/A_{280} ratio of > 2.0. qRT-PCR was performed on a LightCycler® 96 (Roche, IN) using iScript™ One-Step RT-PCR kit with SYBR green (Bio-Rad Laboratories, CA) and gene-specific primers, using the protocol recommended by the manufacturer The reaction volume was 25 µL, with 50 ng of RNA per reaction and 0.15 µM of each primer. The threshold cycle numbers (C_t), were obtained using the Light Cycler system software (Roche, CA). Fold-changes in expression with NE exposure relative to untreated cells were calculated using the $\Delta\Delta C_t$ method (165), and the *rrsG* (rRNA G) transcript was used as the housekeeping gene for data normalization. All qRT-PCR experiments were repeated with three different cultures and two technical replicates per culture.

IV.4 Results and discussion

IV.4.1 The QseC signaling pathway induces TynA and FeaB expression

To study the signaling pathway that induces the enzymes that convert norepinephrine (NE) into the chemoattractant DHMA, we first studied the chemotaxis responses of mutant strains of *E. coli* lacking the relevant sensor kinases (*qseC* or *qseE*) and the corresponding response regulators (*qseB* or *qseF*), using the quantitative Motility Migration Coefficient (MMC) assay (159). All strains responded normally to the control attractant, 10 μM *L*-serine (**Fig. 4.1**). The wild-type strain, CV1, and the CV1Δ*qseE* mutant responded strongly, and essentially identically, to NE in the MMC assay, suggesting that *qseE* is not involved in the conversion of NE to DHMA (Fig. 1). On the other hand, the Δ*qseC* mutant did not respond to NE as an attractant in the MMC assay (Fig. 1), which confirms that QseC plays an essential role. The CV1Δ*qseB* mutant also did not respond to NE, whereas the CV1Δ*qseF* mutant gave a somewhat attenuated chemotaxis response. These results demonstrate that the QseBC histidine kinase/response regulator system is required for induction of TynA and FeaB.

Although the histidine kinase QseE does not seem to play an important role, QseF, the cognate response regulator activated by QseE, does seem to be involved. This observation is consistent with that of Moreira and Sperandio (153), who showed that QseF can also be a substrate for phosphorylation by QseC in *Salmonella*. The MMC values for the CV1, CV1Δ*qseE* and CV1Δ*qseF* strains were all highest when the NE concentration was 50 μM and were lower at both 5 and 500 μM.

FIG. 4.1. Chemotaxis of *E. coli* RP437 and mutants to NE. Cells were exposed to 0, 5, 50, or 500 µM NE in the microfluidic device, as described in Materials and Methods. Serine (10 µM) was used as the positive control. The Motility Migration Coefficients (MMCs) are shown. Data presented are the means and standard deviations from 3 independent experiments carried out in duplicate. * and ** indicate statistical significance for the mutant compared to WT at the given NE concentration, using the Student t-test at a significance level of $p < 0.05$ and 0.005 respectively. # indicates statistical significance for serine compared to the buffer control (no NE) in each strain, using the Student t-test at a significance level of $p < 0.0001$.

It should be noted that the dose-response curve for NE is shifted to higher concentrations by two orders of magnitude compared to that of DHMA (159). This seems to be a reasonable effect, given that NE must be converted to DOPEGAL by TynA in the periplasm, be taken into the cell as DOPEGAL, be converted to DHMA by FeaB, and then exported back to the periplasm to interact with the periplasmic sensory domain of Tsr. We see the same general pattern for the dose response to a step increase in concentration for

both DHMA and NE, as measured in the MMC assay, although shifted to a 100-fold higher concentration with NE.

IV.4.2 Role of FeaR in the signaling pathway

The FeaR transcription factor is required for the expression of the *tynA* and *feaB* genes (164, 166). The *feaR*, *tynA* and *feaB* genes are clustered in the *E. coli* chromosome, with *feaR* being transcribed divergently from the other two. We therefore tested the ability of the CV1Δ*feaR* mutant to respond to NE. These cells responded normally to 10 μM *L*-serine but failed to respond to NE at any concentration tested (**Fig. 4.2**). Thus, FeaR is required for *E. coli* to produce a chemotaxis response to NE, presumably through its role in transcription of the *tynA* and *feaB* genes.

We then determined whether expression of *feaR* increases in cells exposed to NE. **Figure 4.3** shows that *feaR* transcription, as measured by qRT-PCR, increased by 2.7 fold more when CV1 cells were incubated for 60 min with 8 μM NE than when the cells were incubated for 60 min in the absence of NE. No difference in the increase in *feaR* transcription over time, with or without NE incubation, was observed with the CV1Δ*qseC* and CV1Δ*qseB* strains, a result that is consistent with their lack of response in the MMC assay. The increase in the induction of *feaR* transcription in the CV1Δ*qseE* mutant after 60 min exposure to NE relative to incubation of this strain for 60 min without NE was similar to that seen with CV1 (2.8 fold), indicating that QseE plays little or no role in the signaling pathway. On the other hand, the increase in the transcription of *feaR* in the CV1Δ*qseF* mutant after 60 min exposure to NE was 1.6-fold higher than the increase after
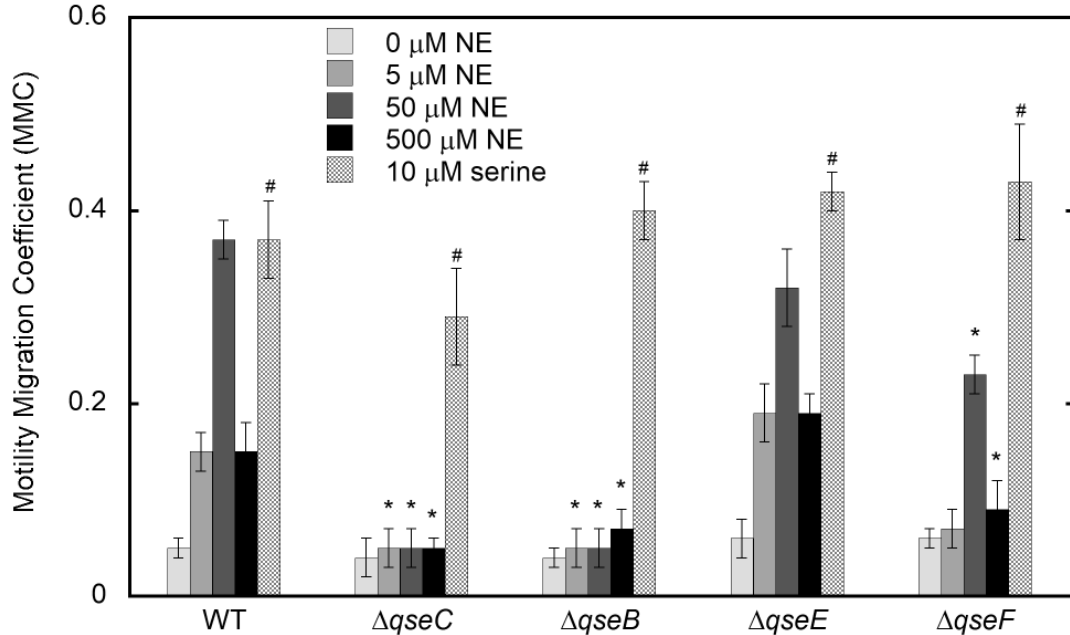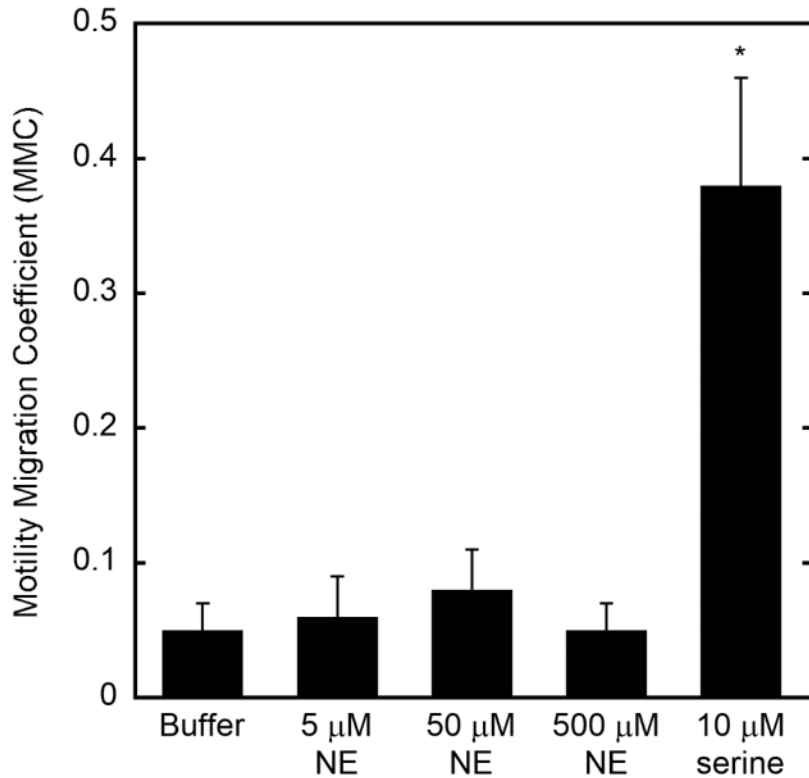
FIG. 4.2. Chemotaxis of *E. coli* RP437 Δ*feaR* to NE**.** Cells were exposed to 0, 5, 50, and 500 µM NE in the microfluidic device as described in Materials and Methods. Serine (10 µM) was used as the positive control. The Motility Migration Coefficients (MMCs) are shown. Data shown are the means and standard deviations from 3 independent experiments carried out in duplicate. * indicates statistical significance for serine compared to the buffer control (no NE), using the Student t-test at a significance level of p<0.0001.

60 min of incubation without NE. This modest decrease in *feaR* expression suggests that

QseF plays some role in the induction of *feaR* transcription. Even in the absence of QseE,

phosphorylation of QseF by QseC apparently produces enough QseF-P for full induction

of *feaR* transcription.
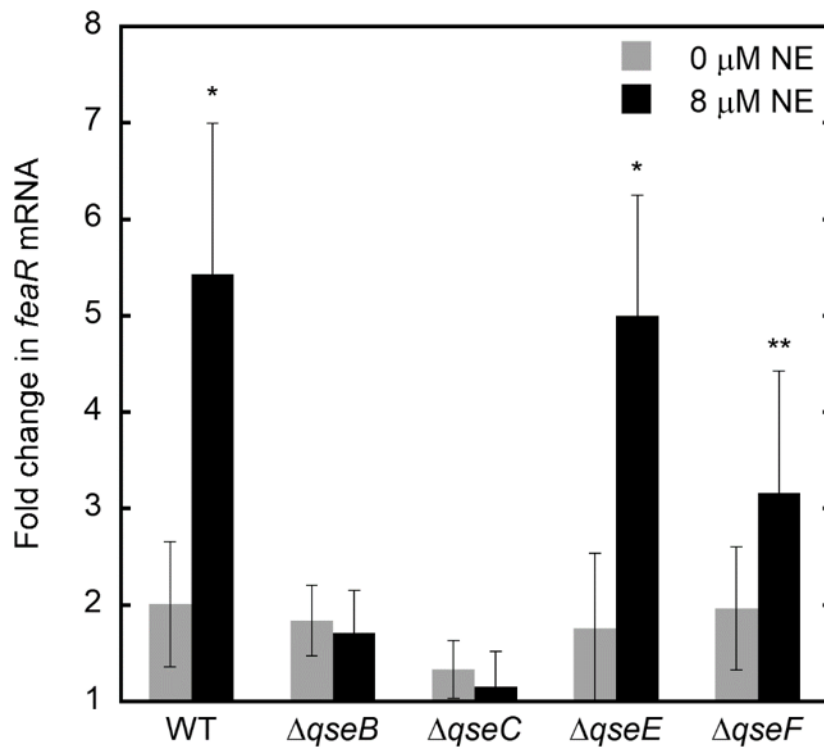
FIG. 4.3. Induction of *feaR* transcription in wild-type *E. coli* RP437 and the Δ*qse* mutants. The expression of *fea*R was quantified by qRT-PCR before and after incubation for 60 min in cells treated with 8 µM NE. Cells that were incubated with 0 mM NE for 60 min were used as the negative control. The fold-increase in *fea*R mRNA after incubation is shown. Data shown are the means and standard deviations from three independent experiments carried out in duplicate. * and ** indicate statistical significance for NE treatment compared to control, using the Student t-test at a significance level of $p < 0.005$ and 0.05, respectively.

IV.4.3 Induction of TynA and FeaB

Because NE increased the transcription of *feaR,* which in turn is known to regulate *tynA* and *feaB*, we next investigated how the transcription of *tynA* and *feaB* changes upon incubation with NE in the wild-type and mutant strains. **Figures 4.4** show that the transcription of both *tynA* and *feaB* increased by 2.4-fold more in CV1 cells incubated
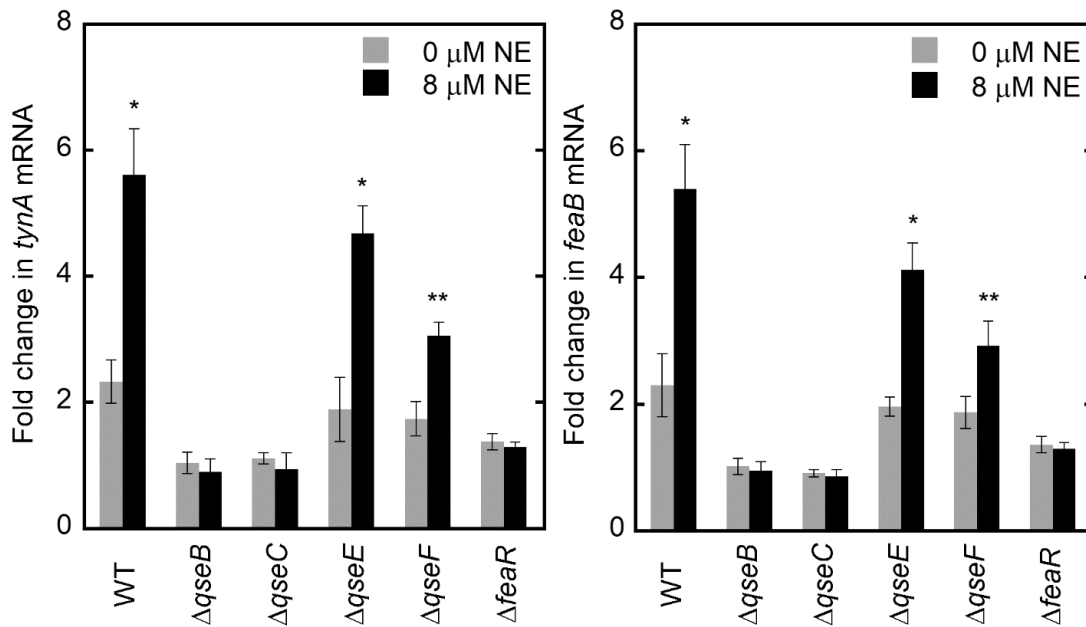
FIG. 4.4. Induction of *tynA* and *feaB* transcription in wild-type *E. coli* RP437 and Δ*qse* mutants**.** The expression of *tynA* and *feaB* was quantified by qRT-PCR before and after incubation for 60 min in cells treated with 8 µM NE. Cells that were incubated without NE for 60 min were used as the negative control. The fold-increase in *tyn*A and *fea*B mRNA after incubation is shown. Data shown are the means and standard deviations from three independent experiments carried out in duplicate. * indicates statistical significance for NE treatment compared to control, using the Student t-test at a significance level of p < 0.005.

for 60 min with NE relative to cells incubated for 60 min in the absence of NE. Consistent

with the data in **Figure 4.3**, the increase in transcription of *tynA* and *feaB* in the CV1Δ*qseE*

mutant (2.5 and 2.9-fold more after 60 min incubation with NE compared to 60 min of

incubation without NE, respectively) was similar to the wild type. No difference in the

increase in *tynA* or *feaB* transcription with or without NE was seen in the CV1Δ*qseC,*

CV1Δ*qseB* or CV1Δ*feaR* mutants. The CV1Δ*qseF* strain again fell into an intermediate

category, with NE boosting transcription of *tynA* and *feaB* 1.8 and 1.6 fold, respectively, after incubation with NE compared to incubation without NE.

IV.4.4 Sequence analysis of the *feaR* promoter

An examination of the regulatory region of the *fearR*, *tynA* and *feaB* genes suggests a mechanism that could explain our results. Both the MMC chemotaxis assay and the analysis of the induction of *feaR*, *feaB* and *tynA* transcription by pretreatment with NE show that QseC and QseB are essential for production of FeaB and TynA by an indirect mechanism involving the FeaR transcription factor. The data also suggest that the response regulator QseF, which can be phosphorylated by both its cognate histidine kinase QseE and by cross talk from QseC, is required for maximal induction by NE.

Inspection of the *feaR* regulatory region shows that it contains three promoters (164) and two predicted binding sites for QseB (**Fig. 4.5**, shown in cyan) (167) in the *feaR* regulatory region, based on the consensus binding site of QseB determined for *qseBC* and *flhDC*. One of the QseB-binding sites, which matches the C**AA**TT**A**CGAATT**A** consensus sequence (167) at 9/13 positions and at all four of the highly conserved A bases (in bold and underlined), overlaps the P_m transcription start site and is 11 base pairs upstream of the -35 region of the P_1 promoter. The other, which matches the consensus at 7/13 positions and at all four of the highly conserved A residues, overlaps the P_2 transcription start site. Although we do not know which of the three *feaR* promoters is responsible for the induction of *feaR* transcription, the position of the putative QseB-

feaR Pm

TCAGCT**GTGACA**AGCTCCGCAAATCGT**GACAAT**AACCGCTTATGTCTCTATG

     -35   **-10**

feaR P1

C**CTGACA**AGACTTATTTCC**TATAGT**CAGGCTCATTAGCTTCGTTTA**TTGCAA**

-35   **-10**   **-35**

feaR P2   FeaR start

CACAAATGC**AACAAT**AAAAATACATTTCACACAGCGAAAACGTGCC ATG

           -10

FIG. 4.5. Analysis of the *fea*R promoter. The *feaR* promoter sequence and the predicted QseB binding sites (32; highlighted in cyan) are shown. The last four and three bases (GACA and ACA) of the 3' ends of the possible QseF binding sites (33) are highlighted in yellow; the two-base overlap between the promoter-distal putative QseF and QseB-binding sites are highlighted in purple. Proposed promoter elements (-35 and -10) associated with the three mapped transcription start sites (164), shown by horizontal rightward-pointing arrows, are underlined.

binding sites suggests that the P_1 promoter is the most likely candidate. Also, the P_1 promoter has the closest match to the σ^{70} -35 and -10 consensus sequences.

It is possible that the activity of P_2, and perhaps even transcription initiated at P_1, would be inhibited by the binding of QseB to its downstream binding site. If the affinity of QseB-P for the upstream site is higher than the affinity for the downstream site, *feaR* transcription could be maximally induced at intermediate levels of QseB-P and repressed at higher levels of QseB-P.

The consensus binding site for QseF has been determined for only one gene, *glmY*, which encodes a small non-coding regulatory RNA (168). There is no obvious match to the 18-base QseF consensus sequence in the FeaR regulatory region, although the GACA bases that overlap the -10 region of Pm and the ACA bases that overlap the -35 region of

75

P$_2$ (highlighted in yellow in **Fig. 4.5**) are the last four and three bases, respectively, of the reported QseF consensus binding site. Although we can make no definitive statement about whether QseF interacts with the *feaR* regulatory region, the short sequence homologies we observe are perhaps in the right position for QseF to bind in conjunction with QseB.

IV.5 Conclusion

Based on our results, we propose a model to explain how NE induces its own metabolism to DHMA (**Fig. 4.6**). In this model, NE binds to QseC to activate its kinase activity. QseC then phosphorylates its cognate response regulator, QseB, and to a lesser extent, its non-cognate response regulator, QseF. The phosphorylated response regulators induce transcription of the *feaR* gene, perhaps by binding upstream of the P$_1$ *feaR* promoter. The FeaR protein, in turn, activates the transcription of the *feaB* and *tynA* genes, whose products convert NE to DHMA. Note that, because of the convoluted way in which NE serves as an attractant, high levels of both TynA and FeaB may be needed to produce enough DHMA to be sensed as an attractant by Tsr.

The paradigm we have just outlined suggests that the extraordinarily thorough work of Julius Adler in the 1960s and 1970s (169) may have missed some important chemoeffectors for *E. coli*, including biological signaling molecules in addition to nutrients For example, we found that the quorum-sensing signal autoinducer-2 is an attractant for *E. coli* that is sensed by binding to the periplasmic LsrB protein, which then
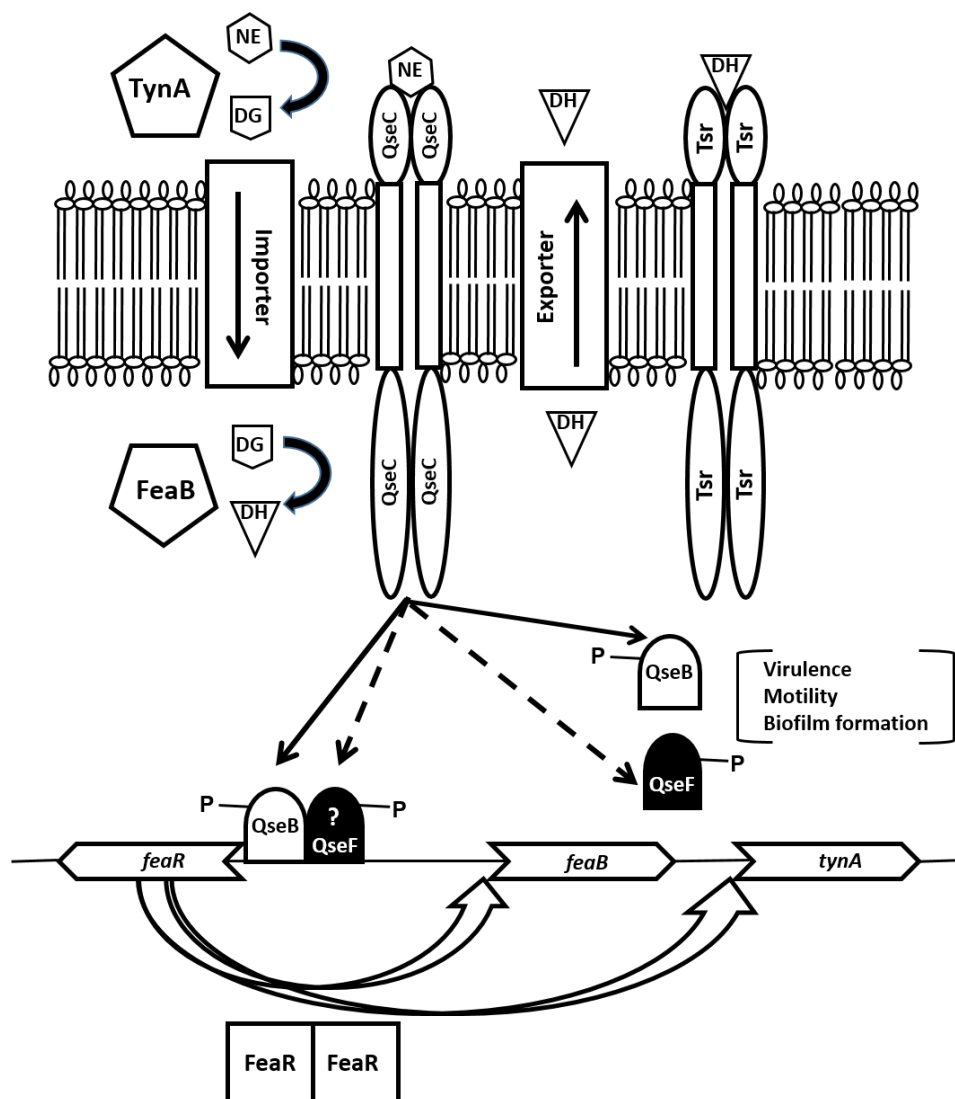
FIG.4.6. Proposed model for conversion of NE to DHMA. NE binds to QseC, which leads to phosphorylation of QseB and, to a lesser extent, QseF. QseF will also be phosphorylated by QseE (not shown) if QseE is present. Phosphorylated QseB, with help from QseF, induces transcription of the *fea*R gene. The FeaR dimer induces the transcription of the *feaB* and *tynA* genes (open arrows) by binding upstream of their respective promoters. Note that QseB-P and QseF promote transcription of many other genes than *feaR* (152, 155, 156) and that *feaR* is regulated by numerous other transcription factors than QseB and QseF (164). The TynA protein is exported to the periplasm, where it acts as a monoamine oxidase to convert NE to DOPEGAL (DG). DG is taken into the cytoplasm by an uncharacterized transporter, where the aromatic aldehyde dehydrogenase FeaB oxidizes it to DHMA (DH). DH is delivered to the periplasm by an uncharacterized exporter, where it binds to the Tsr chemoreceptor to evoke an attractant chemotaxis response.

interacts with Tsr (97). The realization that a host molecule like NE must be metabolized to DHMA for it to be sensed as an attractant suggests that other important chemoeffectors may be produced only by metabolism. Thus, screens for chemoeffectors should be performed after growing cells in the presence of candidate molecules, a procedure that is routinely followed for organisms like *Pseudomonas putida* that can utilize an enormous catalog of possible organic compounds (170). Such processes for generating chemoeffectors might be important for the pathogenesis of enteric pathogens such as EHEC, as we have observed for NE and DHMA (157). Host-derived compounds like NE and DHMA might also play important roles in interactions among the many organisms of the microbiome.

CHAPTER V

MODELING OF CHEMOTAXIS BEHAVIOR OF BACTERIA IN MICROFLUIDIC DEVICES USING PROBABILISTIC APPROCH

V.1 Overview

Mathematical models of bacterial chemotaxis can be used to obtain insights on the effect of various factors on the chemotaxis behavior of bacteria in aqueous solutions. If these models are predictive in nature, they can also be used to minimize the experimental space and the number of experiments needed to comprehensively investigate the chemotaxis response of bacteria to a chemoeffector. While several mathematical models have been developed to describe different aspects of bacterial chemotaxis (100-109), many of them focus on chemotactic processes at cellular level by considering the mechanistic interactions between the intracellular signaling cascades, and do not predict the bacterial migration in a given environment. Accurate description of bacterial migration is essential to account for the effects of spatial and temporal variations on the observed chemotaxis response in flow systems, particularly in microfluidic device.

In this study, we present a probabilistic model to predict the chemotaxis behavior of the bacteria in a stable exponential gradient of chemoeffector in microfluidic devices. Time dependent bacterial distribution profiles were simulated for a $500 \times 50 \times 10$ µm microfluidic device using MATLAB®. The simulations suggest that the time dependent bacterial migration in the microfluidic device is influenced by bulk motion of the fluid and existing concentration gradient of chemoeffector.

V.2 Introduction

The results presented in Chapters III and IV clearly demonstrate the utility of the µFlow assay for investigating the chemotaxis response to molecules such as NE and DHMA. As described earlier (98), a chemoeffector is mixed with buffer in a laminar flow-based diffusive mixing chamber and is introduced into the observation chamber of the device. In the device, a parabolic velocity profile and a stable concentration gradient is maintained. The chemotaxis response is quantified by determining the distribution of bacteria along the width of the chemotaxis chamber near the exit (**Fig.3.1**). The chemotaxis response of the bacteria in the microfluidic device depends on three factors – shape (or steepness) of the concentration gradient, velocity of the fluid stream carrying the chemoeffector, and the maximum concentration used to generate gradient of the chemoeffector molecule. The effect of these three variables is discussed below.

The shape of the concentration gradient plays a significant role in the observed chemotaxis response. Hegde et al (97) have shown that *E. coli* RP437 does not migrate towards serine when the concentration gradient (0 – 200 µM) is linear across the width of the chemotaxis chamber. However, when the serine spatial concentration gradient strength is steep (i.e., a non-linear gradient), *E. coli* RP437 demonstrates strong chemotaxis migration towards serine, indicating that the shape of concentration gradient can impact the observed chemotaxis response. Similarly, Englert et al. (90) showed that the velocity of the fluid also affects the extent of spreading across the chemotaxis chamber (98) and hence, and chemotaxis migration coefficient (CMC). It was observed that the CMC value for *E. coli* RP437 in 0 – 225 µM $NiSO_4$ gradient decreased from -0.18 to -0.14 when the

flow rate reduced from 1500 nl/min to 1000 nl/min. The experimental results provided in chapter III (**Fig.3.6**) support the fact that maximum concentration used to generate gradient of the chemoeffector molecule also affects the extent of chemotaxis response in microfluidic device. It was noticed that the CMC value for *E. coli* RP437 increased from 0.12 to 0.21 when the concentration gradient of DHMA was changed from $0 - 5\ \mu M$ to $0 - 50\ \mu M$.

More importantly, the factors that impact chemotaxis are not independent but are coupled. For example, a strong chemotaxis response towards DHMA was observed when *E.coli* RP437 was presented a 0-50 µM non-linear gradient at a flow rate of 2100 nL/min. Changing the concentration gradient or its shape or flow rate results in attenuation of the observed chemotaxis response. As a result, optimization of these coupled variables requires carrying out numerous time and resource intensive experiments.

Pioneering work on mathematical modeling of bacterial chemotaxis has been carried out by Keller and Segal (108), and this model forms the basis for all subsequent mathematical models describing bacterial chemotaxis (171). Originally developed to model the movement of slime molds Keller-Segal model is widely used to describe the changes in density of bacterial population as function of attractant gradient in a given system. However, this model do not account for the active motion of the bacteria and single cell dynamics. In addition, it is always challenging to obtain numerical solutions to Keller-Segal model without several assumptions. Therefore, it is important to develop a mathematical model, which can be used to identify a small set of optimal conditions to be tested for a specific chemoeffector molecule and minimize the number of experiments

required. In this work, we propose a simple and efficient modeling framework based on probability distribution functions to model the bacterial chemotaxis in microfluidic device.

V.3 Model development

We initially considered a 2D plane along the length of the chemotaxis chamber of dimensions $L \times W \times H$ (**Fig.5.1**). The domain is divided in to small units called 'cells' and the total number of cells in the entire domain are m×n. The location of each cell can be represented as (x_i, y_i), and bacteria are allowed to move from one cell to another cell (**Fig.5.2**). For example, if a bacterium initially at (x_i, y_i) moves to $(x_i{}^*, y_i{}^*)$ in time Δt then the probability associated with this event can computed as

$$p(x, y) = \frac{\exp\left(-\dfrac{(x_i - x_i{}^*)^2 + (y_i - y_i{}^*)^2}{2D\Delta t}\right)}{\sqrt{2\pi D\Delta t}}$$
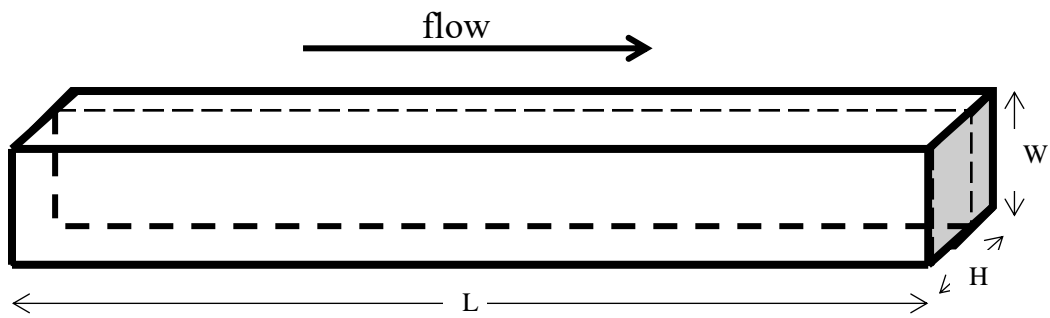
(5.1)

FIG. 5.1. Chemotaxis chamber

Theoretically, bacteria from any one cell may move to other (m×n)-1 cells or may remain in the cell. Therefore, there will be m×n events associated with movement of bacteria from one cell, and corresponding probabilities associated with each event. Since, there are m×n cells and each cell is associated with m×n probabilities, we define the probability matrix of the entire domain as the transition matrix 'T' which is given by:

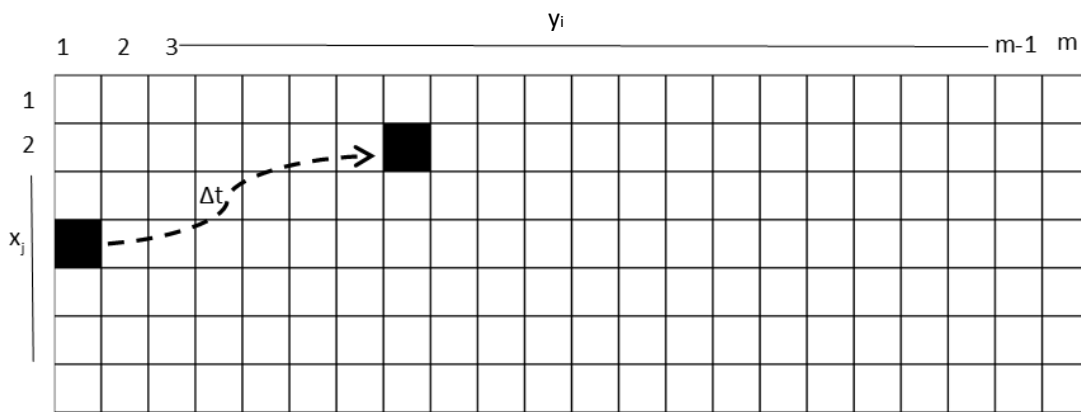$$T = [p(x,y)]_{(m\times n)\,\times\,(m\times n)} \tag{5.2}$$

FIG.5.2. 2D domain of chemotaxis chamber

We now define position matrix, X, whose elements represent the probability of finding the bacteria in any give cell at time 't'. For a given position matrix at time 't', $X_{(m\times n)\,\times\,1}$, the transformed position matrix after time 'Δt' can be calculated as

$$X(t + \Delta t) = T * X(t) \tag{5.3}$$

V.3.1 Incorporation of velocity

It is observed that in the absence of flow the bacteria migrate randomly in all directions, but in the presence of flow bacteria migrate primarily in the direction of flow due to the bulk motion of fluid. To account for this effect, velocity is incorporated in to the eqn.5.1. It is assumed that the flow is laminar and fully developed.

$$p(x,y) = \frac{\exp\left(-\frac{(x_i - x_i^*)^2 + (y_i - y_i^* - v\Delta t)^2}{2D\Delta t}\right)}{\sqrt{2\pi D\Delta t}} \tag{5.4}$$

where

$$v = v_{max}\left(\frac{x_i}{W} - \left(\frac{x_i}{W}\right)^2\right) \tag{5.5}$$

V.3.2 Incorporation of concentration gradient

It is known that bacterial movement is influenced by the presence of chemical gradient. Based on the direction of migration with respect to the chemical gradient the response is called either attraction or repulsion. To account for this effect concentration term is incorporated in to the eqn.5.4. It is assumed that the gradient is exponential.

$$p(x,y) = \frac{\exp\left(-\frac{(x_i - x_i^* \pm C)^2 + (y_i - y_i^* - v\Delta t)^2}{2D\Delta t}\right)}{\sqrt{2\pi D\Delta t}} \tag{5.6}$$

where

$$C = C' exp\left(\frac{ax_i}{w}\right) \tag{5.7}$$

V.3.3 Extending the model to 3D

Eqn. 6 can be used to determine the probability associated with the event in which the bacteria moves from (x_i, y_i) to (x_i^*, y_i^*) in 2D space containing velocity and concentration gradients. By incorporating the 'z' co-ordinate eqn. 5.6 can be written as

$$p(x, y, z) = \frac{\exp\left(-\frac{(x_i - x_i^* \pm C)^2 + (y_i - y_i^* - v\Delta t)^2 + (z_i - z_i^*)^2}{2D\Delta t}\right)}{\sqrt{2\pi D\Delta t}} \qquad (5.8)$$

Eqn. 5.8 can be used to determine the probability associated with the event of bacterial movement from (x_i, y_i, z_i) to (x_i^*, y_i^*, z_i^*) in 3D space containing velocity and concentration gradient.

V.4 MATLAB® simulations

Theoretical validation of the proposed model was carried out by computing the transition matrix 'T' for a chemotaxis chamber with dimensions $500 \times 50 \times 10$ µm. For a given position matrix, X(t), the transformed position matrix X(t+Δt) was computed as per eqn. 5.3. The cells were introduced near the entrance (length =0, width =25, height =5) and the distribution of probability in 3D was shown in the **Figures 5.3, 5.4 5.5, and 5.6.** The simulation results are categorized into the following cases: (1) no flow and no concentration gradient, (2) flow with no concentration gradient (3) flow with concentration gradient (attraction), and (4) flow with concentration gradient (repulsion). **Figures 5.3** and **5.4** depict the effect of fluid flow on the temporal bacterial distribution in

the chemotaxis chamber. As it can be seen from the simulations for the case of no flow and no concentration gradient, the bacteria are distributed around the entrance point after 2 s (**Fig. 5.3A**) and remained at the entrance (with more spread) even 10 s **(Fig. 5.3B)** after their introduction into the chamber, whereas appreciable migration of bacteria can be seen in the case of flow with no concentration gradient (**Fig.5.4**). In this case, bacteria has reached approximately middle of the chamber in 2 s (**Fig. 5.4A** and the end of the chamber in 5 s (**Fig. 5.4A**) after their introduction. Case 3 and 4 are simulated by assuming an exponential concentration gradient and by changing the sign of C' in the equation 8. For a positive C' attraction response is observed (**Fig. 5.5**) similarly for negative C' repulsion response is observed (**Fig. 5.6**). Although, the bacterial distribution appear to be similar for the case of 3 and 4 around at 2 s (**Fig. 5.5A, Fig. 5.6A**), the bacteria migrated towards the higher concentration (**Fig. 5.5B**), and towards the lower concentration (**Fig. 5.5B**) within 5 s of their introduction in the chemotaxis chamber.

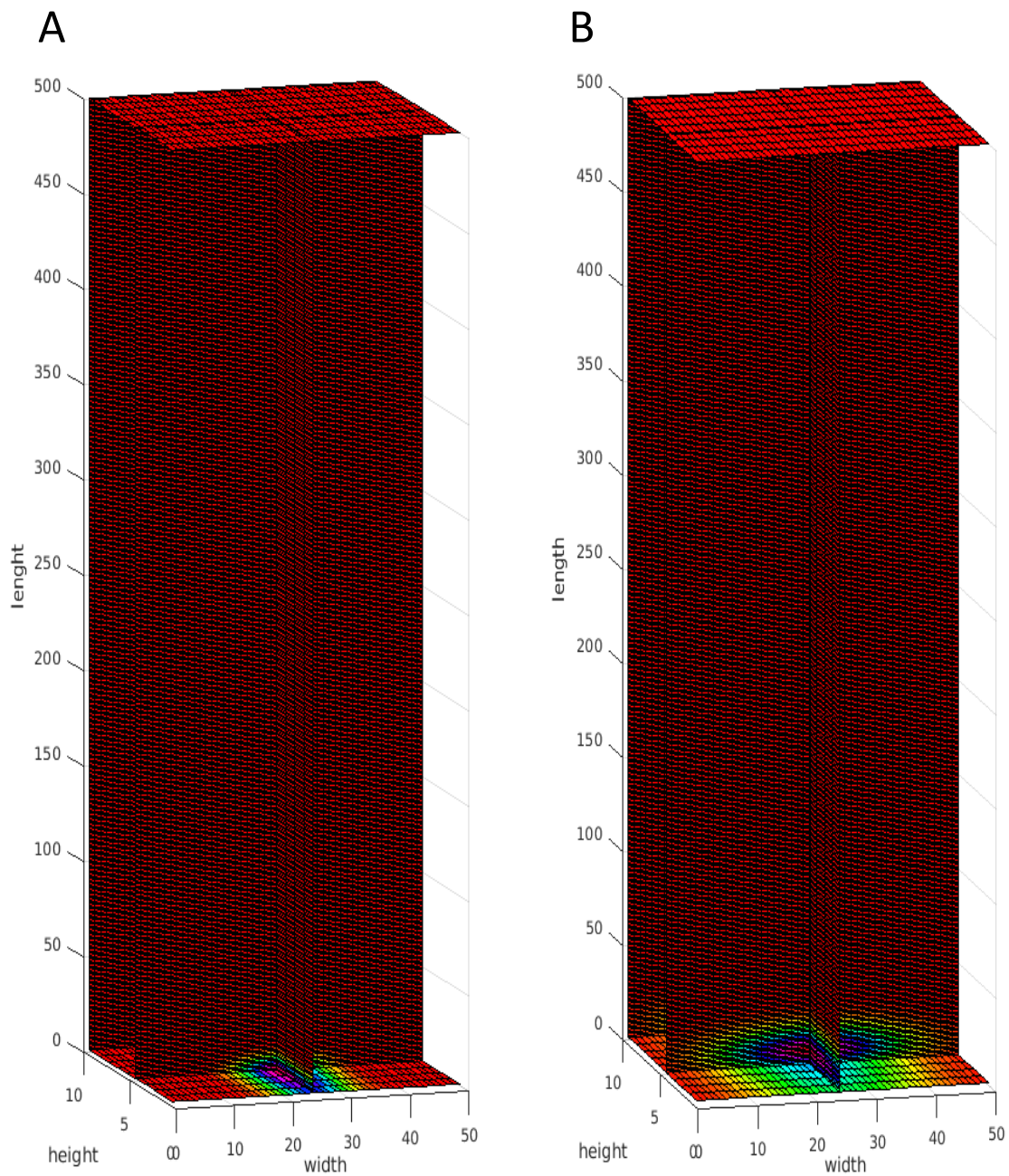**FIG. 5.3.** Temporal probability distribution of bacteria in 3D space for the case of no flow and no concentration gradient. Migration of bacteria in the chemotaxis chamber of 500 × 50 × 10 µm size after (A) 2 s and (B) 10 s of their introduction.
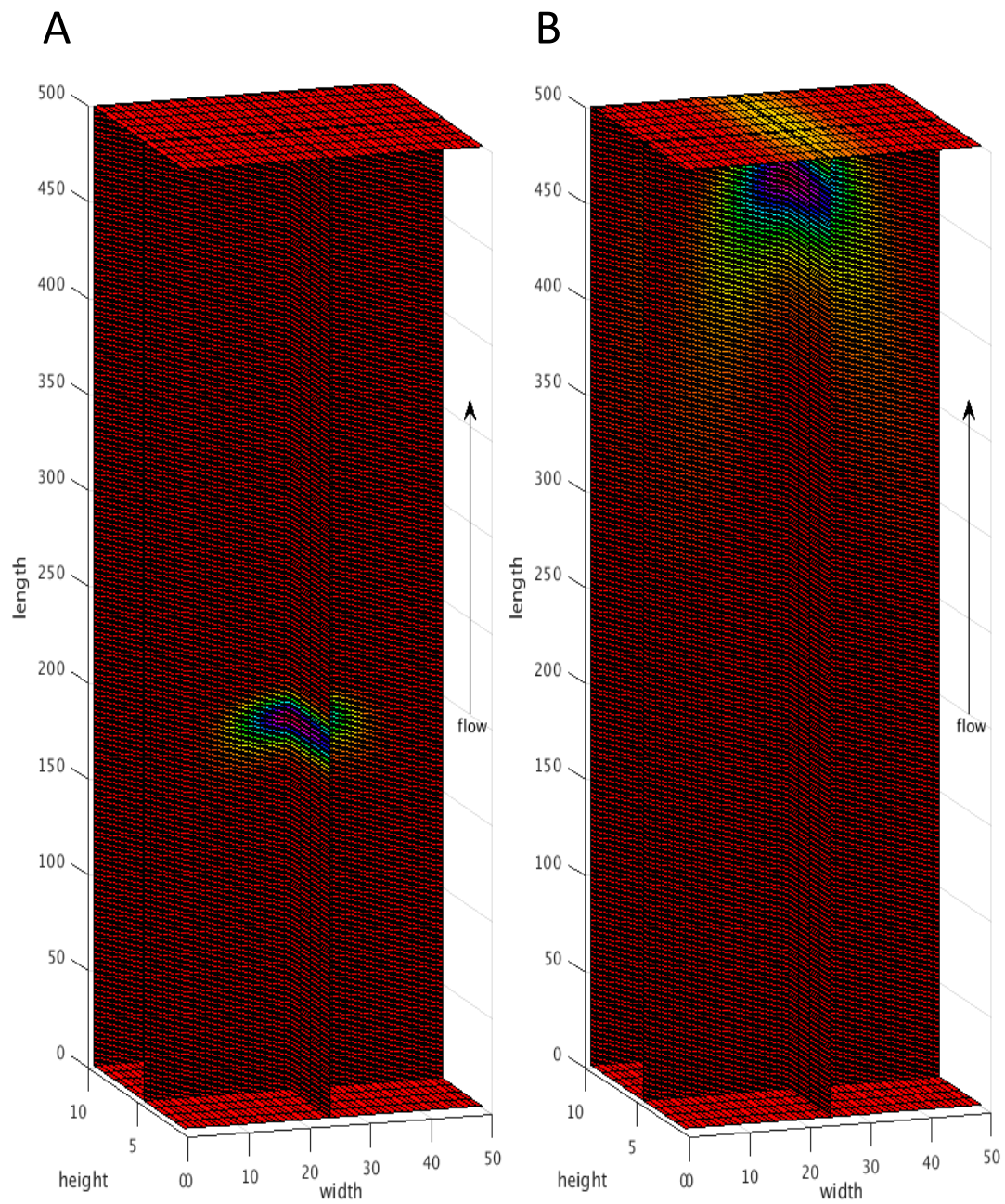
FIG. 5.4. Temporal probability distribution of bacteria in 3D space for the case of flow and no concentration gradient. Migration of bacteria in the chemotaxis chamber of 500 × 50 × 10 µm size after (A) 2 s and (B) 5 s of their introduction.

FIG. 5.5. Temporal probability distribution of bacteria in 3D space for the case of flow and concentration gradient (attractant). Migration of bacteria in the chemotaxis chamber of $500 \times 50 \times 10$ µm size after (A) 2 s and (B) 5 s of their introduction.

FIG. 5.6. Temporal probability distribution of bacteria in 3D space for the case of flow and concentration gradient (repellent). Migration of bacteria in the chemotaxis chamber of $500 \times 50 \times 10$ µm size after (A) 2 s and (B) 5 s of their introduction.
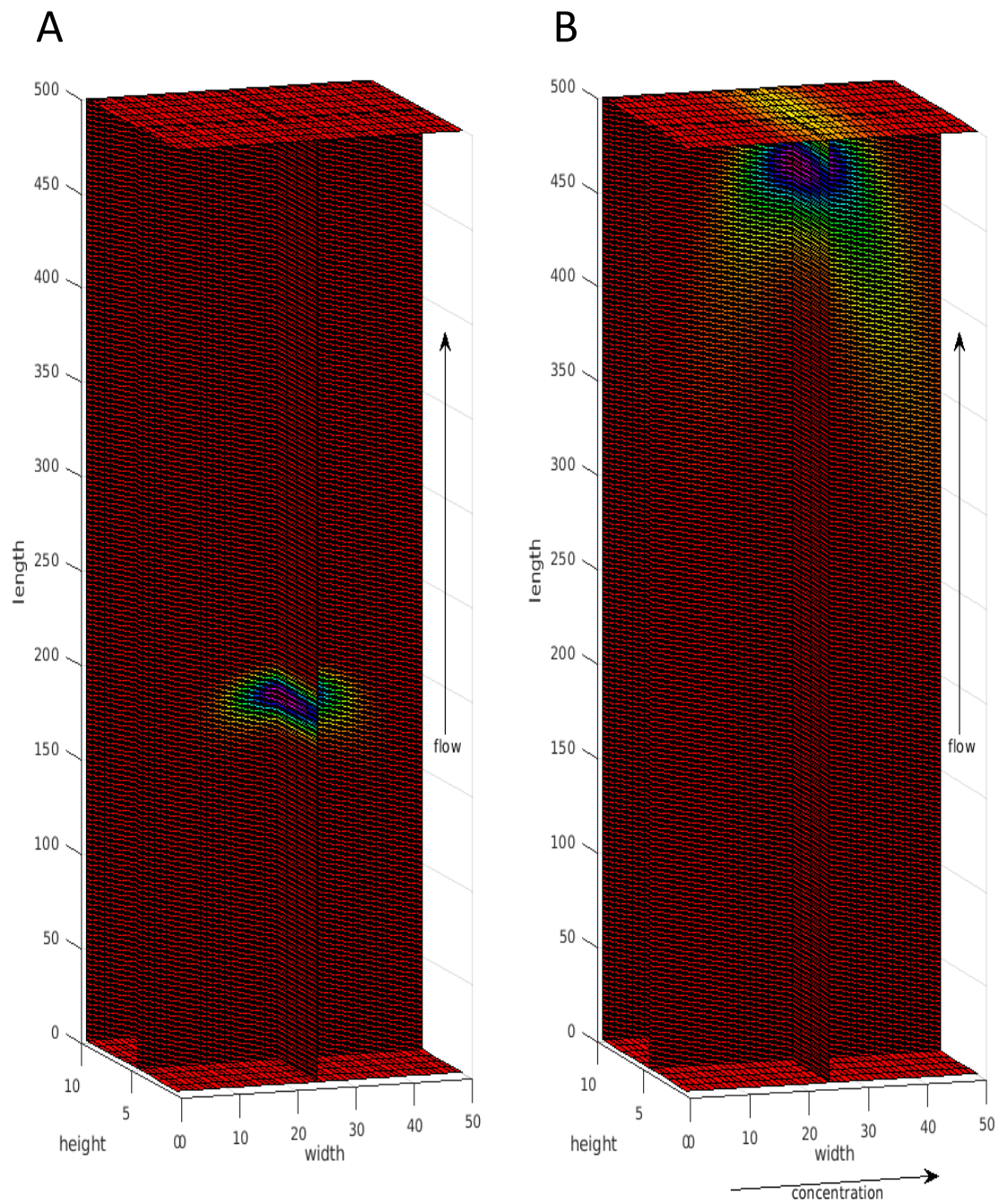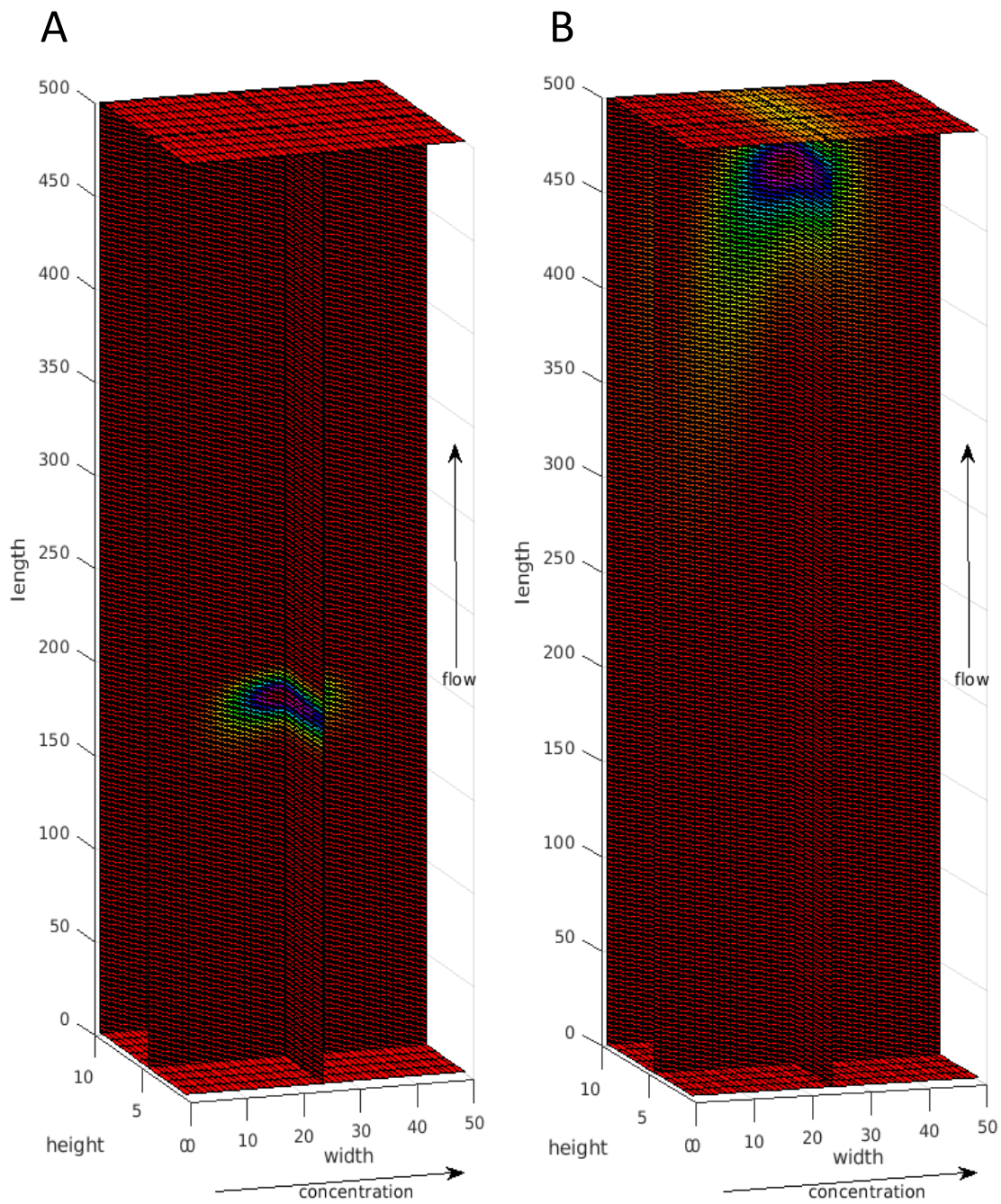
V.5 Discussion

The probabilistic model presented in this Chapter provides a simple yet efficient way to model bacterial migration in the µFlow device. For theoretical validation of the model we used a random bacterial motility coefficient (D) of 1×10^{-7} cm^2/s and chemotactic sensitivity coefficient (C') of 2×10^{-7} cm^2/s. These values are an order of magnitude lower than the values reported previously for other wild-type strains of *E. coli* in a bulk aqueous environment. The explanation for using such low values of D and C' is that the dimension of our chemotaxis chamber used in simulations are 10-fold smaller in length and width compared to the chemotaxis chamber of microfluidic device used in the experiments. In addition, we used a velocity of 100 µm/s for the fluid flow which is also an order of magnitude smaller than the velocity in the microfluidic device. Therefore, using low values of D and C' is particularly important to visually notice the temporal changes in the bacterial distribution within the chemotaxis chamber.

While our results show good agreement between simulations and experimental data for a smaller dimension, it was not possible to extend the simulations to the actual microfluidic device dimensions because of the associated computational cost. The transition matrix that is generated in these simulations is extremely expensive in terms of computational memory. For example, to compute the Transition Matrix (T) for three dimensional space of $500 \times 50 \times 10$ µm requires ~2 TB of computational memory of supercomputer. If we use syntax T=zeros(m,n) to initialize the matrix. Later, we found that utilizing the sparse allocation method of matrix initialization (T=spalloc(m,n,nnz(T))) greatly reduces the memory required, however, the problem with this type of syntax is

very long execution time. **Table 5.1** provides comparative information between the new and old syntax operations. From the **Table 5.1** it is clear that the new syntax is more memory efficient but takes more time to compute. Therefore, more efficient programming code needs to be developed to minimize the computational time and memory.

Table 5.1. Comparison between old and new syntax in terms of computational memory and time.

Size	Size of 'T' Matrix		Computational time	
(L ×W×H)	Old Syntax	New Syntax	Old Syntax	New Syntax
10 ×10×10	8 MB	1 MB	0.5 s	25 s
20 ×10×10	32 MB	2 MB	1 s	200 s
20 ×20×10	120 MB	4 MB	5 s	25 min
40 ×20×10	480 MB	8 MB	20 s	200 min
40 ×40×10	1.8 GB	16 MB	80 s	25 h

CHAPTER VI

SUMMARY AND FUTURE DIRECTIONS

VI.1 Summary

We investigated the chemotaxis response of *E. coli* RP437 towards NE using a microfluidic device (Chapter III) and determined that the response to NE requires priming the cells during growth with a lower concentration of NE. We further determined that a non-linear concentration gradient of NE was required for detecting a significant chemotaxis response to NE. In addition, we identified that priming with NE during growth was required for NE chemotaxis and *de novo* expression of two enzymes TynA and FeaB was required for chemotaxis. Together, this led to the novel finding that NE was converted to DHMA by TynA and FeaB enzymatic activity, and DHMA was the actual chemoattractant for *E. coli* RP437.

We further demonstrated that chemotaxis to DHMA requires the Tsr chemoreceptor and the minimum concentration required for a detectable chemotaxis response through Tsr was ~5 nM. We also observed significant reduction in the chemotaxis response at DHMA concentrations greater than 50 µM and determined that negative cooperativity between the two serine binding sites resulted in attenuation of chemotaxis at concentrations greater than 50 µM.

We also investigated the mechanism underlying the conversion of NE to DHMA (Chapter IV) in *E. coli* RP437. We identified that the conversion of NE into DHMA requires the QseC histidine kinase and its cognate response regulator QseB, and to a lesser

extent, the response regulator QseF. Our data also suggest that the *feaR* transcription factor

is a downstream target for QseB and is required for *tynA* and *feaB* expression. This work

is significant as it suggest that host-derived signals such as NE can be converted by

commensal bacteria to a potent chemoattractant, which can then recruit pathogens that

possess Tsr-like receptors to the site of infection.

We also developed a probabilistic model to simulate the chemotaxis behavior of

bacteria in microfluidic devices (Chapter V). The time-dependent distribution of bacteria

in the chemotaxis chamber was simulated using MATLAB®. We determined that the time

dependent bacterial migration in the micro-flow device is influenced by bulk motion of

the fluid and existing concentration gradient of chemoeffector. The probabilistic model

can be used to reduce the experimental space required to test the response of an unknown

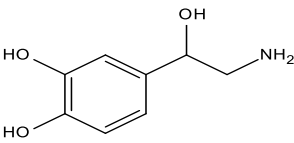chemoeffector in the microfluidic device.

VI.2 Future directions
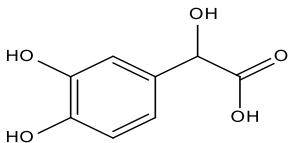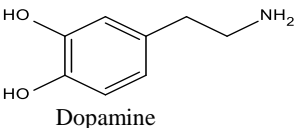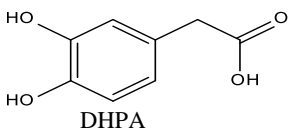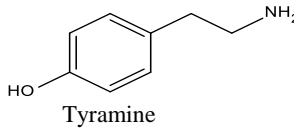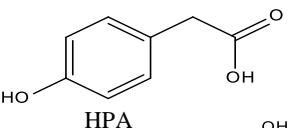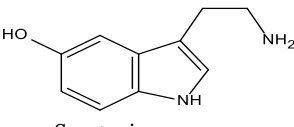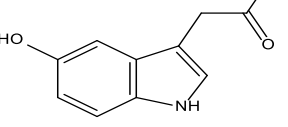
Identification of the NE metabolite DHMA as a chemoattractant for *E. coli* leads to

the hypothesis that metabolites from other aromatic neurotransmitters and hormones can

also be chemoattractants. Specifically, dopamine, tyramine and serotonin are all aromatic

compounds with primary amines that are present in the GI tract. A survey of the data in

the Kyoto Encyclopedia of Genes and Genomes (KEGG) REACTION database indicates

that these molecules are potential substrates for primary amine oxidases like TynA or other

monoamine oxidases. The expected products from these neurotransmitters upon

deamination and oxidation (the reactions carried out by TynA and FeaB, respectively) are

3,4-dihydroxyphenylacetate (DHPA), 4-hydroxyphenylacetate (HPA) and 5-hydroxyindoleactetate (HIA) (**Table 6.1**). Therefore, these metabolites can be tested to determine if they generate a chemotaxis response. Furthermore, it is also possible that DHMA is not the final product in NE metabolism and DHMA can be further metabolized into other compounds such as vanillylmandelic acid (VMA, also known as 4-hydroxy 3-methoxymandelic acid). Therefore, another line of investigation could be to determine if metabolites derived from DHMA are also chemoattractants for *E. coli* RP437. Lastly, it is of interest to determine the structure-function relationship between DHMA and Tsr that leads to chemotaxis. Specifically, the role of the 3'- and 4'-hydroxyl groups in interacting with the DHMA binding site in Tsr needs to be investigated further.

Since DHMA induces virulence and pathogenesis in EHEC O157:H7 (157), one hypothesis emerging out of this work is that DHPA, HPA, and HIA also promote virulence in pathogenic bacteria. The effect of these metabolites to induce the expression of the locus of enterocyte effacement (LEE) genes in EHEC O157:H7 can be tested using qRT-PCR. In addition, the effect of metabolites on EHEC O157:H7 attachment to cultured intestinal epithelial cells *in vitro* can also be investigated.

Our results show that QseB or QseF are required for *feaR* expression. However, we have not yet determined if these transcription factors directly bind to the *feaR* promoter or whether their effects are mediated through a different transcription factor. Interactions between QseB and *feaR* promoter DNA can be tested using Electrophoretic Mobility Shift Assay (EMSA). QseB/QseF protein can be purified under native conditions as described previously (172) by overexpression in a CV1Δ*qseB*/p*qseB*$^+$ or CV1Δq*seF*/p*qseF*$^+$ strain.

Table 6.1 Metabolite candidates for identifying those that are both virulence factors and chemoattractants.

Host enteric neurotransmitters	Metabolic products from primary amine oxidase and aldehyde dehydrogenase reactions
NE	DHMA
Dopamine	DHPA
Tyramine	HPA
Serotonin	HIA

The purified QseB/QseF protein should be mostly unphosphorylated while its sensor kinase, QseC or QseE, will be expressed at normal, wild-type levels. The *feaR* promoter region can be amplified using polymerase chain reaction (PCR) and end-labelled with [γ-32P]-dATP. Mobility shift assays using *feaR* promoter fragments and purified QseB/QseF can be carried out using standard protocols for protein-DNA interactions (173). If QseB or QseF directly bind to the *feaR* promoter region, we expect the protein-DNA complex to migrate slower than the DNA or the free protein.

The probabilistic model that was developed in chapter V can be validated by comparing model simulations with actual experimental data from the response to canonical chemoattractants such as serine and aspartate. After obtaining the fitted parameters of the model, D and C', simulations can be run with different flow rates and concentration gradients and shape of gradients to obtain optimal response space for a new ligand that binds directly to Tsr or Tar. Finally, the model can be extended to capture the response of bacteria to ligands with different binding affinity towards the receptor by incorporating another parameter (K_d) into the model. A *cheRB* mutant strain can be used to obtain the experimental data to fit the model parameter K_d.

REFERENCES

1. **Ley RE, Peterson DA, Gordon JI.** 2006. Ecological and evolutionary forces shaping microbial diversity in the human intestine. Cell **124:**837-848.

2. **Hooper LV, Gordon JI.** 2001. Commensal host-bacterial Relationships in the Gut. Science **292:**1115-1118.

3. FOOD Tool | CDC. https://wwwn.cdc.gov/foodborneoutbreaks/. Accessed on 15 Nov. 2017.

4. **Mellmann A, Bielaszewska M, Karch H.** 2009. Intrahost genome alterations in enterohemorrhagic *Escherichia coli*. Gastroenterology **136:**1925-1938.

5. **Boyer O, Niaudet P.** 2011. Hemolytic uremic syndrome: new developments in pathogenesis and treatment. Int J Nephrol **2011:**908407.

6. Hemolytic uremic syndrome (HUS) | Complications. http://www.mayoclinic.org/diseases-conditions/hemolytic-uremic-syndrome/symptoms-causes/dxc-20204144. Accessed on 15 Nov. 2017.

7. **Moxley RA.** 2004. *Escherichia coli* 0157:H7: an update on intestinal colonization and virulence mechanisms. Anim Health Res Rev **5:**15-33.

8. **Lewis SB, Cook V, Tighe R, Schuller S.** 2015. Enterohemorrhagic *Escherichia coli* colonization of human colonic epithelium in vitro and ex vivo. Infect Immun **83:**942-949.

9. **Franzin FM, Sircili MP.** 2015. Locus of enterocyte effacement: a pathogenicity island involved in the virulence of enteropathogenic and enterohemorragic *Escherichia coli* subjected to a complex network of gene regulation. Biomed Res Int **2015:**534738.

10. **Nguyen Y, Sperandio V.** 2012. Enterohemorrhagic *E. coli* (EHEC) pathogenesis. Front Cell Infect Microbiol **2:**90.

11. **Kaper JB, Nataro JP, Mobley HL.** 2004. Pathogenic *Escherichia coli*. Nat Rev Microbiol **2:**123-140.

12. **Torres AG, Kaper JB.** 2003. Multiple elements controlling adherence of enterohemorrhagic *Escherichia coli* O157:H7 to HeLa cells. Infect Immun **71:**4985-4995.

13. **Vlisidou I, Lyte M, van Diemen PM, Hawes P, Monaghan P, Wallis TS, Stevens MP.** 2004. The neuroendocrine stress hormone norepinephrine augments *Escherichia coli* O157:H7-induced enteritis and adherence in a bovine ligated ileal loop model of infection. Infect Immun **72:**5446-5451.

14. **Jewitt DE, Reid D, Thomas M, Mercer CJ, Valori C, Shillingford JP.** 1969. Free noradrenaline and adrenaline excretion in relation to the development of cardiac arrhythmias and heart-failure in patients with acute myocardial infarction. Lancet **1:**635-641.

15. **Thierry AM, Fekete M, Glowinski J.** 1968. Effects of stress on the metabolism of noradrenaline, dopamine and serotonin (5HT) in the central nervous system of the rat. (II). Modifications of serotonin metabolism. Eur J Pharmacol **4:**384-389.

16. **Lyte M, Arulanandam BP, Frank CD.** 1996. Production of Shiga-like toxins by *Escherichia coli* O157:H7 can be influenced by the neuroendocrine hormone norepinephrine. J Lab Clin Med **128:**392-398.

17. WHO's first ever global estimates of foodborne diseases find children under 5 account for almost one third of deaths. http://www.who.int/mediacentre/news/releases/2015/foodborne-disease-estimates/en/. Accessed on 15 Nov. 2017.

18. CDC (2011) | CDC Estimates of Foodborne Illness in the United States. https://www.cdc.gov/foodborneburden/2011-foodborne-estimates.html. Accessed on 15 Nov. 2017.

19. **Frenzen PD, Drake A, Angulo FJ.** 2005. Economic cost of illness due to *Escherichia coli* O157 infections in the United States. J Food Prot **68:**2623-2630.

20. **Scharff RL.** 2012. Economic burden from health losses due to foodborne illness in the United States. J Food Prot **75:**123-131.

21. **Tuttle J, Gomez T, Doyle MP, Wells JG, Zhao T, Tauxe RV, Griffin PM.** 1999. Lessons from a large outbreak of *Escherichia coli* O157:H7 infections: insights into the infectious dose and method of widespread contamination of hamburger patties. Epidemiol Infect **122:**185-192.

22. **Obrig TG.** 2010. Escherichia coli Shiga Toxin Mechanisms of Action in Renal Disease. Toxins (Basel) **2:**2769-2794.

23. **Meirieu O, Pairet M, Sutra JF, Ruckebusch M.** 1986. Local release of monoamines in the gastrointestinal tract: an in vivo study in rabbits. Life Sci **38:**827-834.

24.	**Aneman A, Eisenhofer G, Olbe L, Dalenbäck J, Nitescu P, Fändriks L, Friberg P.** 1996. Sympathetic discharge to mesenteric organs and the liver. Evidence for substantial mesenteric organ norepinephrine spillover. J Clin Investig **97:**1640-1646.

25.	**Lyte M.** 2004. Microbial endocrinology and infectious disease in the 21st century. Trends Microbiol **12:**14-20.

26.	**Lyte M, Arulanandam B, Nguyen K, Frank C, Erickson A, Francis D.** 1997. Norepinephrine induced growth and expression of virulence associated factors in enterotoxigenic and enterohemorrhagic strains of *Escherichia coli*. Adv Exp Med Biol **412:**331-339.

27.	**Bansal T, Englert D, Lee J, Hegde M, Wood TK, Jayaraman A.** 2007. Differential effects of epinephrine, norepinephrine, and indole on *Escherichia coli* O157:H7 chemotaxis, colonization, and gene expression. Infect Immun **75:**4597-4607.

28.	**Kim DN.** 2012. Inter-kingdom Recognition of Norepinephrine by *E. Coli* : Identification of the Receptors Involved in ChemotaxisTexas A&M University, College Station, TX.

29.	**Mesibov R, Adler J.** 1972. Chemotaxis toward amino acids in *Escherichia coli*. J Bacteriol **112:**315-326.

30.	**Pasupuleti S, Sule N, Cohn WB, MacKenzie DS, Jayaraman A, Manson MD.** 2014. Chemotaxis of *Escherichia coli* to Norepinephrine (NE) Requires Conversion of NE to 3,4-Dihydroxymandelic Acid. J Bacteriol **196:**3992-4000.

31.	**Hazelbauer GL, Falke JJ, Parkinson JS.** 2008. Bacterial chemoreceptors: high-performance signaling in networked arrays. Trends Biochem Sci **33:**9-19.

32.	**Lloyd-Price J, Abu-Ali G, Huttenhower C.** 2016. The healthy human microbiome. Genome Med **8:**51.

33.	**Conrad R, Vlassov A.** 2015. The human microbiota: composition, functions, and therapeutic potential. Med Sci Rev **2:**92-103.

34.	**Abubucker S, Segata N, Goll J, Schubert AM, Izard J, Cantarel BL, Rodriguez-Mueller B, Zucker J, Thiagarajan M, Henrissat B, White O, Kelley ST, Methe B, Schloss PD, Gevers D, Mitreva M, Huttenhower C.** 2012. Metabolic reconstruction for metagenomic data and its application to the human microbiome. PLoS Comput Biol **8:**e1002358.

35. HUMAN MICROBIOTA: DEFINITION, COMPOSITION, FUNCTIONS, ANTIBIOTICS. http://www.tuscany-diet.net/2015/11/28/human-microbiota-definition-composition-functions/. Accessed on 15 Nov. 2017.

36. **Grice EA, Segre JA.** 2011. The skin microbiome. Nat Rev Microbiol **9:**244-253.

37. **Cho I, Blaser MJ.** 2012. The human microbiome: at the interface of health and disease. Nat Rev Genet **13:**260-270.

38. **Tortora GJ, Derrickson BH.** 2008. Principles of anatomy and physiology. John Wiley & Sons, Hoboken, NJ.

39. **Helander HF, Fandriks L.** 2014. Surface area of the digestive tract - revisited. Scand J Gastroenterol **49:**681-689.

40. **Flannigan KL, Geem D, Harusato A, Denning TL.** 2015. Intestinal antigen-presenting cells: key regulators of immune homeostasis and inflammation. Am J Pathol **185:**1809-1819.

41. **Berg RD.** 1996. The indigenous gastrointestinal microflora. Trends Microbiol **4:**430-435.

42. **Ouwehand A, Isolauri E, Salminen S.** 2002. The role of the intestinal microflora for the development of the immune system in early childhood. Eur J Nutr **41:**i32-i37.

43. **Donaldson GP, Lee SM, Mazmanian SK.** 2016. Gut biogeography of the bacterial microbiota. Nat Rev Microbiol **14:**20-32.

44. **Canny GO, McCormick BA.** 2008. Bacteria in the intestine, helpful residents or enemies from within? Infectand Immun **76:**3360-3373.

45. **Kleessen EBJMB.** 2000. Culture-based knowledge on biodiversity, development and stability of human gastrointestinal microflora. Microb Ecol Health Dis **12:**53-63.

46. **Purchiaroni F, Tortora A, Gabrielli M, Bertucci F, Gigante G, Ianiro G, Ojetti V, Scarpellini E, Gasbarrini A.** 2013. The role of intestinal microbiota and the immune system. Eur Rev Med Pharmacol Sci **17:**323-333.

47. **Bibbo S, Ianiro G, Giorgio V, Scaldaferri F, Masucci L, Gasbarrini A, Cammarota G.** 2016. The role of diet on gut microbiota composition. Eur Rev Med Pharmacol Sci **20:**4742-4749.

48. **Canny GO, McCormick BA.** 2008. Bacteria in the intestine, helpful residents or enemies from within? Infect Immun **76:**3360-3373.

49. **Jandhyala SM, Talukdar R, Subramanyam C, Vuyyuru H, Sasikala M, Nageshwar Reddy D.** 2015. Role of the normal gut microbiota. World J Gastroenterol **21:**8787-8803.

50. **Thursby E, Juge N.** 2017. Introduction to the human gut microbiota. Biochem J **474:**1823-1836.

51. **Round JL, Mazmanian SK.** 2009. The gut microbiome shapes intestinal immune responses during health and disease. Nat Rev Immunol **9:**313-323.

52. **Macpherson AJ, Harris NL.** 2004. Interactions between commensal intestinal bacteria and the immune system. Nat Rev Immunol **4:**478-485.

53. **Lutgendorff F, Akkermans LM, Soderholm JD.** 2008. The role of microbiota and probiotics in stress-induced gastro-intestinal damage. Curr Mol Med **8:**282-298.

54. **Abraham C, Cho JH.** 2009. Inflammatory bowel disease. N Engl J Med **361:**2066-2078.

55. **D'Aversa F, Tortora A, Ianiro G, Ponziani FR, Annicchiarico BE, Gasbarrini A.** 2013. Gut microbiota and metabolic syndrome. Intern Emerg Med **8:**S11-15.

56. **Matsuoka K, Kanai T.** 2015. The gut microbiota and inflammatory bowel disease. Semin Immunopathol **37:**47-55.

57. **Sekirov I, Russell SL, Antunes LC, Finlay BB.** 2010. Gut microbiota in health and disease. Physiol Rev **90:**859-904.

58. **Sheflin AM, Whitney AK, Weir TL.** 2014. Cancer-promoting effects of microbial dysbiosis. Curr Oncol Rep **16:**406-406.

59. **Lee J-H, Wood TK, Lee J.** 2015. Roles of indole as an interspecies and interkingdom signaling molecule. Trends Microbiol **23:**707-718.

60. **Xavier KB, Bassler BL.** 2005. Regulation of uptake and processing of the quorum-sensing autoinducer AI-2 in *Escherichia coli*. J Bacteriol **187:**238-248.

61. **Cogan TA, Thomas AO, Rees LE, Taylor AH, Jepson MA, Williams PH, Ketley J, Humphrey TJ.** 2007. Norepinephrine increases the pathogenic potential of *Campylobacter jejuni*. Gut **56:**1060-1065.

62. **Lyte M, Bailey MT.** 1997. Neuroendocrine-bacterial interactions in a neurotoxin-induced model of trauma. J Surg Res **70:**195-201.

63. **Sperandio V, Torres AG, Jarvis B, Nataro JP, Kaper JB.** 2003. Bacteria-host communication: the language of hormones. Proc Natl Acad Sci U S A **100:**8951-8956.

64. **Goyal RK, Hirano I.** 1996. The enteric nervous system. N Engl J Med **334:**1106-1115.

65. **Musacchio JM.** 1975. Enzymes involved in the biosynthesis and degradation of catecholamines, p 1-35. *In* Iversen LL, Iversen SD, Snyder SH (ed), Biochemistry of Biogenic Amines. Springer US, Boston, MA.

66. **Freestone P.** 2013. Communication between bacteria and their hosts. Scientifica **2013:**15.

67. **Freestone PP, Haigh RD, Williams PH, Lyte M.** 1999. Stimulation of bacterial growth by heat-stable, norepinephrine-induced autoinducers. FEMS Microbiol Lett **172:**53-60.

68. **Lyte M, Ernst S.** 1992. Catecholamine induced growth of gram negative bacteria. Life Sci **50:**203-212.

69. **Stevens MP.** 2010. Modulation of the interaction of enteric bacteria with intestinal mucosa by stress-related catecholamines, p 111-134. *In* Lyte M, Freestone PPE (ed), Microbial Endocrinology: Interkingdom Signaling in Infectious Disease and Health. Springer New York, New York, NY.

70. **Hegde M, Wood TK, Jayaraman A.** 2009. The neuroendocrine hormone norepinephrine increases Pseudomonas aeruginosa PA14 virulence through the las quorum-sensing pathway. Appl Microbiol Biotechnol **84:**763-776.

71. **Moreira CG, Weinshenker D, Sperandio V.** 2010. QseC mediates *Salmonella enterica* serovar typhimurium virulence in vitro and in vivo. Infect Immun **78:**914-926.

72. **Naresh R, Hampson DJ.** 2011. Exposure to norepinephrine enhances *Brachyspira pilosicoli* growth, attraction to mucin and attachment to Caco-2 cells. Microbiology **157:**543-547.

73.   **Eisenhofer G, Kopin IJ, Goldstein DS.** 2004. Catecholamine metabolism: a contemporary view with implications for physiology and medicine. Pharmacol Rev **56:**331-349.

74.   **Vladimirov N, Sourjik V.** 2009. Chemotaxis: how bacteria use memory. Biol Chem **390:**1097-1104.

75.   **Adler J.** 1965. Chemotaxis in *Escherichia coli*. Cold Spring Harb Symp Quant Biol **30:**289-292.

76.   **Adler J.** 1969. Chemoreceptors in Bacteria. Science **166:**1588-1597.

77.   **Adler J, Hazelbauer GL, Dahl M.** 1973. Chemotaxis toward sugars in *Escherichia coli*. J Bacteriol **115:**824-847.

78.   **Adler J.** 1966. Chemotaxis in bacteria. Science **153:**708-716.

79.   **Adler J.** 1973. A method for measuring chemotaxis and use of the method to determine optimum conditions for chemotaxis by *Escherichia coli*. J Gen Microbiol **74:**77-91.

80.   **Adler J.** 1975. Chemotaxis in bacteria. Annu Rev Biochem **44:**341-356.

81.   **Englert DL, Adase CA, Jayaraman A, Manson MD.** 2010. Repellent taxis in response to nickel ion requires neither Ni(2+) transport nor the periplasmic NikA binding protein. J Bacteriol **192:**2633-2637.

82.   **Oosawa K, Imae Y.** 1983. Glycerol and ethylene glycol: members of a new class of repellents of *Escherichia coli* chemotaxis. J Bacteriol **154:**104-112.

83.   **Tso WW, Adler J.** 1974. Negative chemotaxis in *Escherichia coli*. J Bacteriol **118:**560-576.

84.   **Sarkar MK, Paul K, Blair D.** 2010. Chemotaxis signaling protein CheY binds to the rotor protein FliN to control the direction of flagellar rotation in *Escherichia coli*. Proc Nati Acade Sci U S A **107:**9370-9375.

85.   **Berg HC, Brown DA.** 1972. Chemotaxis in *Escherichia coli* analysed by three-dimensional tracking. Nature **239:**500-504.

86.   **Parkinson JS.** 2004. Signal amplification in bacterial chemotaxis through receptor teamwork. ASM News **70:**575-582.

87. **Segall JE, Block SM, Berg HC.** 1986. Temporal comparisons in bacterial chemotaxis. Proc Nati Acad Sci U S A **83:**8987-8991.

88. **Eisenbach M, Begley TP.** 2007. Chemotaxis, Wiley Encyclopedia of Chemical Biology. John Wiley & Sons, Inc.

89. **Sourjik V, Wingreen NS.** 2012. Responding to chemical gradients: bacterial chemotaxis. Curr Opin Cell Biol **24:**262-268.

90. **Englert DL, Jayaraman A, Manson MD.** 2009. Microfluidic techniques for the analysis of bacterial chemotaxis. Methods Mol Biol **571:**1-23.

91. **Kearns DB.** 2010. A field guide to bacterial swarming motility. Nat Rev Microbiol **8:**634-644.

92. **Yu HS, Alam M.** 1997. An agarose-in-plug bridge method to study chemotaxis in the Archaeon *Halobacterium salinarum*. FEMS Microbiol Lett **156:**265-269.

93. **Li J, Go AC, Ward MJ, Ottemann KM.** 2010. The chemical-in-plug bacterial chemotaxis assay is prone to false positive responses. BMC Res Notes **3:**77-77.

94. **Englert DL, Manson MD, Jayaraman A.** 2009. Flow-based microfluidic device for quantifying bacterial chemotaxis in stable, competing gradients. Appl Environ Microbiol **75:**4557-4564.

95. **Mao H, Cremer PS, Manson MD.** 2003. A sensitive, versatile microfluidic assay for bacterial chemotaxis. Proc Natl Acad Sci U S A **100:**5449-5454.

96. **Li Jeon N, Baskaran H, Dertinger SK, Whitesides GM, Van de Water L, Toner M.** 2002. Neutrophil chemotaxis in linear and complex gradients of interleukin-8 formed in a microfabricated device. Nat Biotechnol **20:**826-830.

97. **Hegde M, Englert DL, Schrock S, Cohn WB, Vogt C, Wood TK, Manson MD, Jayaraman A.** 2011. Chemotaxis to the quorum-sensing signal AI-2 requires the Tsr chemoreceptor and the periplasmic LsrB AI-2-binding protein. J Bacteriol **193:**768-773.

98. **Englert DL, Manson MD, Jayaraman A.** 2010. Investigation of bacterial chemotaxis in flow-based microfluidic devices. Nat Protoc **5:**864-872.

99. **Ford RM, Cummings PT.** 1998. Mathematical Models of Bacterial Chemotaxis, p 228-269. *In* Koch AL, Robinson JA, Milliken GA (ed), Mathematical Modeling in Microbial Ecology. Springer US, Boston, MA.

100. **Block SM, Segall JE, Berg HC.** 1982. Impulse responses in bacterial chemotaxis. Cell **31:**215-226.

101. **Le Novere N, Shimizu TS.** 2001. STOCHSIM: modelling of stochastic biomolecular processes. Bioinformatics **17:**575-576.

102. **Levin MD, Morton-Firth CJ, Abouhamad WN, Bourret RB, Bray D.** 1998. Origins of individual swimming behavior in bacteria. Biophys J **74:**175-181.

103. **Lipkow K, Andrews SS, Bray D.** 2005. Simulated diffusion of phosphorylated CheY through the cytoplasm of *Escherichia coli*. J Bacteriol **187:**45-53.

104. **Alt W.** 1980. Biased random walk models for chemotaxis and related diffusion approximations. J Math Biol **9:**147-177.

105. **Erban R, Othmer HG.** 2004. From individual to collective behavior in bacterial chemotaxis. SIAM J Appl Math **65:**361-391.

106. **Ford RM, Cummings PT.** 1992. On the relationship between cell balance equations for chemotactic cell populations. SIAM J Appl Math **52:**1426-1441.

107. **Keller EF, Segel LA.** 1970. Initiation of slime mold aggregation viewed as an instability. J Theor Biol **26:**399-415.

108. **Keller EF, Segel LA.** 1971. Model for chemotaxis. J Theor Biol **30:**225-234.

109. **Rivero MA, Tranquillo RT, Buettner HM, Lauffenburger DA.** 1989. Transport models for chemotactic cell populations based on individual cell behavior. Chem Eng Sci **44:**2881-2897.

110. **Romanczuk P, Erdmann U, Engel H, Schimansky-Geier L.** 2008. Beyond the Keller-Segel model. Eur Phys J Spec Top **157:**61-77.

111. **Freestone PP, Lyte M, Neal CP, Maggs AF, Haigh RD, Williams PH.** 2000. The mammalian neuroendocrine hormone norepinephrine supplies iron for bacterial growth in the presence of transferrin or lactoferrin. J Bacteriol **182:**6091-6098.

112. **Green BT, Brown DR.** 2016. Interactions between bacteria and the gut mucosa: do enteric neurotransmitters acting on the mucosal epithelium influence intestinal colonization or infection? Adv Exp Med Biol **874:**121-141.

113. **Clarke MB, Hughes DT, Zhu C, Boedeker EC, Sperandio V.** 2006. The QseC sensor kinase: a bacterial adrenergic receptor. Proc Natl Acad Sci U S A **103:**10420-10425.

114. **Moreira CG, Sperandio V.** 2016. The epinephrine/norepinephrine/autoinducer-3 interkingdom signaling system in *Escherichia coli* O157:H7. Adv Exp Med Biol **874:**247-261.

115. **Karavolos MH, Winzer K, Williams P, Khan CM.** 2013. Pathogen espionage: multiple bacterial adrenergic sensors eavesdrop on host communication systems. Mol Microbiol **87:**455-465.

116. **Lyte M, Vulchanova L, Brown DR.** 2011. Stress at the intestinal surface: catecholamines and mucosa-bacteria interactions. Cell Tissue Res **343:**23-32.

117. **Roshchina VV.** 2010. Evolutionary considerations of neurotransmitters in microbial, plant, and animal cells, p 17-52. *In* Lyte M, Freestone PPE (ed), Microbial Endocrinology: Interkingdom signaling in infectious disease and health. Springer New York, New York, NY.

118. **Kostakioti M, Hadjifrangiskou M, Pinkner JS, Hultgren SJ.** 2009. QseC-mediated dephosphorylation of QseB is required for expression of genes associated with virulence in uropathogenic *Escherichia coli*. Mol Microbiol **73:**1020-1031.

119. **Pullinger GD, Carnell SC, Sharaff FF, van Diemen PM, Dziva F, Morgan E, Lyte M, Freestone PP, Stevens MP.** 2010. Norepinephrine augments *Salmonella enterica*-induced enteritis in a manner associated with increased net replication but independent of the putative adrenergic sensor kinases QseC and QseE. Infect Immun **78:**372-380.

120. **Parkinson JS, Houts SE.** 1982. Isolation and behavior of *Escherichia coli* deletion mutants lacking chemotaxis functions. J Bacteriol **151:**106-113.

121. **Baba T, Ara T, Hasegawa M, Takai Y, Okumura Y, Baba M, Datsenko KA, Tomita M, Wanner BL, Mori H.** 2006. Construction of *Escherichia coli* K-12 in-frame, single-gene knockout mutants: the Keio collection. Mol Syst Biol **2:**2006.0008.

122. **Wang H, Bian X, Xia L, Ding X, Muller R, Zhang Y, Fu J, Stewart AF.** 2014. Improved seamless mutagenesis by recombineering using ccdB for counterselection. Nucleic Acids Res **42:**e37.

123. **Bernard P, Couturier M.** 1992. Cell killing by the F plasmid CcdB protein involves poisoning of DNA-topoisomerase II complexes. J Mol Biol **226:**735-745.

124. **Jaffe A, Ogura T, Hiraga S.** 1985. Effects of the ccd function of the F plasmid on bacterial growth. J Bacteriol **163:**841-849.

125. **Volkmer B, Heinemann M.** 2011. Condition-dependent cell volume and concentration of *Escherichia coli* to facilitate data conversion for systems biology modeling. PLoS ONE **6:**e23126.

126. **Stock JB, Rauch B, Roseman S.** 1977. Periplasmic space in *Salmonella typhimurium* and *Escherichia coli*. J Biol Chem **252:**7850-7861.

127. **Rankin LD, Bodenmiller DM, Partridge JD, Nishino SF, Spain JC, Spiro S.** 2008. *Escherichia coli* NsrR regulates a pathway for the oxidation of 3-nitrotyramine to 4-hydroxy-3-nitrophenylacetate. J Bacteriol **190:**6170-6177.

128. **Lai RZ, Manson JM, Bormans AF, Draheim RR, Nguyen NT, Manson MD.** 2005. Cooperative signaling among bacterial chemoreceptors. Biochemistry **44:**14298-14307.

129. **Sourjik V, Berg HC.** 2004. Functional interactions between receptors in bacterial chemotaxis. Nature **428:**437-441.

130. **Tajima H, Imada K, Sakuma M, Hattori F, Nara T, Kamo N, Homma M, Kawagishi I.** 2011. Ligand specificity determined by differentially arranged common ligand-binding residues in bacterial amino acid chemoreceptors Tsr and Tar. J Biol Chem **286:**42200-42210.

131. **Lin LN, Li J, Brandts JF, Weis RM.** 1994. The serine receptor of bacterial chemotaxis exhibits half-site saturation for serine binding. Biochemistry **33:**6564-6570.

132. **Gardina PJ, Bormans AF, Manson MD.** 1998. A mechanism for simultaneous sensing of aspartate and maltose by the Tar chemoreceptor of *Escherichia coli*. Mol Microbiol **29:**1147-1154.

133. **Gardina PJ, Manson MD.** 1996. Attractant signaling by an aspartate chemoreceptor dimer with a single cytoplasmic domain. Science **274:**425-426.

134. **Ames P, Zhou Q, Parkinson JS.** 2008. Mutational analysis of the connector segment in the HAMP domain of Tsr, the *Escherichia coli* serine chemoreceptor. J Bacteriol **190:**6676-6685.

135. **Zhou Q, Ames P, Parkinson JS.** 2009. Mutational analyses of HAMP helices suggest a dynamic bundle model of input-output signalling in chemoreceptors. Mol Microbiol **73:**801-814.

136. **Biemann HP, Koshland DE, Jr.** 1994. Aspartate receptors of *Escherichia coli* and *Salmonella typhimurium* bind ligand with negative and half-of-the-sites cooperativity. Biochemistry **33:**629-634.

137. **Englert DL.** 2009. Microfluidic systems for investigating bacterial chemotaxis and colonization. PhD Dissertation. Texas A&M University, College Station, TX.

138. **Maddock JR, Shapiro L.** 1993. Polar location of the chemoreceptor complex in the *Escherichia coli* cell. Science **259:**1717-1723.

139. **Block SM, Segall JE, Berg HC.** 1982. Impulse responses in bacterial chemotaxis. Cell **31:**215-226.

140. **Block SM, Segall JE, Berg HC.** 1983. Adaptation kinetics in bacterial chemotaxis. J Bacteriol **154:**312-323.

141. **Cluzel P, Surette M, Leibler S.** 2000. An ultrasensitive bacterial motor revealed by monitoring signaling proteins in single cells. Science **287:**1652-1655.

142. **Adler J, Hazelbauer GL, Dahl MM.** 1973. Chemotaxis toward sugars in *Escherichia coli*. J Bacteriol **115:**824-847.

143. **Eugene PK.** 1970. The lactose permease system of *Escherichia coli*. p. 49–92. *In* Beckwith, JR, Zipser, D (eds.), The Lactose Operon. Cold Spring Harbor Laboratory, Cold Spring Harbor, NY.

144. **Irving Z, Audrée VF.** 1970. β -galactosidase and thiogalactoside transacetylase. p. 24–47. *In* Beckwith, JR, Zipser, D (eds.), The Lactose Operon. Cold Spring Harbor Laboratory, Cold Spring Harbor, NY.

145. **Boos W.** 1969. The galactose binding protein and its relationship to the beta-methylgalactoside permease from *Escherichia coli*. Eur J Biochem **10:**66-73.

146. **Kondoh H, Ball CB, Adler J.** 1979. Identification of a methyl-accepting chemotaxis protein for the ribose and galactose chemoreceptors of *Escherichia coli*. Proc Natl Acad Sci U S A **76:**260-264.

147. **Etienne-Mesmin L, Chassaing B, Sauvanet P, Denizot J, Blanquet-Diot S, Darfeuille-Michaud A, Pradel N, Livrelli V.** 2011. Interactions with M cells and macrophages as key steps in the pathogenesis of enterohemorrhagic *Escherichia coli* infections. PLoS ONE **6:**e23594.

148. **Li M, Hazelbauer GL.** 2004. Cellular stoichiometry of the components of the chemotaxis signaling complex. J Bacteriol **186:**3687-3694.

149. **Hansen MC, Palmer RJ, Udsen C, White DC, Molin S.** 2001. Assessment of GFP fluorescence in cells of *Streptococcus gordonii* under conditions of low pH and low oxygen concentration. Microbiology **147:**1383-1391.

150. **Lyte M, Erickson AK, Arulanandam BP, Frank CD, Crawford MA, Francis DH.** 1997. Norepinephrine-induced expression of the K99 pilus adhesin of enterotoxigenic *Escherichia coli*. Biochem Biophy Res Commun **232:**682-686.

151. **Lyte M, Freestone PP, Neal CP, Olson BA, Haigh RD, Bayston R, Williams PH.** 2003. Stimulation of *Staphylococcus epidermidis* growth and biofilm formation by catecholamine inotropes. Lancet **361:**130-135.

152. **Hughes DT, Clarke MB, Yamamoto K, Rasko DA, Sperandio V.** 2009. The QseC adrenergic signaling cascade in Enterohemorrhagic *E. coli* (EHEC). PLoS Pathog **5:**e1000553.

153. **Moreira CG, Sperandio V.** 2012. Interplay between the QseC and QseE bacterial adrenergic sensor kinases in *Salmonella enterica* serovar typhimurium pathogenesis. Infect Immun **80:**4344-4353.

154. **Reading NC, Torres AG, Kendall MM, Hughes DT, Yamamoto K, Sperandio V.** 2007. A novel two-component signaling system that activates transcription of an enterohemorrhagic *Escherichia coli* effector involved in remodeling of host actin. J Bacteriol **189:**2468-2476.

155. **Sperandio V, Torres AG, Kaper JB.** 2002. Quorum sensing *Escherichia coli* regulators B and C (QseBC): a novel two-component regulatory system involved in the regulation of flagella and motility by quorum sensing in *E. coli*. Mol Microbiol **43:**809-821.

156. **Weigel W, Demuth D.** 2016. QseBC, a two-component bacterial adrenergic receptor and global regulator of virulence in *Enterobacteriaceae* and *Pasteurellaceae*. Mol Oral Microbiol **31:**379-397.

157. **Sule N, Pasupuleti S, Kohli N, Menon R, Dangott LJ, Manson MD, Jayaraman A.** 2017. The norepinephrine metabolite 3,4-dihydroxymandelic acid is Produced by the commensal microbiota and promotes chemotaxis and virulence gene expression in enterohemorrhagic *Escherichia coli*. Infect Immun **85:** e00431-17

158. **Walters M, Sperandio V.** 2006. Autoinducer 3 and epinephrine signaling in the kinetics of locus of enterocyte effacement gene expression in enterohemorrhagic *Escherichia coli*. Infect Immun **74:**5445-5455.

159. **Pasupuleti S, Sule N, Cohn WB, MacKenzie DS, Jayaraman A, Manson MD.** 2014. Chemotaxis of *Escherichia coli* to norepinephrine (NE) requires conversion of NE to 3,4-dihydroxymandelic acid. J Bacteriol **196:**3992-4000.

160. **Iwama T, Nakao K-I, Nakazato H, Yamagata S, Homma M, Kawagishi I.** 2000. Mutational analysis of ligand recognition by Tcp, the citrate chemoreceptor of *Salmonella enterica* serovar typhimurium. J Bacteriol **182:**1437-1441.

161. **Wang Q, Mariconda S, Suzuki A, McClelland M, Harshey RM.** 2006. Uncovering a large set of genes that affect surface motility in *Salmonella enterica* serovar typhimurium. J Bacteriol **188:**7981-7984.

162. **Dahl MK, Boos W, Manson MD.** 1989. Evolution of chemotactic-signal transducers in enteric bacteria. J Bacteriol **171:**2361-2371.

163. **Craven RC, Montie TC.** 1983. Chemotaxis of *Pseudomonas aeruginosa*: involvement of methylation. J Bacteriol **154:**780-786.

164. **Zeng J, Spiro S.** 2013. Finely tuned regulation of the aromatic amine degradation pathway in *Escherichia coli*. J Bacteriol **195:**5141-5150.

165. **Livak KJ, Schmittgen TD.** 2001. Analysis of relative gene expression data using real-time quantitative PCR and the 2(-Delta Delta C(T)) method. Methods **25:**402-408.

166. **Hanlon SP, Hill TK, Flavell MA, Stringfellow JM, Cooper RA.** 1997. 2-phenylethylamine catabolism by *Escherichia coli* K-12: gene organization and expression. Microbiology **143:**513-518.

167. **Clarke MB, Sperandio V.** 2005. Transcriptional regulation of flhDC by QseBC and sigma (FliA) in enterohaemorrhagic *Escherichia coli*. Mol Microbiol **57:**1734-1749.

168. **Gopel Y, Luttmann D, Heroven AK, Reichenbach B, Dersch P, Gorke B.** 2011. Common and divergent features in transcriptional control of the homologous small RNAs GlmY and GlmZ in *Enterobacteriaceae*. Nucleic Acids Res **39:**1294-1309.

169. **Kresge N, Simoni RD, Hill RL.** 2006. Julius Adler's Contributions to Understanding Bacterial Chemotaxis. J Biol Chem **281:**e33.

170. **Parales RE, Luu RA, Hughes JG, Ditty JL.** 2015. Bacterial chemotaxis to xenobiotic chemicals and naturally-occurring analogs. Curr Opin Biotechnol **33:**318-326.

171. **Tindall MJ, Maini PK, Porter SL, Armitage JP.** 2008. Overview of mathematical approaches used to model bacterial chemotaxis II: bacterial populations. Bull Math Biol **70:**1570-1607.

172. **Clarke MB, Sperandio V.** 2005. Transcriptional autoregulation by quorum sensing Escherichia coli regulators B and C (QseBC) in enterohaemorrhagic *E. coli* (EHEC). Mol Microbiol **58:**441-455.

173. **Hellman LM, Fried MG.** 2007. Electrophoretic mobility shift assay (EMSA) for detecting protein-nucleic acid interactions. Nat Protoc **2:**1849-1861.